Australian Government
Department of Defence
Defence Science and
Technology Organisation

The Effects of Selected Modelling Parameters on the Computed Optical Frequency Signatures of Naval Platforms

Susan Smith

Maritime Platforms Division
Defence Science and Technology Organisation

DSTO-TR-2277

ABSTRACT

An investigation has been carried out into the effects of wireframe detail and model sub-processing on the predicted optical frequency (OF) signature of a platform. This report describes the results of that investigation. Overall it is concluded that to be able to compare the computed OF signatures of different platforms with validity, the models of the platforms have to incorporate the same level of wireframe detail, especially in internally-heated regions such as their stacks. They also have to be processed using subdivisions of very similar size, based on the same method of facet subdivision.

RELEASE LIMITATION

Approved for public release

Published by

Maritime Platforms Division
DSTO Defence Science and Technology Organisation
506 Lorimer St
Fishermans Bend, Victoria 3207 Australia

Telephone: (03) 9626 7000
Fax: (03) 9626 7999

© Commonwealth of Australia 2008
AR-014-501
April 2009

APPROVED FOR PUBLIC RELEASE

The Effects of Selected Modelling Parameters on the Computed Optical Frequency Signatures of Naval Platforms

Executive Summary

Computer-based modelling plays an important part in the assessment of the optical frequency (OF) signatures of naval platforms. The nature of such signatures means that they are heavily dependent on the prevailing environmental conditions and a platform's settings, such as its heading and speed. Measurements of OF signatures are expensive, difficult to perform and only give a single snapshot of the signature under the conditions in which they are taken. Modelling allows the prediction of the signature of a platform under any conditions and in any location. Modelling can also be used to predict the signature of a future platform. It therefore has a role in the acquisition process, assessing and comparing the signatures of competing platform designs, and in the upgrade process, examining the effects on the OF signature of proposed changes to a platform. It may also be used to help determine which platform in a group is most suited to perform a given mission.

Although OF signature modelling is an established capability, it has not previously been ascertained how the level of detail in a wireframe model and the type of model sub-processing used affect the process. These factors are of particular significance when comparing the signatures of different platforms. An investigation has therefore been carried out into their effects on the predicted OF signature of a platform. This report describes the results of that investigation. Overall it is concluded that to be able to compare the computed OF signatures of different platforms with validity, the models of the platforms have to incorporate the same level of wireframe detail, especially in internally-heated regions such as their stacks. They also have to be processed using subdivisions of very similar size, based on the same method of facet subdivision.

Authors

Susan Smith
Maritime Platforms Division

Susan Smith completed a B.Sc. (Hons) in 1986 and a Ph.D. in 1996, both in Computer Science, at the University of Melbourne. She was recruited into DSTO in February 1997 to establish and run a naval infrared signature modelling capability. She has continued to work in the area of naval IR signatures and has been one of the principals in the development of Maritime Platforms Division's expertise in the subject. She currently leads the optical frequency signature modelling area in the division.

Contents

1. INTRODUCTION 1

2. MODELLING CODES 1
2.1 NTCS 2
2.2 MODTRAN 2
2.3 RAVFAC 3
2.4 GEST 4

3. METHODOLOGY 5
3.1 Model differences 5
3.2 Model sub-processing 6
3.3 Computer processing 6
3.4 Platform settings 7
3.5 OF bands 7
3.6 Thermal backgrounds 7
3.7 Observation details 8

4. RESULTS 8
4.1 Model sub-processing 8
4.1.1 Simple wireframe 8
4.1.2 Complex wireframe 9
4.2 Wireframe detail 10
4.2.1 Simple wireframe versus complex wireframe – standard paints 10
4.2.2 Simple wireframe versus complex wireframe – near-infrared reflecting (NIRR) paints 11

5. DISCUSSION 13
5.1 Model sub-processing 13
5.2 Wireframe detail 15

6. CONCLUSIONS 17

7. REFERENCES 18

APPENDIX A: OF CONTRAST SIGNATURE DATA — SIMPLE WIREFRAME MODEL SUB-PROCESSING 19
A.1. Contrast signature plots for the simple wireframe model with user-defined thermal boundary conditions and an exhaust plume 20
A.2. Contrast signature plots for the simple wireframe model with user-defined thermal boundary conditions but no exhaust plume 25
A.3. Contrast signature plots for the simple wireframe model with no user-defined thermal boundary conditions or exhaust plume 30

APPENDIX B: OF CONTRAST SIGNATURE DATA — COMPLEX WIREFRAME MODEL SUB-PROCESSING 35
B.1. Contrast signature plots for the complex wireframe model with user-defined thermal boundary conditions and an exhaust plume 36
B.2. Contrast signature plots for the complex wireframe model with user-defined thermal boundary conditions but no exhaust plume 41
B.3. Contrast signature plots for the complex wireframe model with no user-defined thermal boundary conditions or exhaust plume 46

APPENDIX C: OF CONTRAST SIGNATURE DATA — SIMPLE WIREFRAME VERSUS COMPLEX WIREFRAME, BOTH WITH STANDARD PAINTS 51
C.1. Contrast signature plots for the two models, both with user-defined thermal boundary conditions and an exhaust plume 52
C.2. Contrast signature plots for the two models, both with user-defined thermal boundary conditions but no exhaust plume 58
C.3. Contrast signature plots for the two models, both with no user-defined thermal boundary conditions or exhaust plume 64

APPENDIX D: OF CONTRAST SIGNATURE DATA —SIMPLE WIREFRAME VERSUS COMPLEX WIREFRAME, BOTH WITH NEAR-INFRARED REFLECTING PAINTS (NIRR) 71
D.1. Contrast signature plots for the two models, both with user-defined thermal boundary conditions and an exhaust plume 72
D.2. Contrast signature plots for the two models, both with user-defined thermal boundary conditions but no exhaust plume 77
D.3. Contrast signature plots for the two models, both with no user-defined thermal boundary conditions or exhaust plume 82

1. Introduction

In 2004, the Maritime Platforms Division of the Defence Science and Technology Organisation (DSTO) was required to assess the optical frequency (OF) signatures of four different naval platforms in a limited time frame. In the space of a few weeks, computer models of the four platforms had to be produced, the models processed, their OF signatures calculated and the results both cross-compared and also compared with those for another, pre-existing model. The time constraints were such that it was not possible to generate all of the computer models and compare them before proceeding with the next stage of the work. Immediately each model was completed, it had to be processed and its OF signature calculated. It was therefore not possible to ensure that an equivalent level of detail was incorporated into the corresponding subsections of the wireframes of the four models. It was only possible to ensure that a similar total number of facets was used in each of the wireframes. In addition to the time constraints, computer processing constraints were also placed upon the work. The combination of these and the time constraints meant the size of the largest wireframe facet in each model varied to a sufficient degree that differing restrictions were placed on the sub-processing of each model.

Based on knowledge of the OF signature modelling process and the broad-brush nature of the assessment being undertaken, it was decided that the differences in the wireframes and the sub-processing of the models did not present an issue. It was expected that any effects the differences may have on the computed OF signatures of the platforms would be sufficiently small that they could be neglected for the purposes of the work. However, it was recognised that under different circumstances, where a more rigorous assessment was required, that even a small variation in the calculated signature of a platform may be significant. It was therefore decided that an investigation should be carried out to quantify the effects of wireframe detail and model sub-processing on the predicted OF signature of a platform. This report describes the results of that investigation.

2. Modelling Codes

The primary software package used in DSTO to perform OF contrast signature analysis for naval platforms is the Naval Threat/Countermeasures Simulator (NTCS) [1]. Two third-party programs are supplied with NTCS to perform low-level processing: the Moderate Resolution Transmittance (MODTRAN) code, which is used to generate environmental data and the Radiation View Factor (RAVFAC) code, which performs the model sub-processing. DSTO also uses an alternative code for performing model sub-processing, the General Electromagnetic Signature ToolBox (GEST) [2].

2.1 NTCS

NTCS was developed by Davis Engineering in Ottawa, Canada. This software package is used by many countries and has been adopted as the standard code for maritime OF signature modelling by members of NATO. NTCS performs OF signature modelling of a platform within specified wavebands, given the relevant physical information about the platform, such as its shape and surface coatings, together with its speed, direction and location in both space and time.

NTCS requires the structure of a platform to be input in the form of a wireframe consisting of triangular or flat rectangular facets. The surface materials of the facets are specified in terms of their conductive and radiative properties across the wavebands of interest. The properties of the exhaust plumes, if present, plus the details of any internal heat sources, convective heat transfers and conductive heat paths between superstructure plates, collectively know as the thermal boundary conditions, complete the model of the platform. To calculate the signature of a platform, the model is placed in a thermal background, given a speed and direction and processed to produce a scenario. The thermal background is specified in terms of a date and time, a latitude and longitude, a description of the prevailing climatic conditions (including air and sea surface temperature, relative humidity, cloud cover, rain rate and wind speed and direction), the OF bands of interest and the parameters and parameterisation schemes to be used for the sun, sea, sky and sea glint.

Once a scenario has been constructed for a platform, the OF contrast signature of the platform in the specified background may be calculated for any of the selected wavebands and from any viewing direction and distance. The distance at which a simple, generic missile will lock-on to the platform when launched at it from a selected location can be computed using a simulated missile-platform engagement. Full missile encounters, in which a missile is launched at the platform and the platform attempts to seduce the missile using flares, can be simulated. For such encounters, NTCS predicts if and where the missile will hit the platform.

2.2 MODTRAN

MODTRAN was developed by the U.S. Air Force Research Laboratory, Space Vehicles Directorate, in collaboration with Spectral Sciences, Inc [3-5]. It calculates atmospheric transmittance, atmospheric background radiance, single-scattered solar and lunar radiance, direct solar irradiance and multiple-scattered solar and thermal radiance for frequencies from 0 to 50,000 cm^{-1} (0.2 μm to infinity) at moderate spectral resolution, primarily 2 cm^{-1} (20 cm^{-1} in the UV). A molecular band model is used to calculate molecular transmittance. The effects of molecular scattering and aerosol and hydrometeor absorption and scattering are included. Refraction and earth curvature are considered in the calculation of the atmospheric slant path and attenuation amounts along the path.

MODTRAN provides representative atmospheric, aerosol, cloud and rain models with options to replace them with user-provided values. There are six reference geographical-seasonal model atmospheres (tropical, mid-latitude summer, mid-latitude winter, sub-arctic summer, sub-arctic winter and 1976 US standard), each defining temperature, pressure, density and mixing ratios for H_2O, O_3, CH_4, CO and N_2O as a function of altitude. The in-built

boundary-layer aerosol models represent urban, rural, desert, maritime and fog-bound environments. The stratospheric aerosol models include profiles for different levels of volcanic activity. The cloud and rain models range from the choice of no clouds or rain, through increasing levels of cloud cover then increasing rain rates, all the way to extreme rain.

NTCS calls MODTRAN both to process the thermal background directly and to process the chosen platform in the background [6]. In the former case, MODTRAN is used to generate general environmental data. In the latter, it is used to generate the target-specific environmental data. In addition to inputting the global geographic location and time of day, the NTCS interface to MODTRAN allows the user to select one of the in-built model atmospheres or to input their own model atmosphere. The user can also select the boundary-layer and stratospheric aerosol models and the cloud and rain models to use and input details of the clouds and rain. They can choose not to include solar scattering or to incorporate either single or multiple scattering.

2.3 RAVFAC

RAVFAC was developed by the Thermal Environment Section of the Lockheed Missiles and Space Company [7]. The program calculates diffuse radiation view factors[1] for groups of surfaces, including the effects of shading. It divides each surface into smaller areas called nodes and the nodes into even smaller areas called elements. It calculates the view factors between elements and sums the results to output view factors between nodes. The code incorporates two different methods for calculating the view factors: a finite difference technique and a contour integral technique. Either or both may be used in a computation.

The method of subdivision of a surface is illustrated in Figure 1, where β_{min} and β_{max} define the dimension of the surface in the β direction, γ_{min} and γ_{max} define the dimension of the surface in the γ direction, NVB and NVG are the numbers of nodes per surface in the β and γ directions respectively and NB and NG are the numbers of elements per node in the β and γ directions respectively. Up to 2500 elements can be defined for each surface. The effects of shading are taken into account by checking whether or not two elements can "see" each other based on their centres of area. If they can, the elemental view factor is calculated. If the elements do not present themselves to each other or one or more other opaque surfaces obstruct the vector joining their centres of area, the elemental view factor is set to zero.

NTCS uses RAVFAC to perform the model sub-processing, which determines the interactions between the facets in a platform's wireframe [9]. Two versions of RAVFAC are provided with NTCS: one for Unix-based computer systems, which can process up to 5400 wireframe facets, and one for Windows-based systems, which can process up to 2000 facets. The supplied interface to RAVFAC is embedded within the Model View Editor (MVE) [10]. It generates both the input files used by RAVFAC and script files to facilitate running RAVFAC and converting its output to the format required by NTCS. To help circumvent the surface

[1] Radiation View Factor F_{AB} [7, 8]: The fraction of the radiant energy leaving surface A in all directions, which strikes surface B, determined entirely as a function of geometry. Stated in other words, it is the fraction of surface B which is visible from surface A and ranges from zero to 1. Its units are dimensionless. It is also referred to as the angle factor, shape factor, form factor, geometric factor or configuration factor.

processing limits in RAVFAC, the interface enables the user to split the wireframe of a platform into an unlimited number of groups of interacting facets, which can be processed separately. This feature can, in addition, be used to significantly reduce the RAVFAC runtime for any given set of facets. The MVE interface also allows the user to define the subdivision of the facets. In NTCS each facet requires its own set of view factors but RAVFAC calculates the view factors between nodes. Therefore, within MVE, NVB and NVG are always set to 1, which equates to defining one node per facet. However the user can specify the values of NB and NG. Their default values are 1, giving one element per node and hence one element per facet. Within the interface, the user can specify the maximum desired element length in metres. For each facet, MVE computes the number of elements necessary to ensure the largest element is no longer than the specified value and sets NB and NG accordingly, within the constraint that NB times NG cannot exceed 2500 — if the number exceeds 2500, the user is required to choose a longer element length. Alternatively, if a different fixed subdivision of the facets, such as NB = 3 and NG = 2, is required, it can be set by manually editing the files generated by MVE.

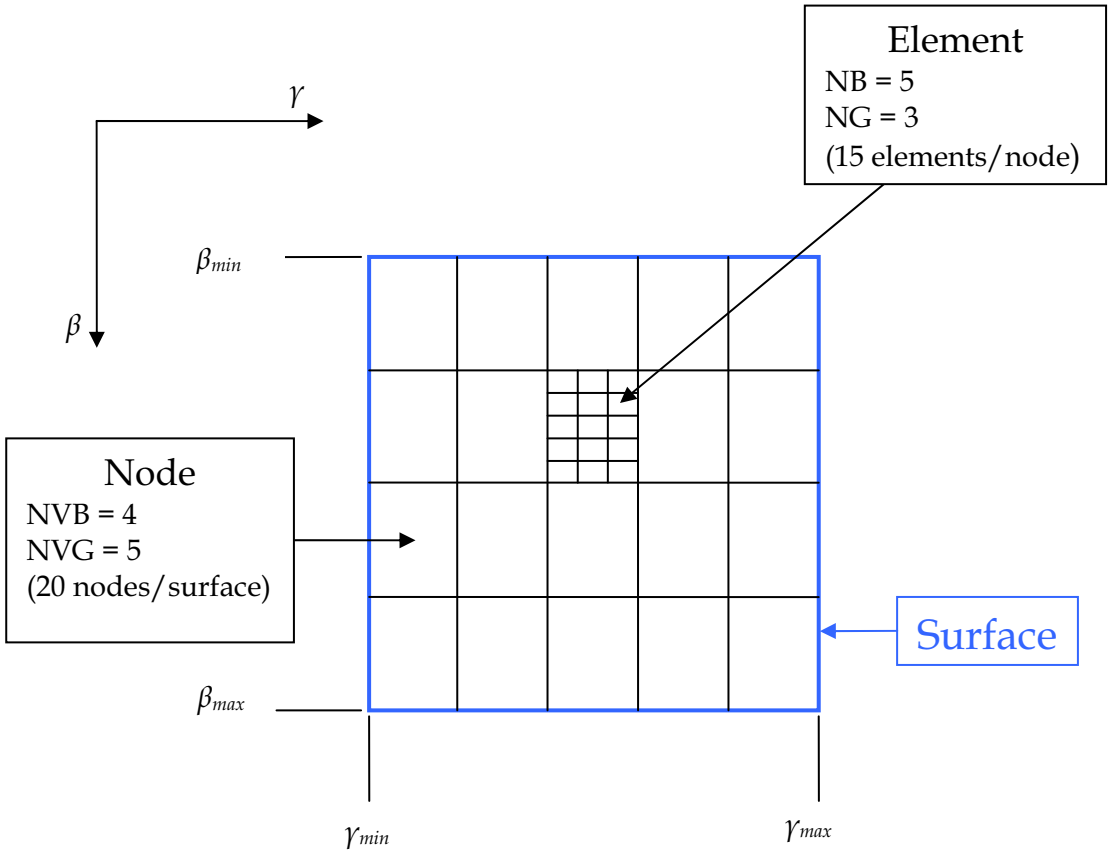

Figure 1: RAVFAC node and element distribution for a surface. (After [7])

2.4 GEST

GEST is an electromagnetic signature prediction suite developed by DSTO [2]. It was intended to be an alternative to NTCS, incorporating different features to the latter, such as diurnal signature variation.

GEST calculates radiation view factors in a manner similar to RAVFAC. However, unlike RAVFAC, it produces a non-uniformly structured subdivision across a wireframe. It treats facets individually, subdividing each one recursively into smaller triangular elements until a user-specified level of convergence or accuracy is reached. The code has advantages over RAVFAC in that it can handle wireframes with over half a million facets and there are no constraints on the number of subdivisions allowed, apart from those imposed by computer processing limitations.

To enable comparisons with NTCS, GEST includes an option to use the same target geometry input file formats. It can also output calculated radiation view factors in the file format required by NTCS. It can therefore be used to perform the model sub-processing for the latter, in place of RAVFAC.

3. Methodology

Two different computer models of the same naval platform were both sub-processed a number of times under varying constraints and their OF contrast signatures calculated using NTCS. In each instance, the signature calculations were performed for three settings of the platform in four wavebands in three different thermal backgrounds at two viewing distances for 360 viewing directions. The results were then compared in order to study the effects of model sub-processing and of wireframe detail on the calculated OF signature.

3.1 Model differences

The most significant differences between the two models were in their wireframes (see Figure 2). The first had a simple wireframe consisting of 866 facets, of which 160 were double-sided, while the second had a complex wireframe consisting of 3666 facets, of which 648 were double-sided. Apart from having more, and hence smaller, facets, the complex wireframe also differed physically from the simple wireframe in three areas: the 76 mm gun, the CIWS and the stack. In the complex wireframe these areas were modelled as detailed curved surfaces, rather than as blocks as in the simple wireframe. The stack area was also made more realistic in the complex wireframe, using the precise details of the exhaust outlets. Hence, in the complex wireframe the exhaust outlets had a larger diameter than in the simple wireframe and were tilted rather than vertical.

Aside from the differences in their wireframes, the models were for practical purposes identical. For the investigations into the effects of model sub-processing, the simple wireframe was assigned standard paints while the complex wireframe was assigned near-infrared reflecting (NIRR) paints. However, for the investigations into wireframe detail, similar material properties were assigned to each – for the first set of analyses, both wireframes were assigned standard paints; for the second set of analyses, both wireframes were assigned NIRR paints. Allowing for the differences in their stack areas, the same exhaust plume and user-defined thermal boundary conditions were used for both models (see Section 3.4).

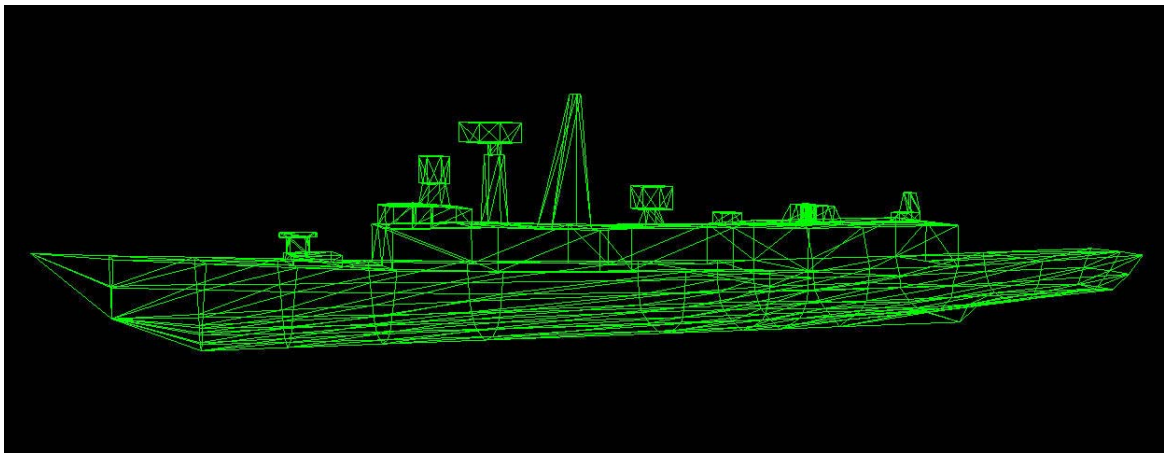

(a) Simple wireframe

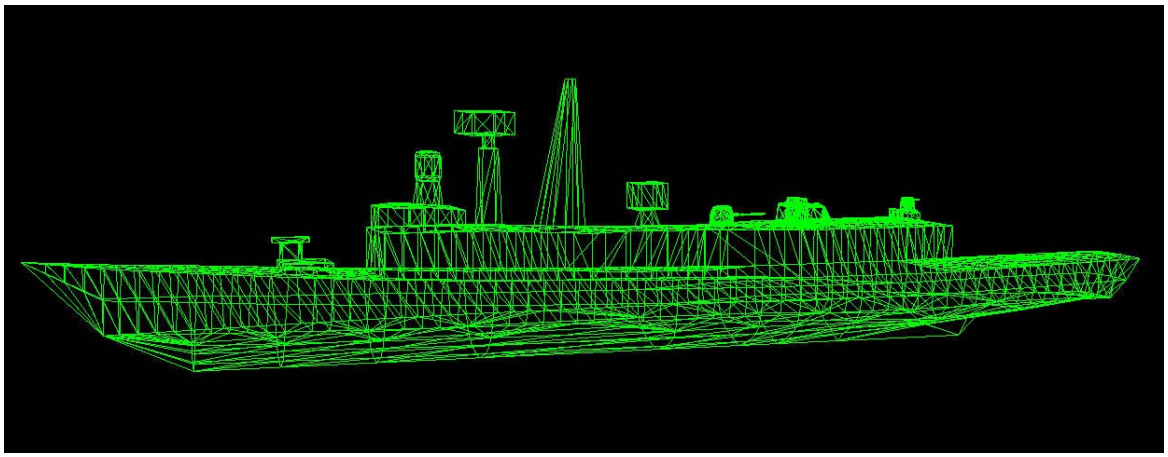

(b) Complex wireframe

Figure 2: The wireframes for the two computer models

3.2 Model sub-processing

The simple wireframe was processed three times. It was processed twice using RAVFAC, once with a maximum desired element length of 1.0 m and once with a maximum desired element length of 0.3 m, and once using GEST with a moderate level of accuracy [2]. The complex wireframe was processed four times, each with RAVFAC. It was processed using the default setting of NB = NG = 1 and also with maximum desired element lengths of 1.0 m, 0.25 m and 0.2 m respectively.

3.3 Computer processing

The calculations were performed under Windows XP. Hence the Windows-based version of RAVFAC, which can process a maximum of 2000 facets in one group, was used for the model sub-processing. MODTRAN4 v1.1 was used for the environmental processing and NTCS v3.1c was used to perform the OF signature calculations. The analysis parameters for the signature

calculations were set such that the output was apparent absolute contrast intensities; the calculations used the absolute pixel-contrast values with the blackbody-equivalent atmospheric attenuation applied [11-13].

3.4 Platform settings

Both models were analysed with three different settings: with no exhaust plume and no user-defined thermal boundary conditions; with user-defined thermal boundary conditions but no exhaust plume; and with both user-defined thermal boundary conditions and an exhaust plume. The plume used was based on that produced by an unsuppressed LM2500 gas turbine engine and it was assigned to the starboard exhaust uptake. The thermal boundary conditions described the convective heat transfers within the starboard uptake resulting from the presence of an exhaust plume and also the effects on the plates of the hull of a heated main engine room. For all the calculations, regardless of the settings, the models were given a speed of 18.4 knots and a heading of due east.

3.5 OF bands

The signature calculations were performed for four representative wavebands covering the OF spectrum from the visible region through to the long-wave infrared (IR). The bands used were:

Visible	0.4 – 0.8 μm
Near-visible IR	1.4 – 1.8 μm
Mid-wave IR	3 – 5 μm
Long-wave IR	8 – 14 μm.

3.6 Thermal backgrounds

Three thermal backgrounds, covering a range of locations and environmental conditions, were used for the analyses. Each was set in a maritime environment with no clouds or rain and no solar scattering. Background 1 was based on the MODTRAN mid-latitude summer model atmosphere and was set mid-afternoon with an ambient temperature of 25°C, a sea surface temperature of 23°C, a relative humidity of 69%, a wind speed of 5 m/s and a wind direction of 9° N of E. Background 2 was also based on the mid-latitude summer model atmosphere but was set at night with ambient and sea surface temperatures both of 16°C, a relative humidity of 35%, a wind speed of 5 m/s and a wind direction of 196° N of E. Background 3 was based on the MODTRAN tropical model atmosphere and was set mid-morning with ambient and sea surface temperatures of 29°C, a relative humidity of 76%, a wind speed of 7 m/s and a wind direction of 255° N of E.

3.7 Observation details

The OF signatures of the models were calculated for two different viewing distances: 2 km and 10 km. For all the calculations, the observer was placed at 10 m above sea level with a viewing angle below the horizontal of 0.03° and a field of view (FOV) chosen such that the broadside of the platform closely filled the image width of 800 pixels. For the viewing distance of 2 km, the FOV was set to 3.00 and for the viewing distance of 10 km, it was set to 0.60.

4. Results

The results of the OF contrast signature calculations for the two computer models are plotted in Appendices A to D and discussed in the following sections. It should be noted that no results are presented for Background 2 and the visible and near-visible IR bands as the platform is not detectable under these conditions. (For details of the backgrounds and the OF wavebands, refer to Section 3.)

4.1 Model sub-processing

4.1.1 Simple wireframe

The simple wireframe was processed twice using RAVFAC, once with a maximum desired element length of 1.0 m and once with a maximum desired element length of 0.3 m, and processed once using GEST with a moderate level of accuracy. Comparative plots of the OF contrast signature data generated for the three cases are presented in Appendix A.

The plots show that for this model, in the visible band and the near-visible IR band, the results for the two RAVFAC subdivisions and the GEST subdivision are for practical purposes identical for all environmental conditions, platform settings and viewing positions (see Figure A1, Figure A8 and Figure A17, for example).

In the long-wave IR band, the results for the two RAVFAC subdivisions are for practical purposes identical, regardless of the choice of thermal background, platform settings or viewing position, and, in general, those for the GEST subdivision are no more than slightly different from the others. For the cases where there are no specified thermal boundary conditions or plume, for Background 2 the results for the GEST subdivision are for practical purposes identical to the others (see Figure A15, for example). For Background 1 (e.g. Figure A14) and Background 3 (e.g. Figure A18), they are marginally smaller on the port broadside of the platform but are for practical purposes identical to the others elsewhere. When the model includes specified thermal boundary conditions, with or without an exhaust plume, for Background 1 (e.g. Figure A2) and Background 3 (e.g. Figure A5), the results for the GEST subdivision are marginally larger on the starboard side but for the remaining viewing angles there is no significant difference between them and the others. However, for Background 2, the results for the GEST subdivision are noticeably larger than those for the RAVFAC subdivisions (see, for example, Figure A3).

In the mid-wave IR band, the differences between the results for the three subdivisions vary from case to case. For those instances where there are no specified thermal boundary conditions or plume, the results for the two RAVFAC subdivisions are for practical purposes identical for all three backgrounds and all viewing positions and those for the GEST subdivision are at most marginally different. For Background 2 (e.g. Figure A16), there is no significant difference between the latter and the others. For Background 1 (e.g. Figure A13) and Background 3 (e.g. Figure A17), the results for the GEST subdivision are marginally smaller on the port broadside of the platform but are for practical purposes identical to the others elsewhere. When the model includes both a plume and specified thermal boundary conditions (Figure A1 to Figure A6), for Background 3 and a viewing distance of 10 km, the results for the two RAVFAC subdivisions differ noticeably for viewing angles on the port forward broadside. In all other cases, there is no significant difference between them. The results for the GEST subdivision are only marginally different to the others for Backgrounds 1 and 3. For Background 2, they follow the same distribution as the others but are noticeably larger, especially on the starboard broadside. When there are specified thermal boundary conditions but not an exhaust plume (Figure A7 to Figure A12), for all three backgrounds and a viewing distance of 10 km, the results for the two RAVFAC subdivisions differ noticeably for viewing angles on the port broadside of the platform. For the remaining viewing angles at this distance and for a viewing distance of 2 km, there is no significant difference between them. The results for the GEST subdivision follow a similar distribution to the others for all three backgrounds. However, while for Backgrounds 1 and 3 they are also similar in size to the others, for Background 2 they are noticeably larger, especially on the starboard broadside.

4.1.2 Complex wireframe

The complex wireframe was processed four times using RAVFAC, once using the default setting of NB = NG = 1 and once each with maximum desired element lengths of 1.0 m, 0.25 m and 0.2 m respectively. Comparative plots of the OF contrast signature data generated for the four cases are presented in Appendix B.

The plots show that for this model, in the visible band and the near-visible IR band, the results for the four RAVFAC subdivisions are for practical purposes identical for all environmental conditions, platform settings and viewing positions (see Figure B1, Figure B8 and Figure B17, for example).

In the long-wave IR band, for Backgrounds 1 and 3, the results for the 0.2, 0.25 and 1.0 m subdivisions are for practical purposes identical, regardless of the choice of platform settings or viewing position. The results for the default subdivision are marginally smaller than the others on the port broadside of the platform but for all other viewing angles are identical for practical purposes (for example, see Figure B6 and Figure B14). For Background 2, there are no significant differences between the results for the four subdivisions in any instance (see Figure B9 and Figure B16 for example).

In the mid-wave IR band, the differences between the results for the four subdivisions vary from case to case. For the cases with no specified thermal boundary conditions or plume (Figure B13 to Figure B18), for Backgrounds 1 and 2 the results for all four subdivisions are for practical purposes identical but for Background 3 the results for the default subdivision are

marginally smaller than the others on the port broadside of the platform. When the model includes specified thermal boundary conditions, with or without a plume, for Background 3, for a viewing distance of 2 km (Figure B5 and Figure B11) the results for the four subdivisions differ marginally on the broadsides of the platform. For a viewing distance of 10 km (Figure B6 and Figure B12), they differ marginally on the starboard broadside but there is no significant difference between them on the port side. For Background 1, for a viewing distance of 2 km there is no significant difference between the results for the four subdivisions (see Figure B1 and Figure B7). For a viewing distance of 10 km, there is no significant difference between the results on the port broadside but they differ noticeably on the starboard side — when there is an exhaust plume, the results are spread out, with those for the default subdivision being the largest and those for a subdivision of 1.0 m being the smallest (see Figure B2); when there is no exhaust plume, the results for the default subdivision are again the largest but the results for the others are grouped closely together (see Figure B8). For Background 2, for a viewing distance of 2 km (Figure B3 and Figure B9), on the port side of the platform there is no significant difference between the results for all four subdivisions. On the starboard side, the results for the 0.2, 0.25 and 1.0 m subdivisions are for practical purposes identical but the results for the default subdivision are larger. For a viewing distance of 10 km (Figure B4 and Figure B10), on the port side the results for the four subdivisions are spread out, with those for the 0.2 m subdivision being the largest and those for the 1.0 m being the smallest. On the starboard side, the results for the 0.2 m, 0.25 m and default subdivisions are for practical purposes identical but those for the 1.0 m subdivision are noticeably smaller.

4.2 Wireframe detail

4.2.1 Simple wireframe versus complex wireframe – standard paints

The simple and the complex wireframes were both processed using RAVFAC with a maximum desired element length of 1.0 m and assigned standard paints. Comparative plots of the OF contrast signature data generated for the two models are presented in Appendix C. For a select number of cases the data is presented twice, using two different scales, in order to demonstrate better the effects of wireframe detail.

The plots show that, in the visible band and the near-visible IR band, for Background 1 the results for the two models are very similar for all platform settings and viewing distances. However, those for the complex wireframe indicate the presence of a strong glint on the starboard broadside of the platform, towards the stern, but those for the simple wireframe do not (see Figure C1 and Figure C10, for example). As well, in both wavebands the results for the complex wireframe show more variation on the port broadside (for example, see Figure C11) and in the near-visible IR band they show more variation in the starboard forward quarter (for example, see Figure C12). In the visible band, the results for the simple wireframe are marginally larger than those for the complex wireframe on the port broadside, while in the near-visible IR band, they are marginally smaller at the stern of the platform (see Figure C3 and Figure C4, for example). For Background 3, in most instances there is no significant difference between the results for the two models. However, as for Background 1, the results for the complex wireframe indicate the presence of a strong glint, in this case on the port side near the bow, while those for the simple wireframe do not (see Figure C15 and Figure C24, for example). In addition, when the models include both specified thermal

boundary conditions and an exhaust plume (Figure C7 and Figure C8), in the visible band the results for the simple wireframe are marginally larger than those for the complex wireframe on the port broadside of the platform.

In the long-wave IR band, for the instances where there are no specified thermal boundary conditions or plume, for Background 2 (e.g. Figure C21) there is no significant difference between the results for the two wireframes. For Background 3 (e.g. Figure C23), the results for the simple wireframe are marginally larger than those for the complex wireframe on the port broadside of the platform. For Background 1 (e.g. Figure C17), the results for the simple wireframe are marginally larger for most viewing angles. When the two models include specified thermal boundary conditions, for Background 2 (e.g. Figure C14) the results for the simple wireframe are smaller than those for the complex wireframe for the majority of viewing angles. For Background 3 (e.g. Figure C16), the results for the simple wireframe are marginally larger on the port broadside but marginally smaller on the starboard side. For Background 1 (e.g. Figure C10), the results for the simple wireframe are smaller than those for the complex wireframe in the region of the bow. In addition, when the models include an exhaust plume, for a viewing distance of 2 km (Figure C1) the results for the simple wireframe are also marginally smaller on the port side near the stern of the platform.

In the mid-wave IR band, for the cases where there are no specified thermal boundary conditions or plume, for Background 2 (Figure C21 and Figure C22) there is no significant difference between the results for the two wireframes. For Background 1 (Figure C17 to Figure C20), the results for the two models are nearly the same. However, those for the complex wireframe indicate the presence of a strong glint on the starboard broadside of the platform, towards the stern, but those for the simple wireframe do not. As well, the results for the simple wireframe are marginally larger than those for the complex wireframe at the stern of the platform. For Background 3 (Figure C23 and Figure C24), there is no significant difference between the results for the two wireframes on the starboard side of the platform. On the port side of the platform, the results for the simple wireframe are marginally larger than those for the complex wireframe for the majority of viewing angles but those for the complex wireframe indicate the presence of a strong glint near the bow, while those for the simple wireframe do not. For the cases where there are specified thermal boundary conditions, in every instance the results for the two models take a similar form but those for the simple wireframe are much smaller than those for the complex wireframe for nearly all viewing angles (see, for example, Figure C1, Figure C2 and Figure C5 to Figure C8). The results for the complex wireframe also indicate the presence of a strong glint on the starboard broadside of the platform towards the stern for Background 1 and on the port side of the platform near the bow for Background 3, while those for the simple wireframe do not (see Figure C9 and Figure C15 for example).

4.2.2 Simple wireframe versus complex wireframe – near-infrared reflecting (NIRR) paints

The simple and the complex wireframes were both processed using RAVFAC with a maximum desired element length of 1.0 m and assigned NIRR paints. Comparative plots of the OF contrast signature data generated for the two models are presented in Appendix D.

The plots show that, in the visible band and the near-visible IR band, the results for the two models are very similar, regardless of the choice of thermal background, platform settings or viewing distance, but they do differ. The results for the complex wireframe indicate the presence of a strong glint on the starboard broadside of the platform towards the stern for Background 1 and on the port side near the bow for Background 3, while those for the simple wireframe do not (see Figure D7 and Figure D11, for example). For Background 1, in addition, the results for the complex wireframe show more variation on the port broadside of the platform than do those for the simple wireframe (for example, see Figure D8) and, in the visible band, the results for the simple wireframe are marginally larger than those for the complex wireframe on the port side (for example, see Figure D1). For Background 3, in the visible band, when the models include both specified thermal boundary conditions and an exhaust plume (e.g. Figure D5) the results for the simple wireframe are marginally larger than those for the complex wireframe on the port broadside of the platform. In the near-visible IR band, the results for the simple wireframe are marginally larger on the port broadside for all platform settings (see Figure D11 and Figure D17 for example).

In the long-wave IR band, for the cases where there are no specified thermal boundary conditions or plume, for Background 2 (e.g. Figure D16) the results for the two wireframes are for practical purposes identical. For Background 3 (e.g. Figure D18), the results for the simple wireframe are marginally larger than those for the complex wireframe on the port broadside of the platform. For Background 1 (e.g. Figure D13), the results for the simple wireframe are marginally larger for approximately half the viewing angles. When the two models include specified thermal boundary conditions, for Background 1 (e.g. Figure D1) and Background 2 (e.g. Figure D3) the results for the simple wireframe are smaller than those for the complex wireframe for the majority of viewing angles. For Background 3 (e.g. Figure D5), the results for the simple wireframe are marginally smaller than those for the complex wireframe on the starboard side of the platform but marginally larger on the port broadside.

In the mid-wave IR band, for the cases where there are no specified thermal boundary conditions or plume, for Background 2 (e.g. Figure D15) there is no significant difference between the results for the two wireframes. For Background 1 (e.g. Figure D13), the results for the two models are nearly the same. However, those for the complex wireframe indicate the presence of a strong glint on the starboard broadside of the platform towards the stern but those for the simple wireframe do not. For Background 3 (e.g. Figure D17), the results for the simple wireframe are marginally larger on the port broadside of the platform. However, those for the complex wireframe indicate the presence of a strong glint on the port side of the platform near the bow, while those for the simple wireframe do not. For the cases where there are specified thermal boundary conditions, in every instance the results for the two models take a similar form but those for the simple wireframe are much smaller than those for the complex wireframe for nearly all viewing angles (see Figure D1 to Figure D12). The results for the complex wireframe also indicate the presence of a strong glint on the starboard broadside of the platform towards the stern for Background 1 and on the port side of the platform near the bow for Background 3, while those for the simple wireframe do not (see Figure D2 and Figure D5, for example).

5. Discussion

5.1 Model sub-processing

In the visible band and the near-visible IR band, the contrast signature is dominated by solar reflections — the emissions from heated plates and exhaust plumes have little effect. In these bands, neither the method used for subdividing the facets (RAVFAC or GEST) nor the choice of subdivision is relevant, regardless of the thermal background selected or whether or not user-defined thermal boundary conditions or an exhaust plume are included in the model. The contrast signatures predicted for all the subdivisions are for practical purposes identical in every case.

In the long-wave IR band, the contrast signature is dominated by the emissions from ambient and near-ambient temperature plates. In this band, the method used for subdividing the facets can have an appreciable effect on the predicted contrast signature, but only in limited circumstances, and the choice of subdivision has little or no effect.

For the simple wireframe, when the model includes neither thermal boundary conditions nor an exhaust plume, for the warm, sunlit environments (Backgrounds 1 and 3) the GEST subdivision produces a marginally smaller contrast signature than the RAVFAC subdivisions when looking toward the solar-heated section of the platform[2]. When the model includes user-defined thermal boundary conditions, with or without a plume, for the cold, dark environment (Background 2) the GEST subdivision produces a markedly larger contrast signature than the RAVFAC subdivisions. For the warm, sunlit environments, when looking towards the starboard broadside, which is both the solar-shaded region of the platform[2] and where the hot uptake is located, the GEST subdivision produces a marginally larger contrast signature. In all other instances, there is no significant difference between the contrast signature produced by the GEST subdivision and those produced by the RAVFAC subdivisions. This indicates that, in the long-wave IR band, using the GEST method of subdivision results in the prediction of higher emissions from internally-heated plates and lower emissions from solar-heated plates than using the RAVFAC method. Thus the choice of method has an effect under most conditions. However the effect is noticeable only when the contrast signature is either dominated by the emissions from sources within the platform or generated solely by emissions from strongly solar-heated plates. In all other instances it can be neglected.

For the complex wireframe, for the warm, sunlit environments the default RAVFAC subdivision of NB = NG = 1 produces a marginally smaller contrast signature than the other RAVFAC subdivisions when looking toward the solar-heated section of the platform. In all other instances for the complex wireframe and in all instances for the simple wireframe, there is no significant difference between the contrast signatures produced by the different

[2] In Background 1, the sun is located at 154° off the port bow so that the starboard forward quadrant of the platform is heavily shaded from the sun, the starboard aft quadrant is partly shaded and the port broadside is solar-heated, especially towards the stern. In Background 3, the sun is located at 33° off the port bow so that the starboard aft quadrant of the platform is heavily shaded, the starboard forward quadrant is partly shaded and the port broadside is solar-heated.

RAVFAC subdivisions. This shows that, while subdivision size does have an effect in the long-wave IR band, the effect is slight and limited to a very small number of cases. Most importantly, reducing the size of the RAVFAC subdivision below 1.0 m produces no appreciable difference in the calculated contrast signature.

In the mid-wave IR band, the contrast signature is dominated by the emissions from exhaust plumes and high temperature plates. In this band both the method used for subdividing the facets and the choice of subdivision have a noticeable effect.

For the simple wireframe, when the model includes neither thermal boundary conditions nor an exhaust plume, for the warm, sunlit environments the GEST subdivision produces a marginally smaller contrast signature than the RAVFAC subdivisions when looking toward the solar-heated section of the platform. When the model includes user-defined thermal boundary conditions, for the warm, sunlit environments the GEST subdivision produces a slightly different contrast signature to the RAVFAC subdivisions. The size of the difference in the predicted contrast signatures varies with viewing angle and distance and whether or not the model includes an exhaust plume. For the cold, dark background, the GEST subdivision produces a much larger contrast signature than the RAVFAC subdivisions. For viewing angles on the starboard side of the platform, where the hot uptake is located, the difference between the predicted contrast signatures decreases with increasing viewing distance when a plume is present and increases when one is not. These results indicate that, in the mid-wave IR band, the method used for subdividing the facets has an effect under most conditions. However it is particularly important under normal platform operating conditions, when the contrast signature is generated either partly or solely by the emissions from sources internal to the platform, including the exhaust plumes.

When the model includes neither thermal boundary conditions nor an exhaust plume, for the complex wireframe and the warm, sunlit, tropical environment the default RAVFAC subdivision produces a marginally smaller contrast signature than the other RAVFAC subdivisions when looking toward the solar-heated section of the platform. In all other cases for this platform setting, the choice of RAVFAC subdivision has no effect. When the model includes user-defined thermal boundary conditions, the choice of RAVFAC subdivision is more important, with the effect of the choice increasing with the complexity of the associated wireframe and with viewing distance. For the simple wireframe, when the model includes an exhaust plume, for the warm, sunlit, tropical environment (Background 3) and a viewing distance of 10 km the two RAVFAC subdivisions produce noticeably different contrast signatures on the port forward broadside of the platform. When the model does not include an exhaust plume, for all three backgrounds and a viewing distance of 10 km the two RAVFAC subdivisions produce noticeably different contrast signatures along the entire port broadside of the platform. In all other cases for the simple wireframe the choice of RAVFAC subdivision has no effect. For the complex wireframe, for a viewing distance of 2 km the four RAVFAC subdivisions produce very similar contrast signatures for the sunlit, temperate climate, similar contrast signatures for the sunlit, tropical environment and somewhat similar contrast signatures for the cold, dark environment, with there being no significant difference between the contrast signatures produced by the two smallest subdivisions (0.2 and 0.25 m). For a viewing distance of 10 km, for the sunlit, tropical environment there is less variation in the contrast signatures for the different subdivisions than for a viewing distance of 2 km but

for the sunlit, temperate and the cold, dark climate there is more variation, especially on the starboard broadside of the platform. Nonetheless, in general, the 0.2 and 0.25 m subdivisions again produce very similar contrast signatures. These results indicate that, in the mid-wave IR band, the choice of RAVFAC subdivision is important under normal platform operating conditions. Using a different subdivision can give quite different contrast signatures, depending on the modelling parameters. However, in all cases using small subdivisions of similar size produces similar contrast signatures.

Overall, the results indicate that the method used for subdividing the facets and the choice of subdivision size are only significant for OF bands where emissions from internal sources, such as exhaust plumes and hot uptakes, affect the contrast signature. The impact of the choices increases with the relative contributions of these internal emissions to the signature and with the complexity of the wireframe structures associated with the sources. The results are not sufficiently extensive to indicate whether one of the methods of subdivision is better than the other or what is the most appropriate RAVFAC subdivision size to use. However they do indicate that using RAVFAC subdivisions of a very similar size is necessary to permit a sound comparison between the contrast signatures calculated for different models.

5.2 Wireframe detail

In the visible band and the near-visible IR band, as noted in Section 5.1, the contrast signature is dominated by solar reflections — the emissions from heated plates and exhaust plumes have little effect. Hence in these bands, as would be expected, the effects of wireframe detail are largely independent of the platform settings but do vary with the thermal background and the choice of paints, albeit to a limited extent. The most noticeable consequence of using a more complex wireframe is to increase the likelihood of predicting the presence of strong glints in the contrast signature; the choice of paints affects the relative strengths of any such glints but not whether and where they are predicted. Using a more complex wireframe may also result in an increase in variation in the calculated contrast signature, depending upon the thermal background. Discounting the presence of glints, using a simpler wireframe in general results in a marginally larger predicted contrast signature when looking towards the solar-heated section of the platform[3]. The effect is less pronounced for standard paints than for NIRR paints but only slightly.

In the long-wave IR band, the contrast signature is dominated by the emissions from ambient and near-ambient temperature plates. Therefore the effects of wireframe detail are highly dependent on the platform settings, due to the differences between the stack areas of the two models (see Section 3.1), and somewhat dependent on the thermal background and the choice of paints. When the models include neither thermal boundary conditions nor exhaust plumes, for the cold, dark environment there are no significant effects due to wireframe detail. For the warm, sunlit environments using a simpler wireframe in general results in a marginally larger predicted contrast signature, except when looking towards the heavily-shaded section of the

[3] In Background 1, the sun is located at 154° off the port bow so that the starboard forward quadrant of the platform is heavily shaded from the sun, the starboard aft quadrant is partly shaded and the port broadside is solar-heated, especially towards the stern. In Background 3, the sun is located at 33° off the port bow so that the starboard aft quadrant of the platform is heavily shaded, the starboard forward quadrant is partly shaded and the port broadside is solar-heated.

platform. When the models include thermal boundary conditions, for the cold, dark environment using a more complex wireframe produces a larger predicted contrast signature, except in regions where the view of the internally-heated plates is obscured. For the sunlit, tropical environment using a more complex wireframe produces a marginally larger predicted contrast signature when looking towards the starboard broadside, which is both the solar-shaded region and where the hot uptake is located. However it produces a marginally smaller contrast signature when looking towards the port broadside, which is both the solar-heated region of the platform and the region where the view of the hot uptake is obscured. For the sunlit, temperate environment, where the solar-shaded region of the platform is not aligned with the location of the hot uptake, using a more complex wireframe in general results in a marginally larger predicted contrast signature, except for viewing angles where the internally-heated plates are obscured. The effect is very noticeable for NIRR paints but less marked for standard paints.

In the mid-wave IR band, the contrast signature is dominated by emissions from exhaust plumes and high temperature plates. Therefore, as in the long-wave IR band, the effects of wireframe detail are highly dependent on the platform settings, due to the differences between the stack areas of the two models, but in this band they are less dependent on the thermal background and the choice of paints. In all cases for the warm, sunlit environments, using a more complex wireframe increases the likelihood of predicting the presence of strong glints in the contrast signature; the choice of paints affects the relative strengths of any such glints slightly but not whether and where they are predicted. When the models include neither thermal boundary conditions nor exhaust plumes, for the cold, dark environment using a simpler wireframe has little effect. Discounting the presence of glints, this is also true for the sunlit, temperate environment. For the sunlit, tropical environment, discounting the presence of glints, using a simpler wireframe produces a marginally larger predicted contrast signature when looking towards the solar-heated section of the ship. When the models include thermal boundary conditions, in all cases using a more complex wireframe produces a larger predicted contrast signature, except in regions where the view of the internally-heated plates is obscured. The effect varies with the choice of paints, the viewing distance and the presence or not of the exhaust plume, but is always significant.

Taken as a whole, the results indicate that changing the level of detail in a wireframe has three major effects. As would be expected, changing the details of internally-heated regions, such as the stack and the exhaust uptakes, has a significant impact on the predicted contrast signature in the mid-wave and long-wave IR bands, under normal platform operating conditions. As might also be expected, increasing the complexity of platform structures increases the likelihood of glints occurring in the contrast signature in the visible through to the mid-wave IR bands. Less obviously, using a more complex wireframe decreases the predicted contrast signature in all OF wavebands, for the regions of the platform where the emissions are dominated by those from solar-heated plates.

6. Conclusions

Both model sub-processing (the method used for subdividing facets and the choice of subdivision size) and wireframe detail (the number of facets in a wireframe and how realistically it represents the superstructure) affect the prediction of the OF contrast signature of a platform, albeit to different extents.

Wireframe detail affects the results for all OF bands and its effect is significant in the majority of cases. Increasing wireframe detail increases the probability of detecting glint conditions in the visible, near-visible IR and mid-wave IR bands. Decreasing wireframe detail increases the effects of solar heating in all OF wavebands. Changing wireframe detail in the internally-heated regions of a platform, such as the stack and the exhaust uptakes, has a significant impact on the computed contrast signature in the mid-wave and long-wave IR bands.

In contrast, model sub-processing only affects the results for the mid-wave and long-wave IR bands, where emissions from internal sources contribute to the contrast signature. Its effect increases with the relative contributions of these emissions to the signature and with the complexity of the wireframe structures associated with the sources of the emissions. However, regardless of the details of the wireframe, small subdivisions of similar size, based on the same method of facet subdivision, produce similar results.

Overall, it can be concluded that to be able to validly compare the computed OF signatures of different platforms, the models of the platforms have to incorporate the same level of wireframe detail, especially in internally-heated regions such as their stacks. They also have to be processed using subdivisions of very similar size, based on the same method of facet subdivision.

7. References

1. *User Manual for the Naval Threat/Countermeasures Simulator (NTCS), Version 2.7*. 2000, Davis Engineering Limited: Ottawa, Ontario.
2. Jewsbury, P., *Personal Communication*. 2004: Melbourne.
3. Kneizys, F.X., Shettle, E.P., Abreu, L.W., Chetwynd, J.H., Anderson, G.P., Gallery, W.O., Selby, J.E.A. and Clough, S.A., *Users Guide to LOWTRAN 7*. 1988, Air Force Geophysics Laboratory: Hanscom AFB, Massachusetts 01731-5000. AFGL-TR-88-0177.
4. Berk, A., Anderson, G.P., Acharya, P.K., Chetwynd, J.H., Bernstein, L.S., Shettle, E.P., Matthew, M.W. and Adler-Golden, S.M., *MODTRAN4 User's Manual*. 1999, Air Force Research Laboratory, Space Vehicles Directorate: Hanscom AFB, MA 01731-3010.
5. *MODTRAN 4 Software*. U.S. Air Force Fact Sheet. [cited 21/11/2007]; Available from: http://www.kirtland.af.mil/afrl_vs/ir_clutter/index.asp.
6. *NTCS Procedural Manual, Version 2.3*. 1997, W.R. Davis Engineering Limited: Ottawa, Ontario.
7. Lovin, J.K., Lubkowitz, A.W. and Spradley, L.W., *User's Manual for 'RAVFAC', a Radiation View Factor Digital Computer Program*. 1973, Lockheed Missiles and Space Company, Inc: Huntsville Research Park, 4800 Bradford Drive, Huntsville, Alabama. LMSC/HREC D148620-A.
8. *Heat Transfer: Glossary*. eFunda: engineering Fundamentals. [cited 27/11/2007]; Available from: http://www.efunda.com/formulae/heat_transfer/home/glossary.cfm?ref=view#view.
9. *Technical Manual for SHIPIR/NTCS, Version 2.9*. 2002, W.R. Davis Engineering Limited: Ottawa, Ontario.
10. *User Manual for the Model View Editor (MVE), Version 1.4*. 2005, W.R. Davis Engineering Limited: Ottawa, Ontario.
11. *NTCS Release Notes (v3.0)*. 2002, Davis Engineering Limited: Ottawa, Ontario. p. 12.
12. *NTCS Release Notes (v3.1-x1), Interim Release*. 2003, Davis Engineering Limited: Ottawa, Ontario. p. 19-21.
13. *NTCS Release Notes (v3.1-x3), Interim Release*. 2003, Davis Engineering Limited: Ottawa, Ontario. p. 9.

Appendix A: OF contrast signature data — Simple wireframe model sub-processing

The following plots depict the apparent absolute contrast intensity data calculated for the model with the simple wireframe that was used in the investigation of model sub-processing. The plots are grouped into three sections: those comparing the results generated for the model with user-defined thermal boundary conditions and an exhaust plume; those comparing the results generated for the model with user-defined thermal boundary conditions but no exhaust plume; and those comparing the results generated for the model with no user-defined thermal boundary conditions or exhaust plume. It should be noted that no results are presented for Background 2 and the visible and near-visible IR bands as the platform is not detectable under these conditions. (For details of the backgrounds and the OF wavebands, refer to Section 3.)

A.1. Contrast signature plots for the simple wireframe model with user-defined thermal boundary conditions and an exhaust plume

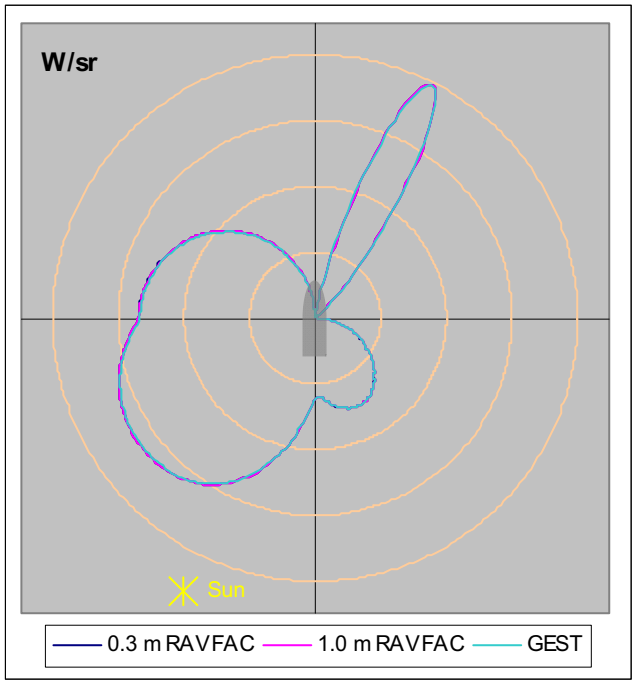

(a) Visible band

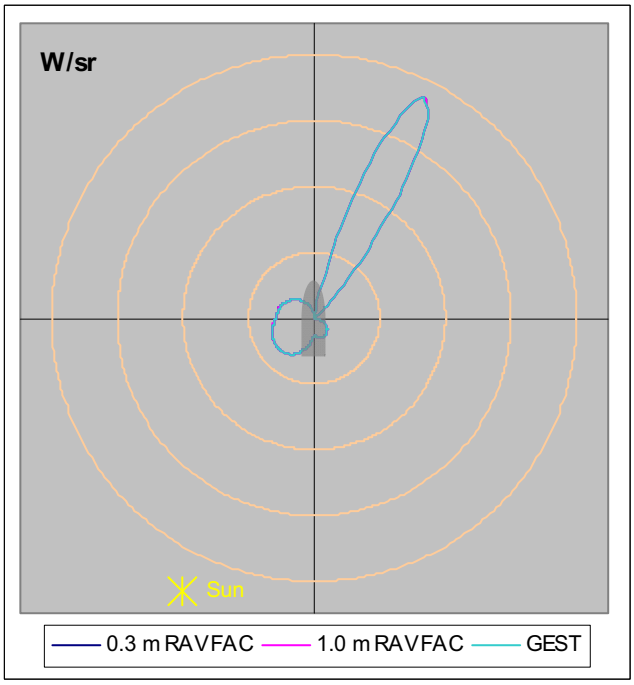

(b) Near-visible IR band

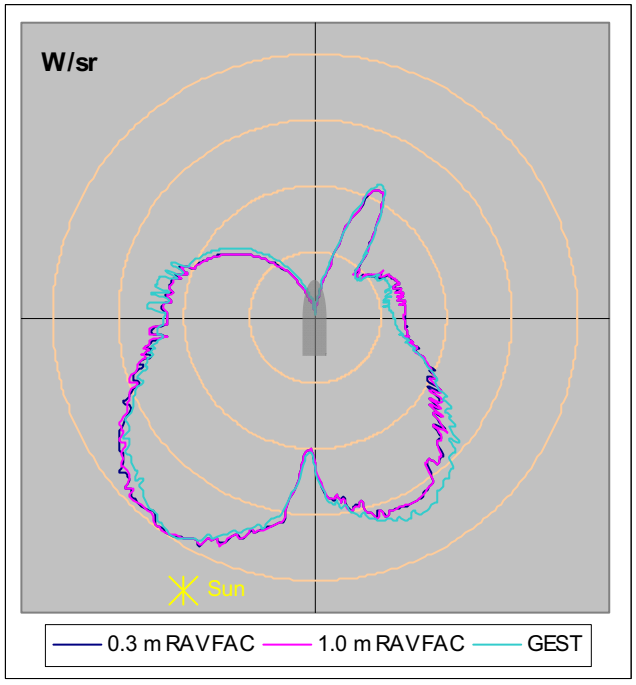

(c) Mid-wave IR band

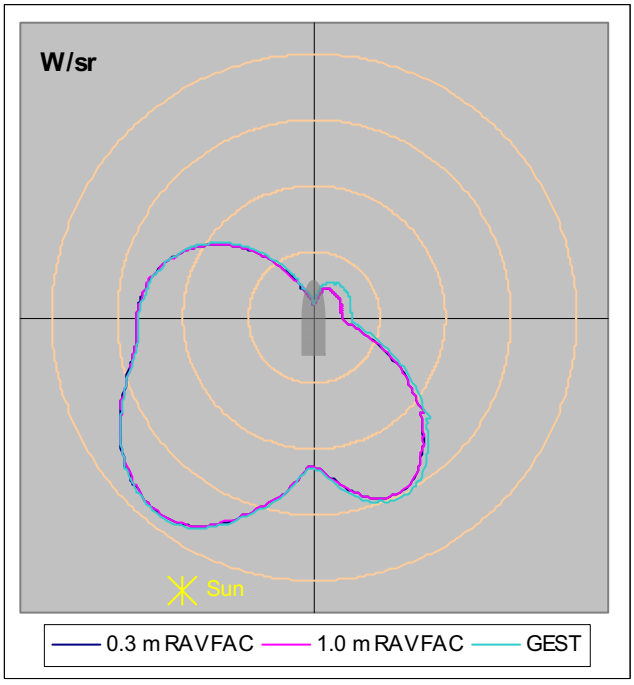

(d) Long-wave IR band

Figure A1 Background 1, 2 km viewing distance

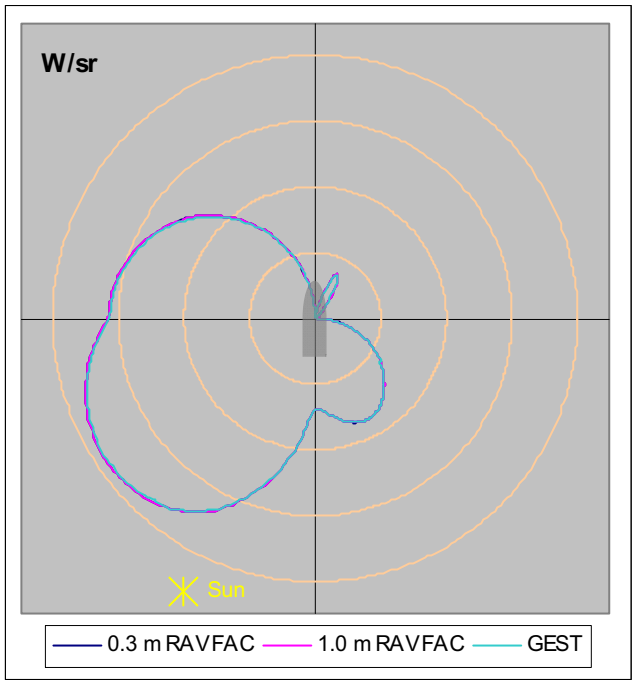

(a) Visible band

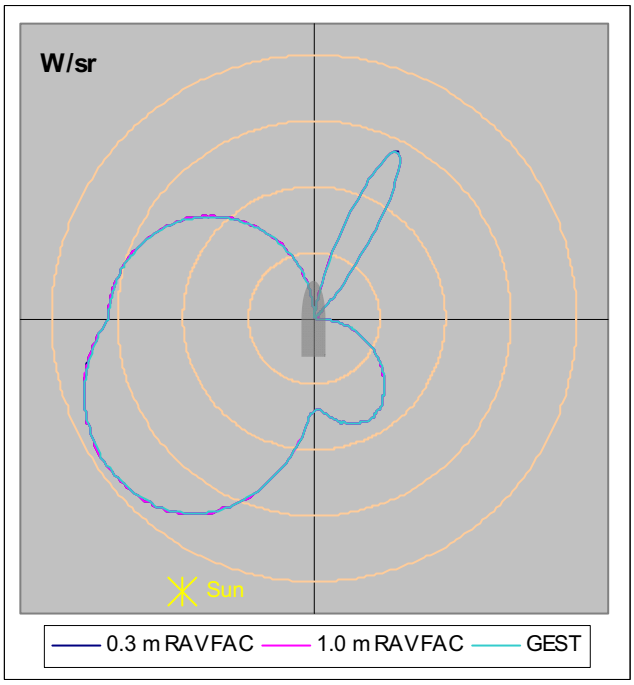

(b) Near-visible IR band

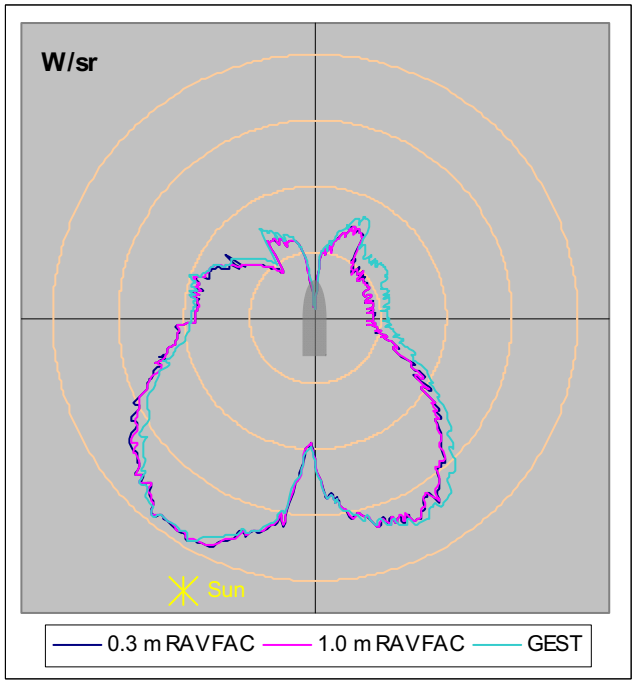

(c) Mid-wave IR band

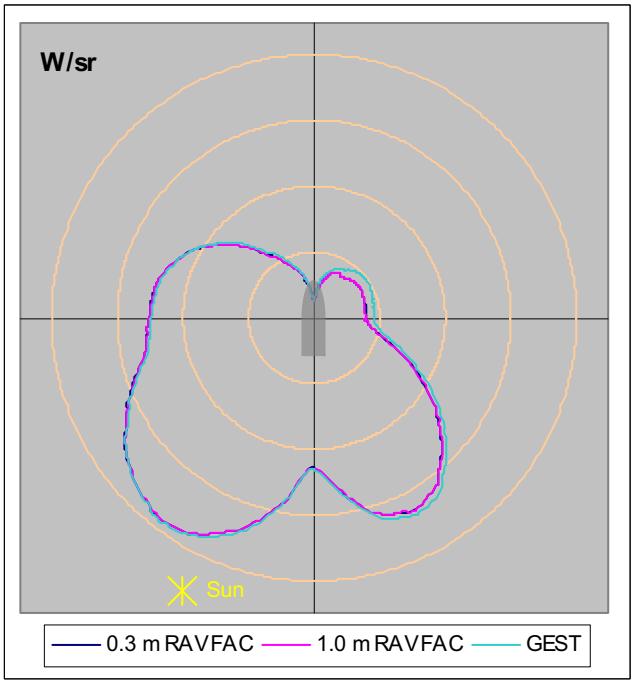

(d) Long-wave IR band

Figure A2 Background 1, 10 km viewing distance

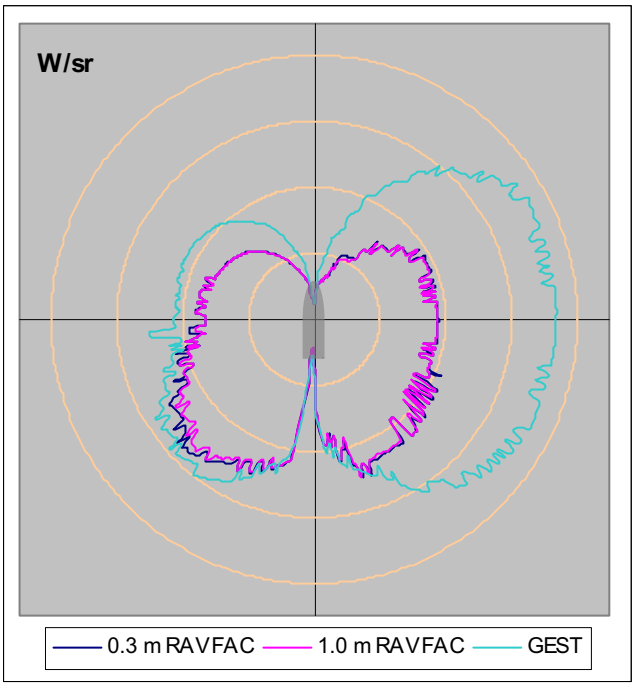

(a) Mid-wave IR band

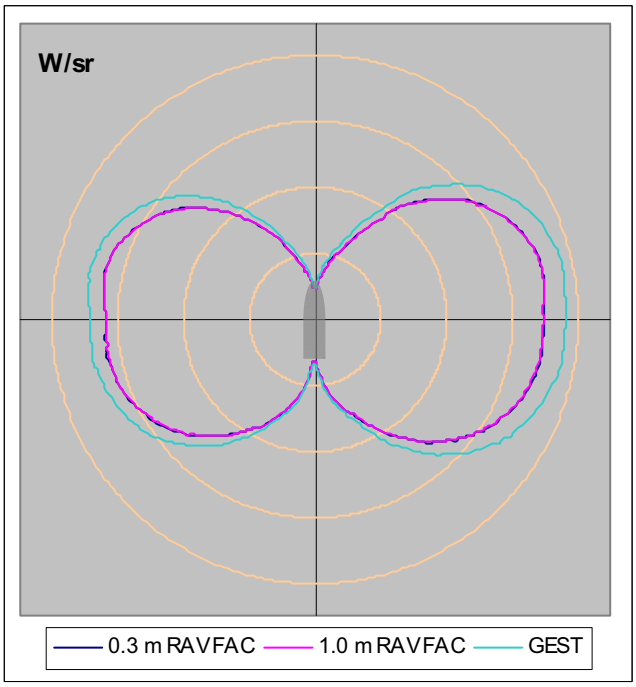

(b) Long-wave IR band

Figure A3 Background 2, 2 km viewing distance

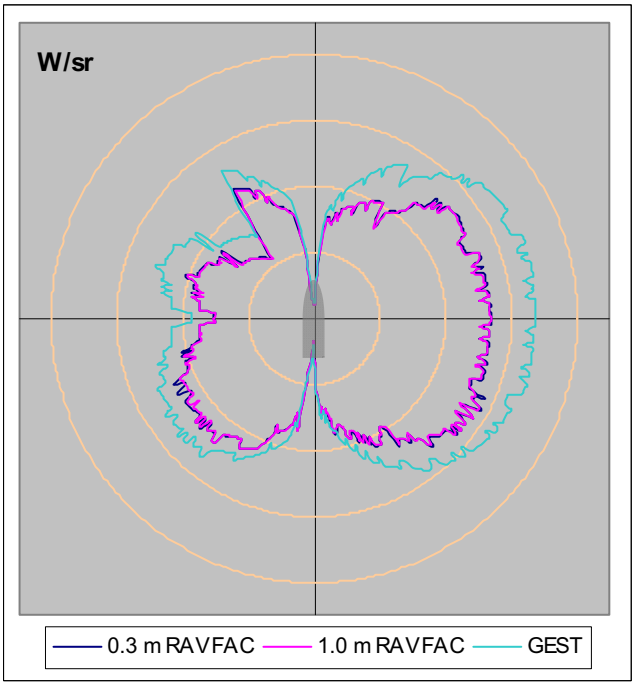

(a) Mid-wave IR band

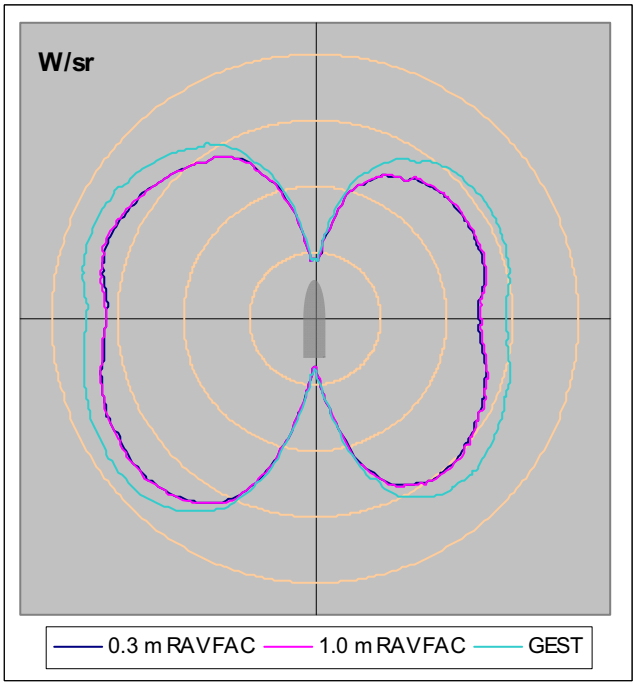

(b) Long-wave IR band

Figure A4 Background 2, 10 km viewing distance

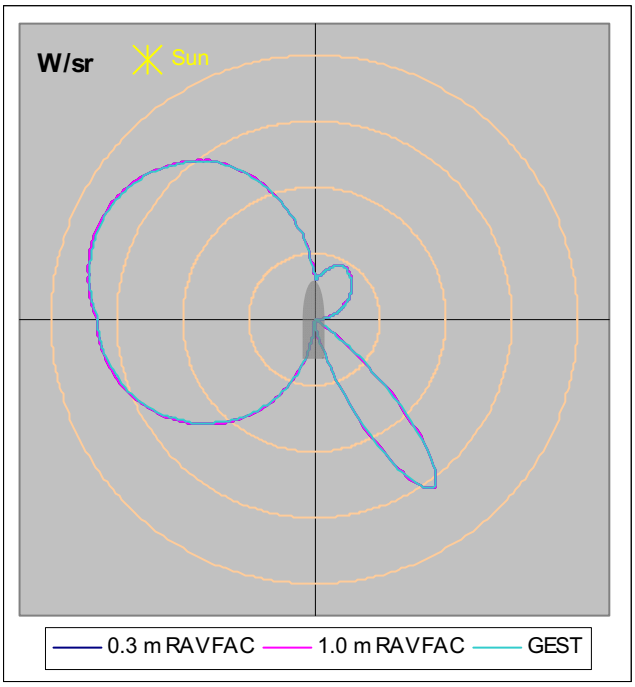

(a) Visible band

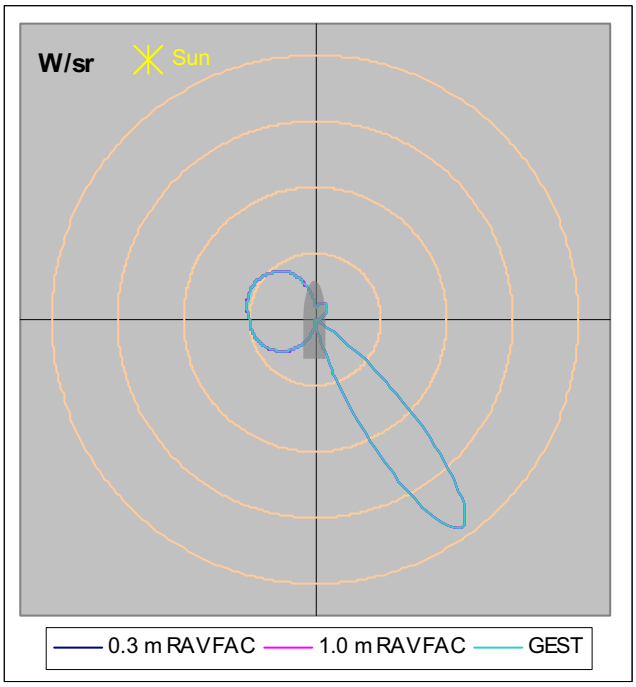

(b) Near-visible IR band

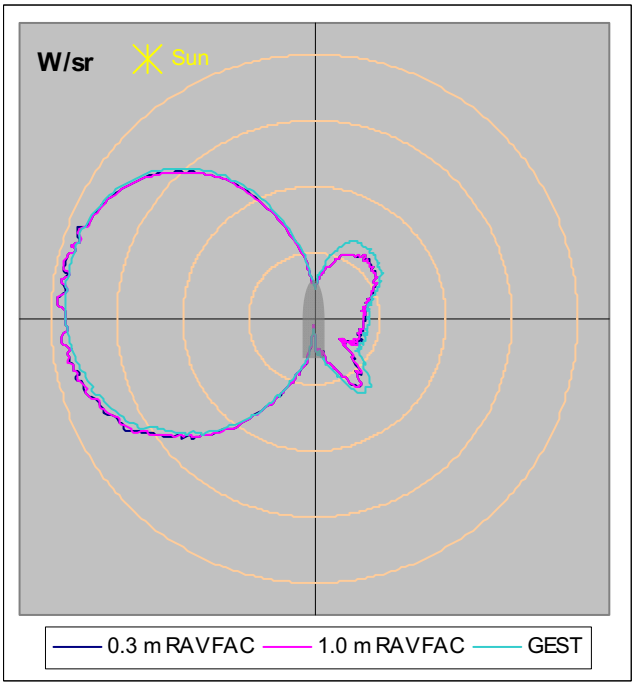

(c) Mid-wave IR band

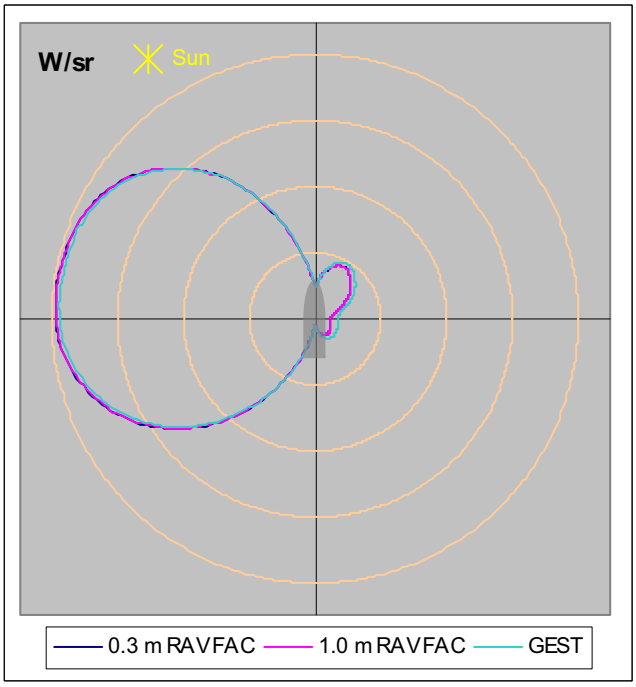

(d) Long-wave IR band

Figure A5 Background 3, 2 km viewing distance

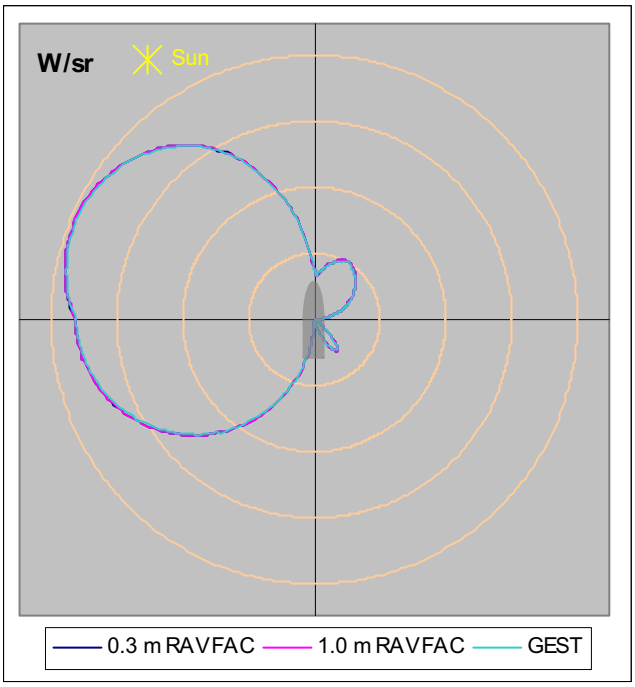

(a) Visible band

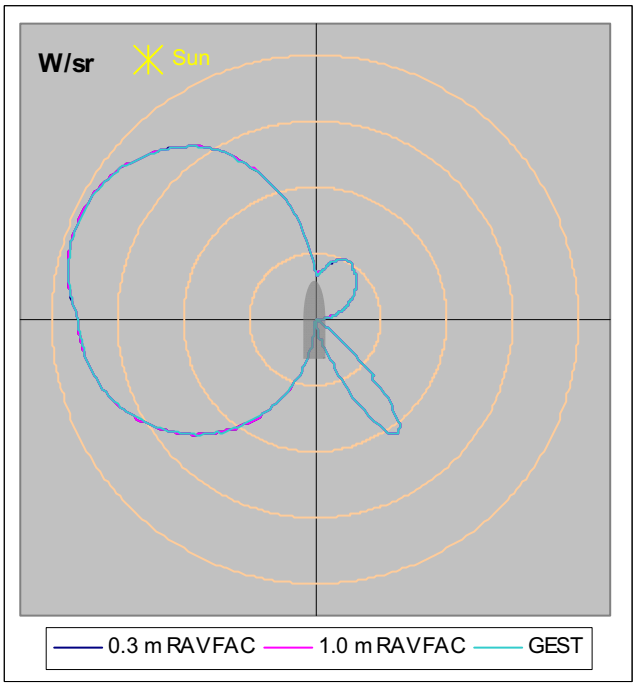

(b) Near-visible IR band

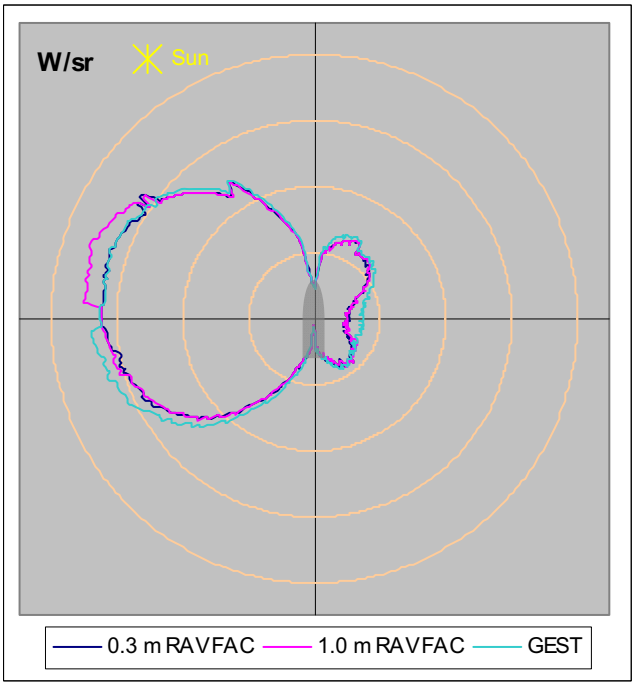

(c) Mid-wave IR band

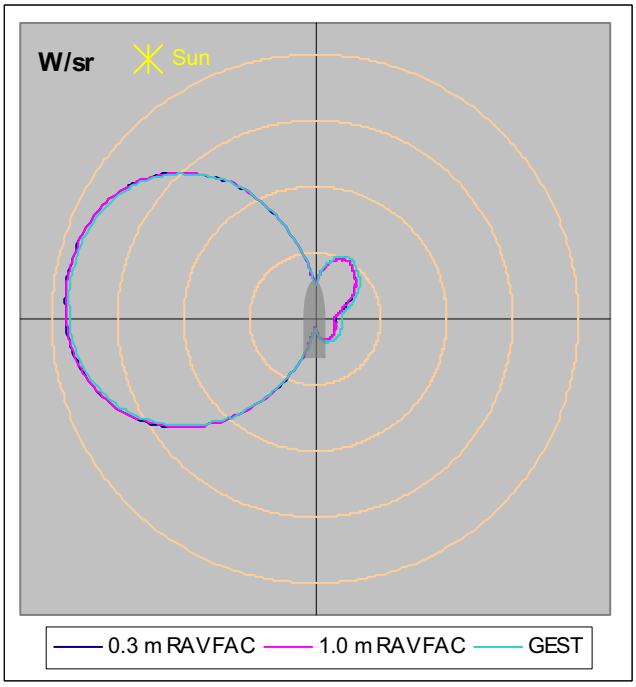

(d) Long-wave IR band

Figure A6 Background 3, 10 km viewing distance

A.2. Contrast signature plots for the simple wireframe model with user-defined thermal boundary conditions but no exhaust plume

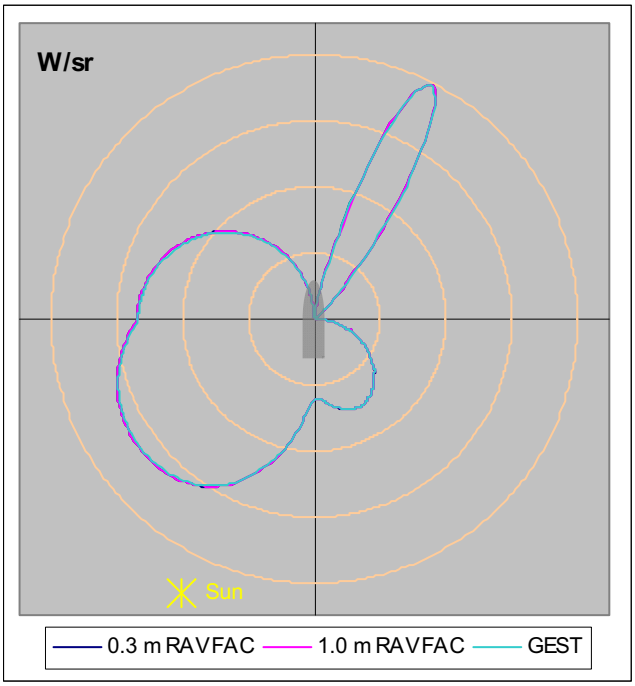

(a) Visible band

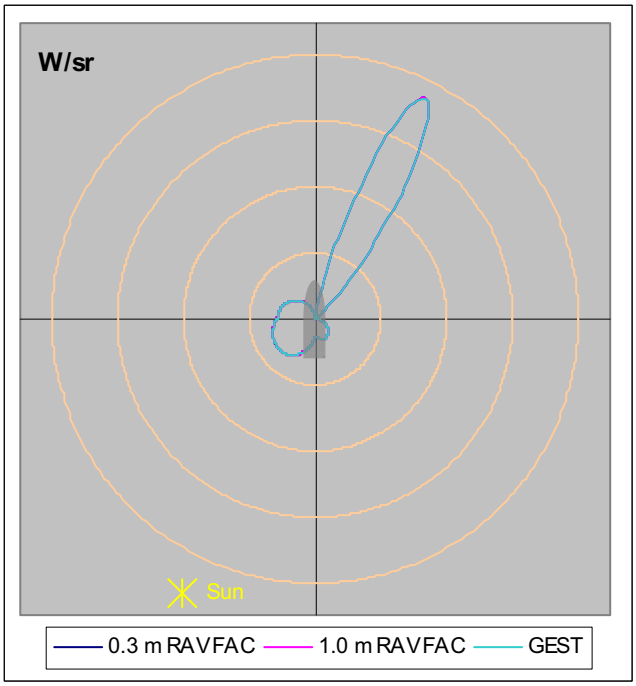

(b) Near-visible IR band

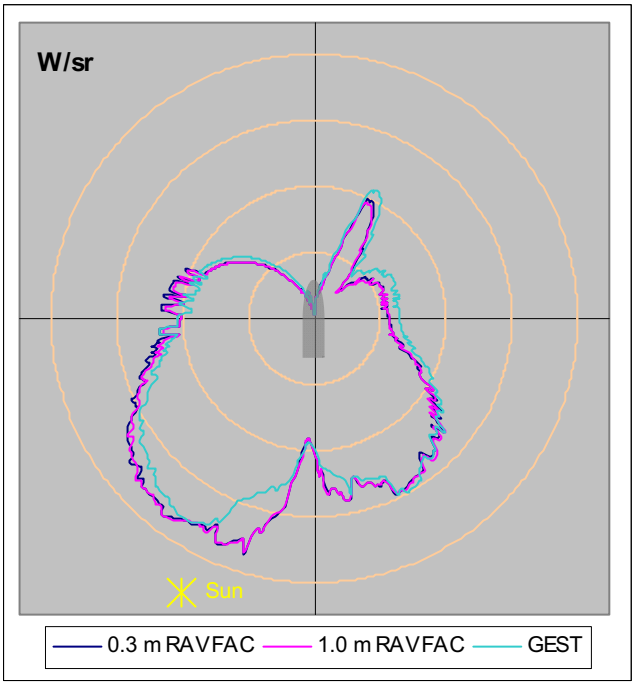

(c) Mid-wave IR band

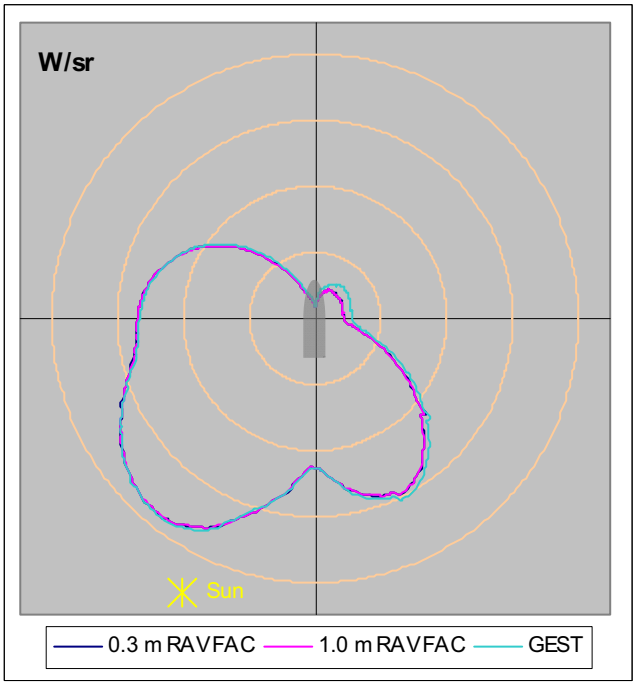

(d) Long-wave IR band

Figure A7 Background 1, 2 km viewing distance

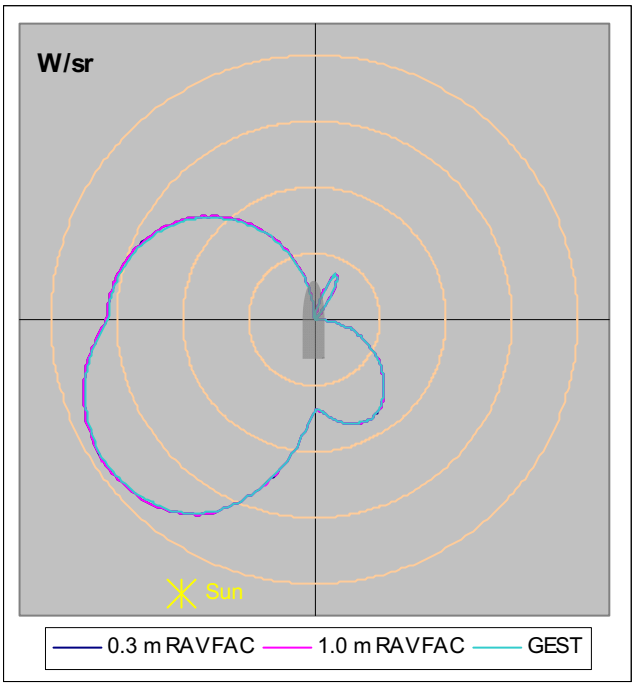

(a) Visible band

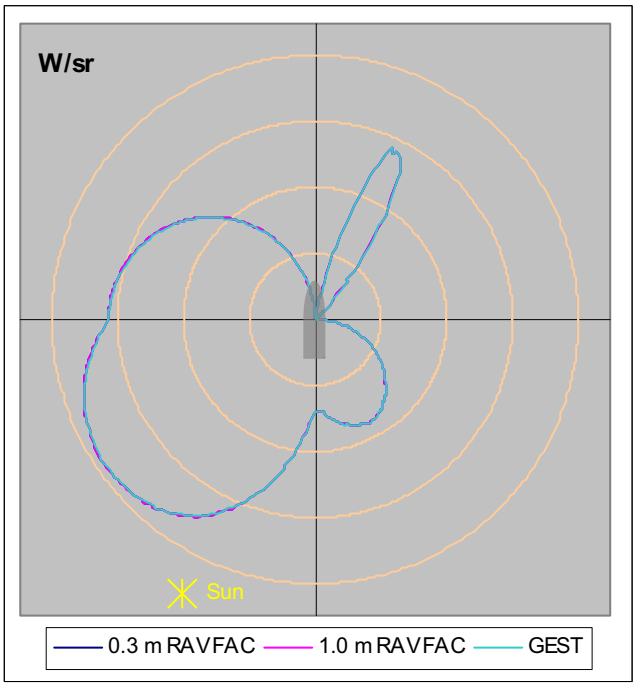

(b) Near-visible IR band

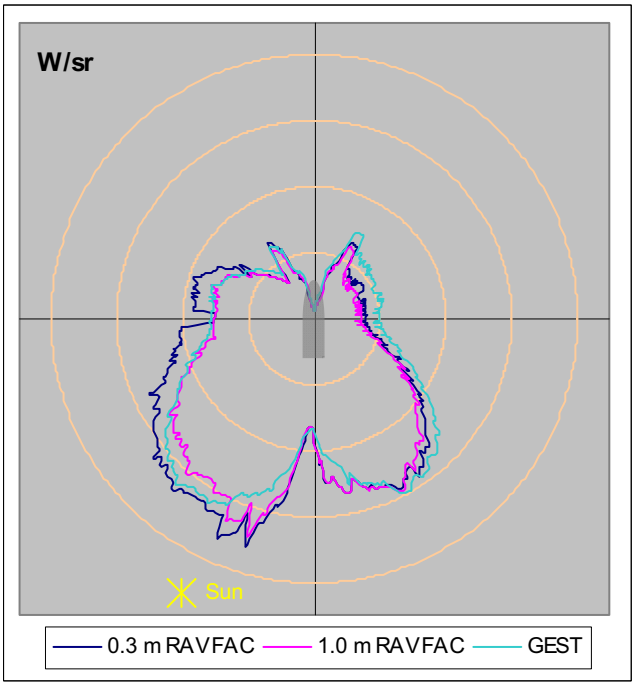

(c) Mid-wave IR band

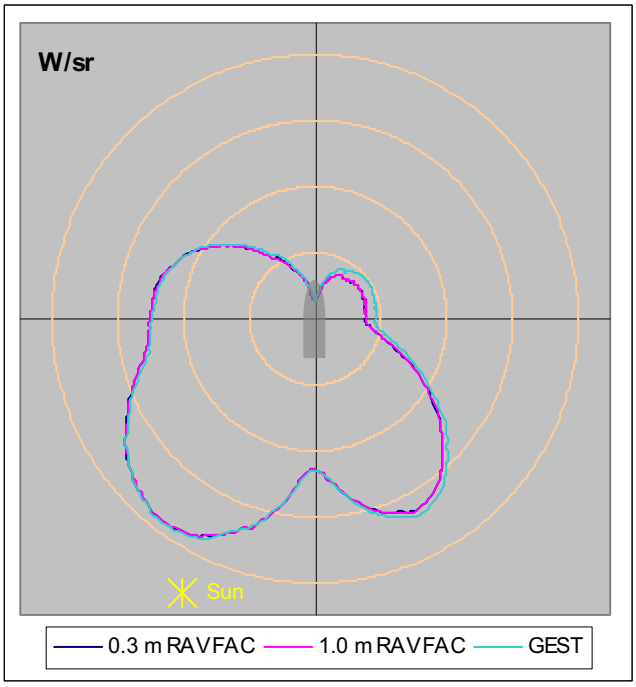

(d) Long-wave IR band

Figure A8 Background 1, 10 km viewing distance

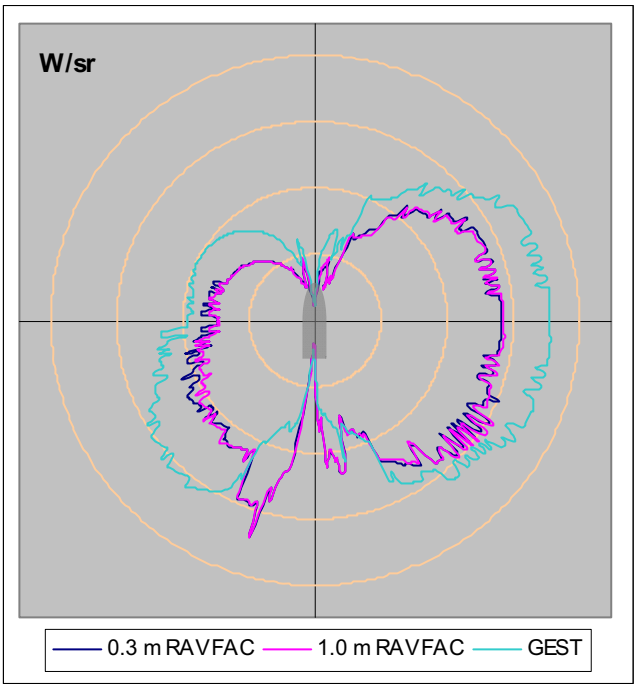

(a) Mid-wave IR band

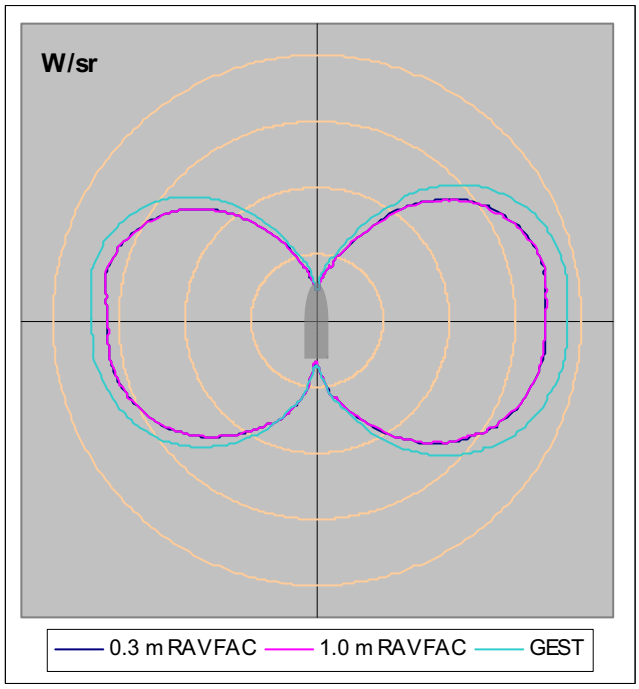

(b) Long-wave IR band

Figure A9 Background 2, 2 km viewing distance

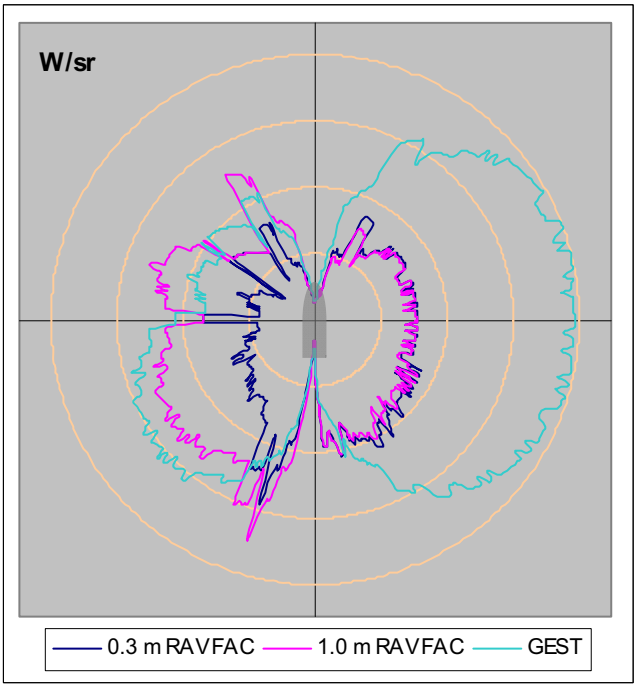

(a) Mid-wave IR band

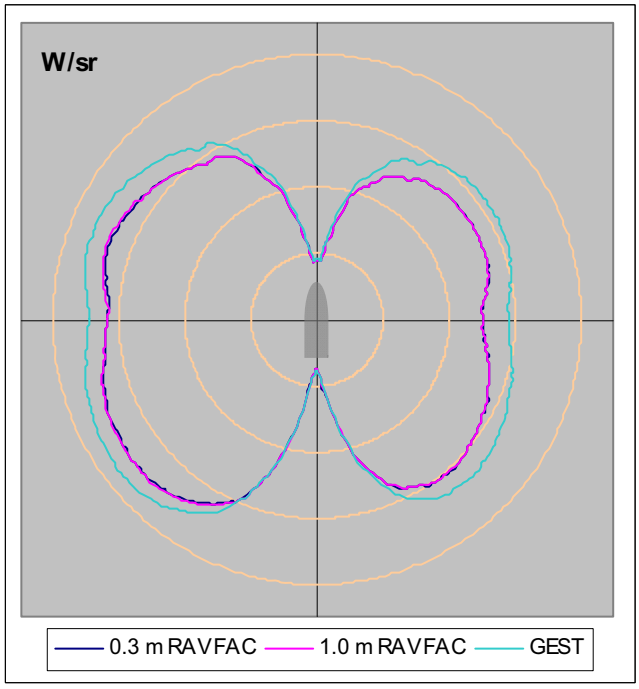

(b) Long-wave IR band

Figure A10 Background 2, 10 km viewing distance

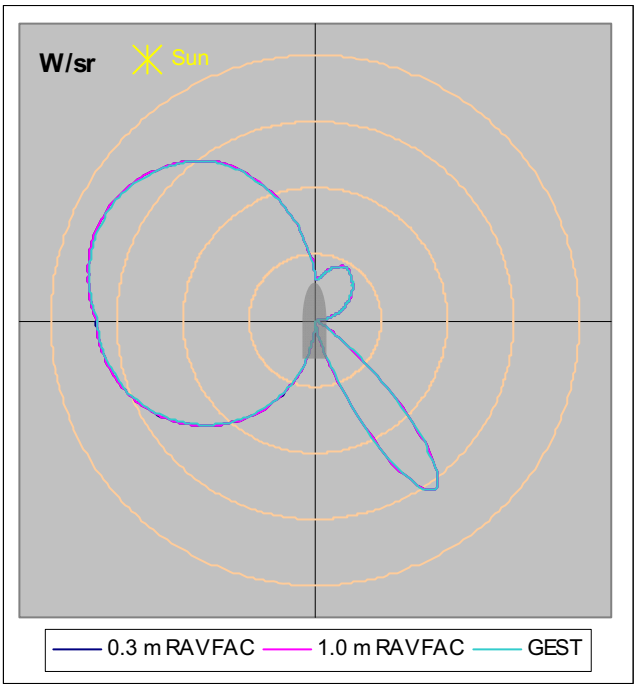

(a) Visible band

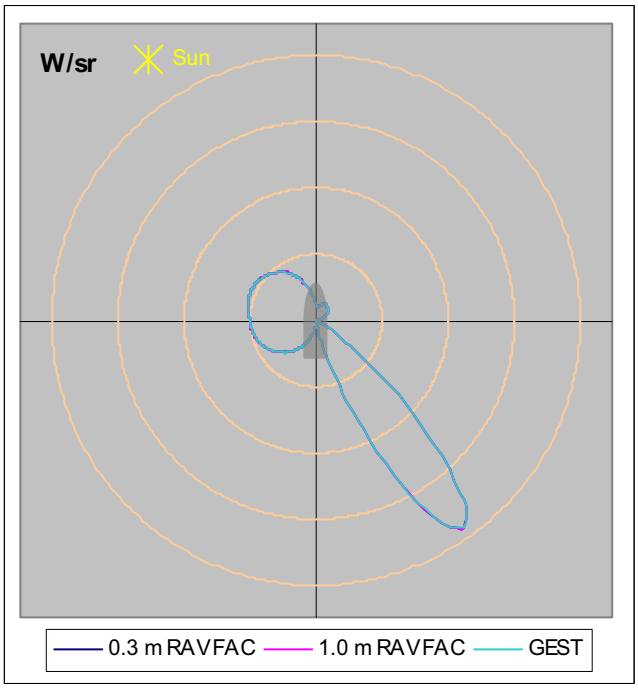

(b) Near-visible IR band

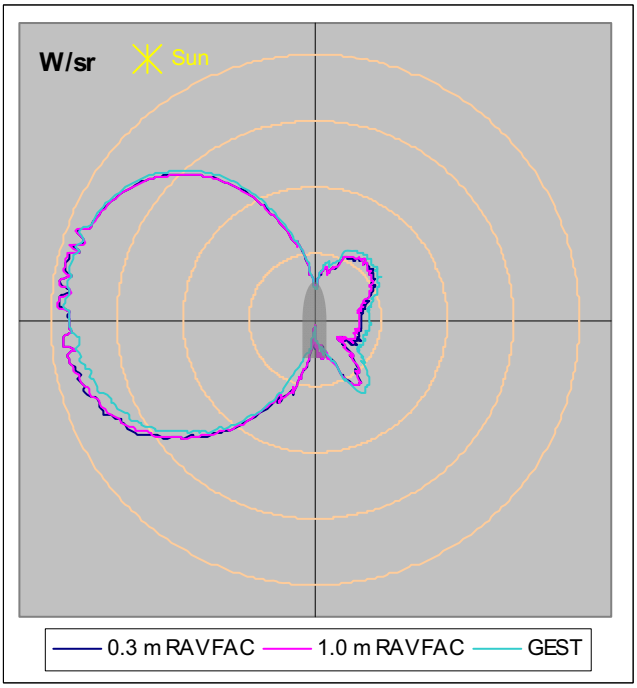

(c) Mid-wave IR band

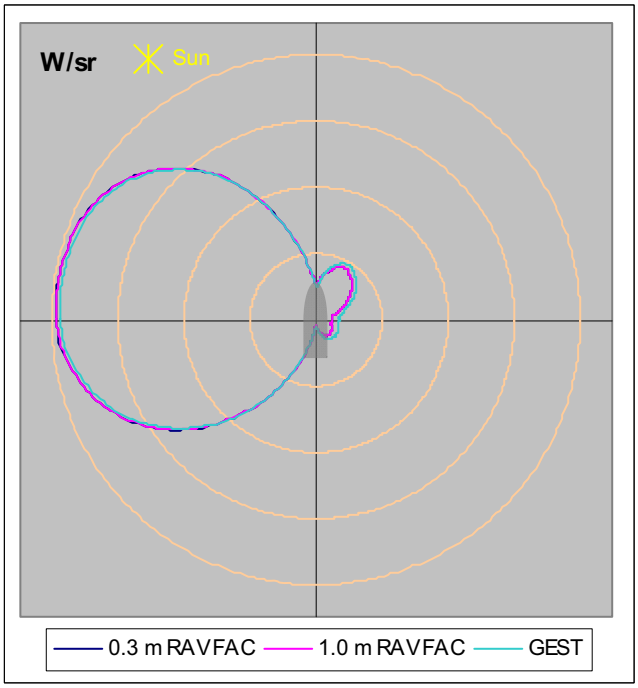

(d) Long-wave IR band

Figure A11 Background 3, 2 km viewing distance

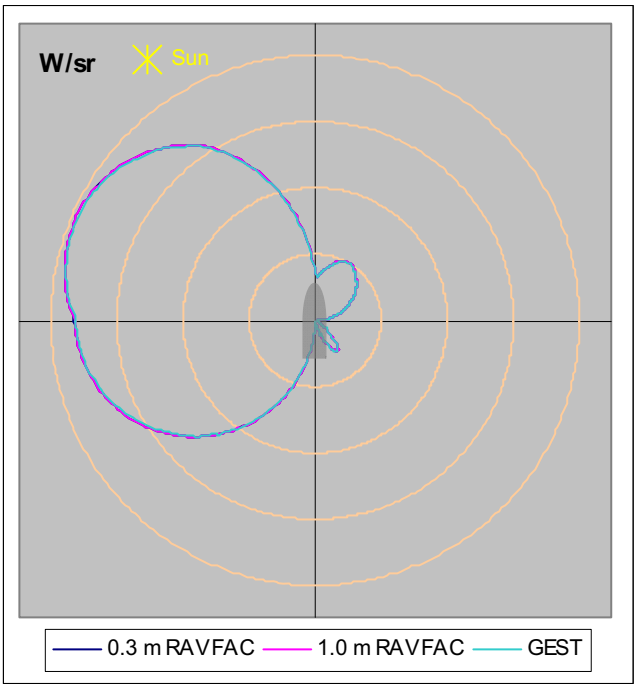

(a) Visible band

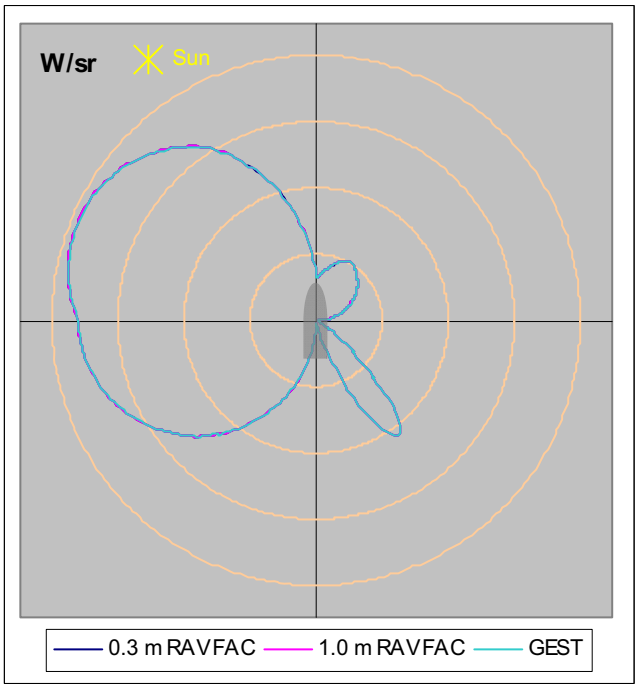

(b) Near-visible IR band

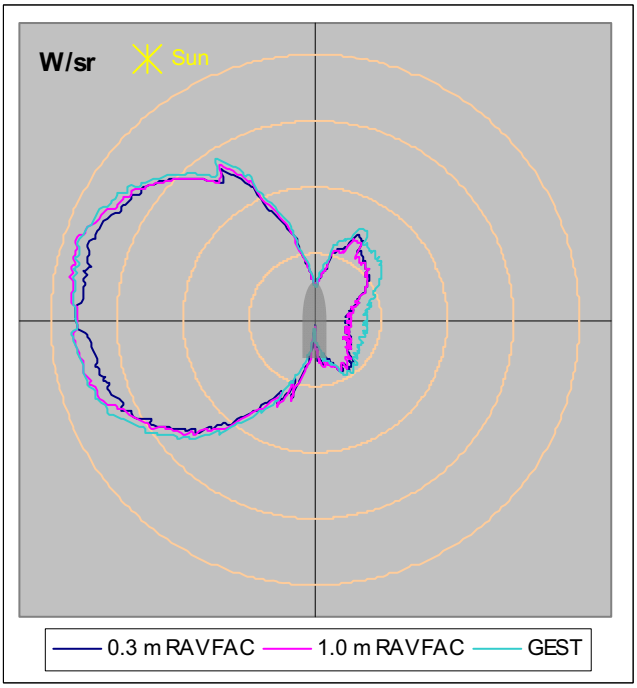

(c) Mid-wave IR band

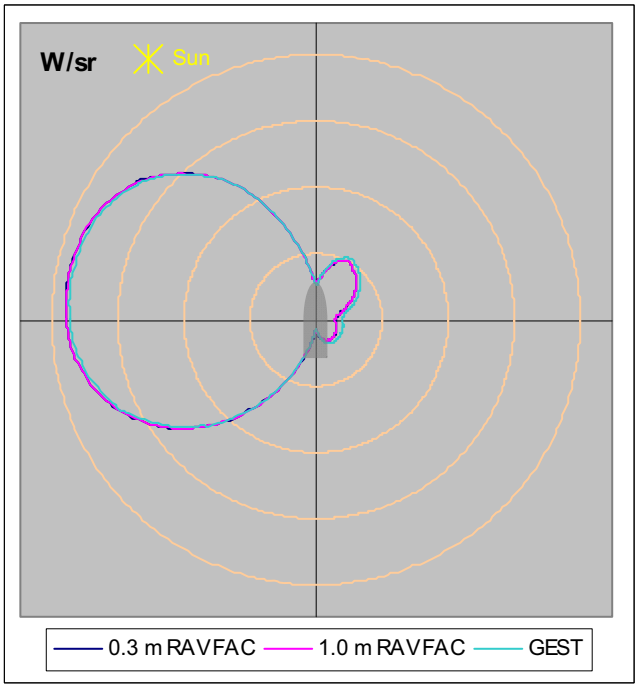

(d) Long-wave IR band

Figure A12 Background 3, 10 km viewing distance

A.3. Contrast signature plots for the simple wireframe model with no user-defined thermal boundary conditions or exhaust plume

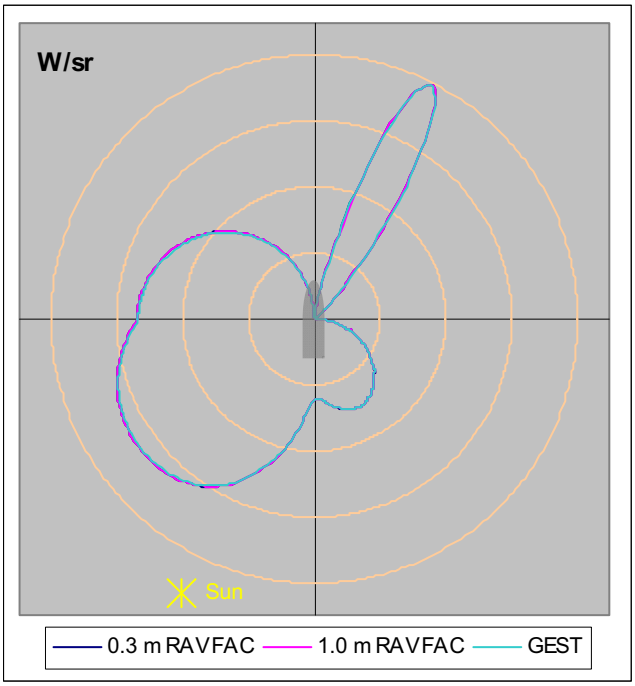

(a) Visible band

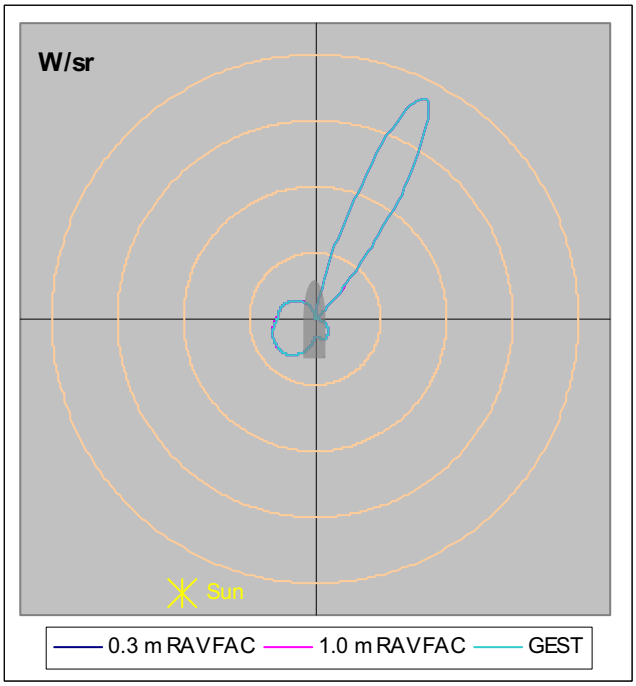

(b) Near-visible IR band

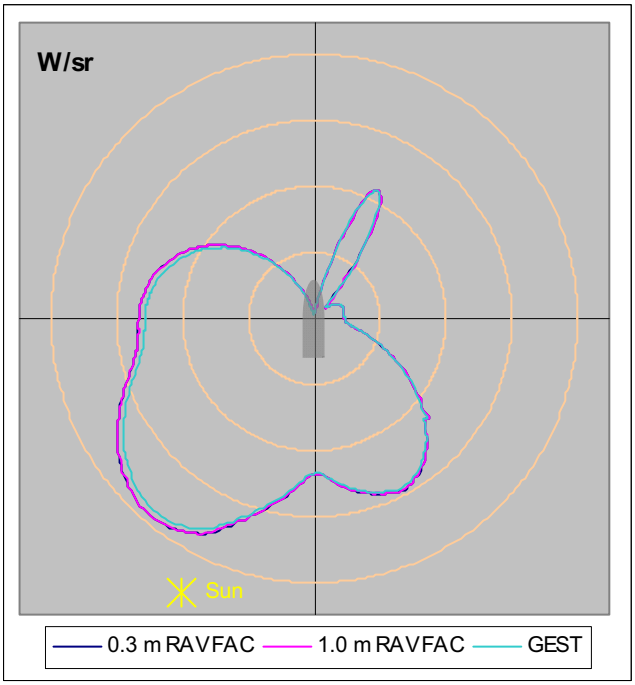

(c) Mid-wave IR band

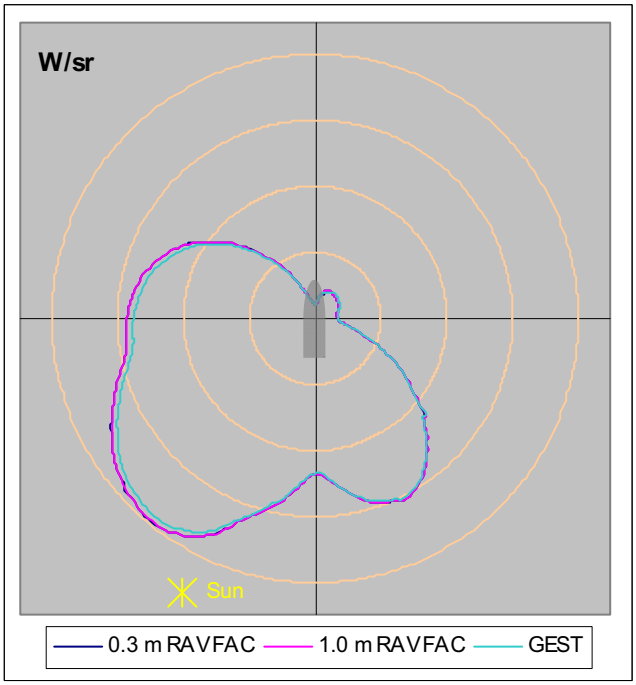

(d) Long-wave IR band

Figure A13 Background 1, 2 km viewing distance

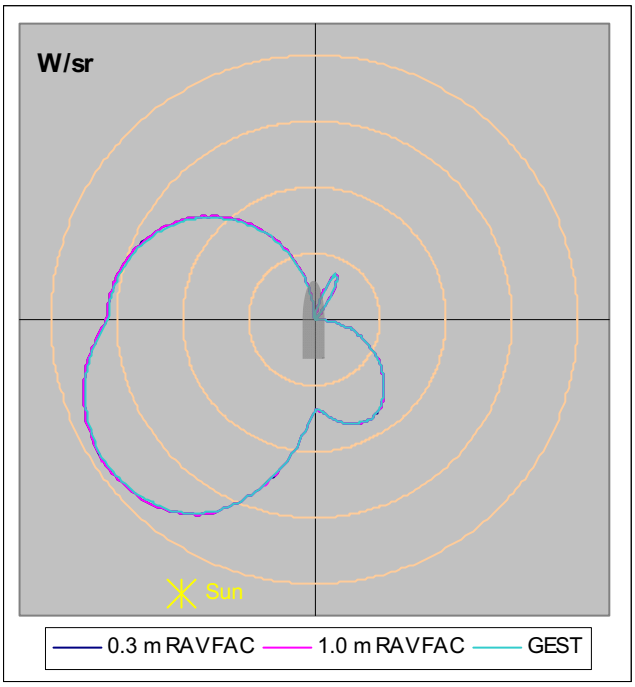

(a) Visible band

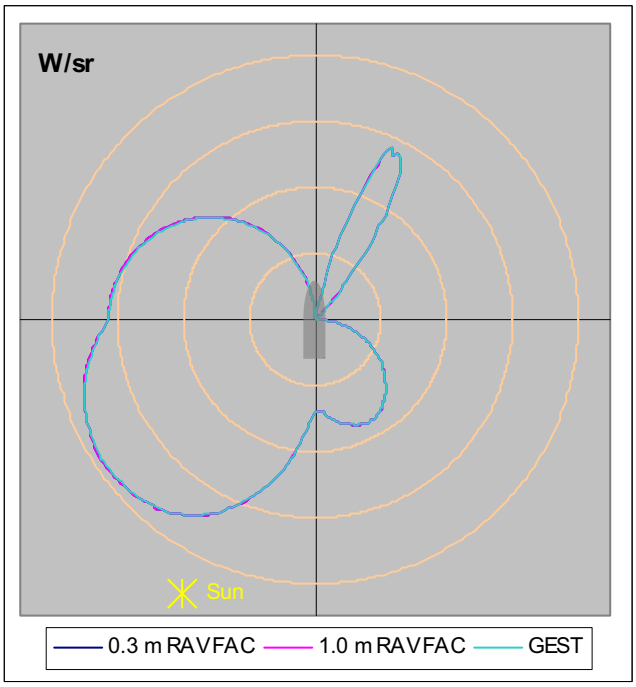

(b) Near-visible IR band

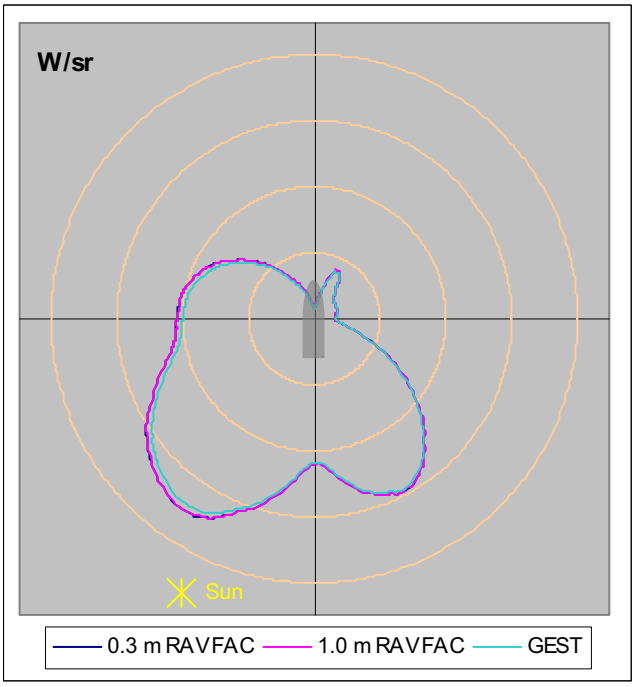

(c) Mid-wave IR band

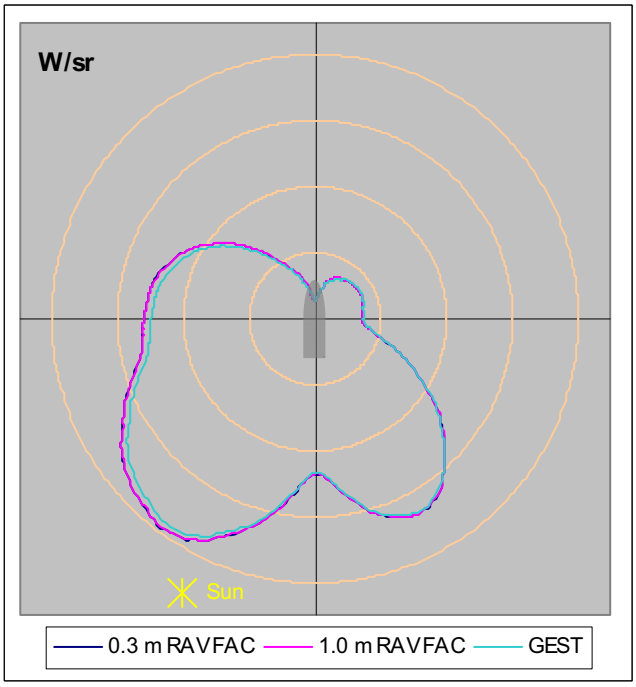

(d) Long-wave IR band

Figure A14 Background 1, 10 km viewing distance

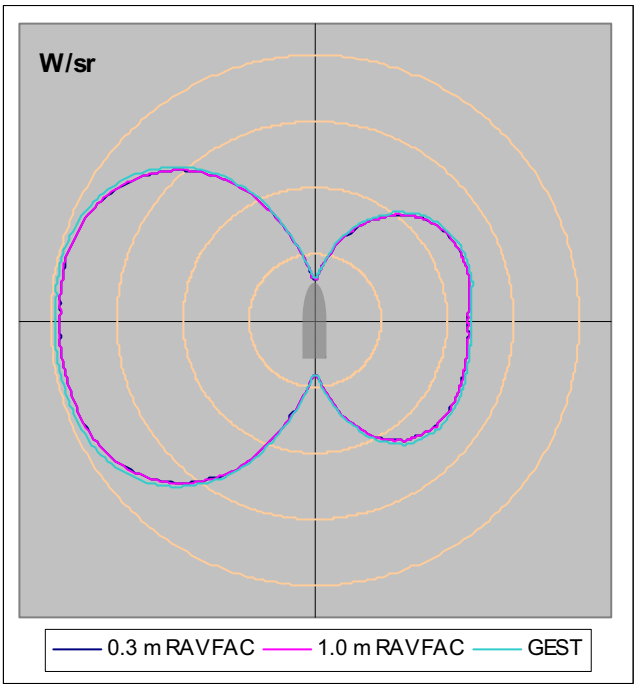

(a) Mid-wave IR band

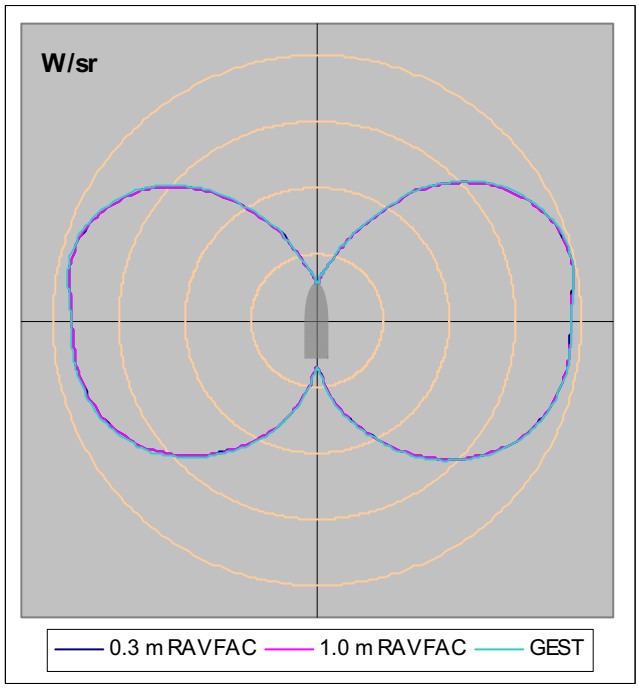

(b) Long-wave IR band

Figure A15 Background 2, 2 km viewing distance

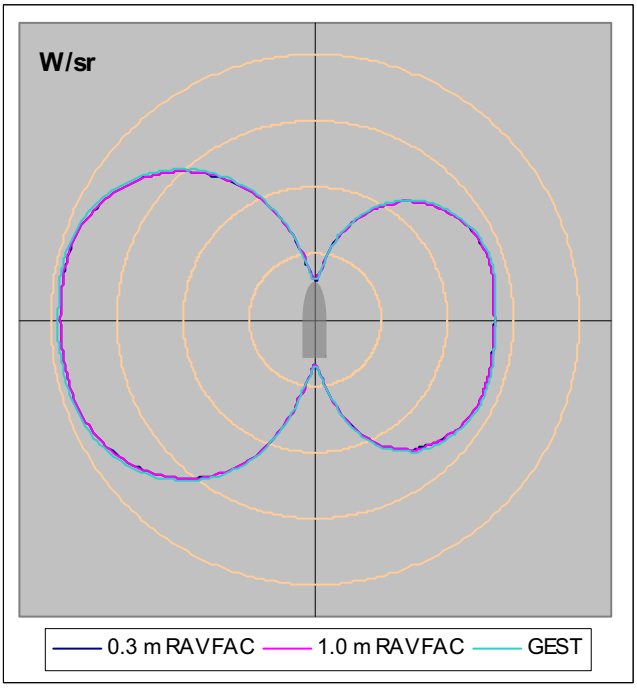

(a) Mid-wave IR band

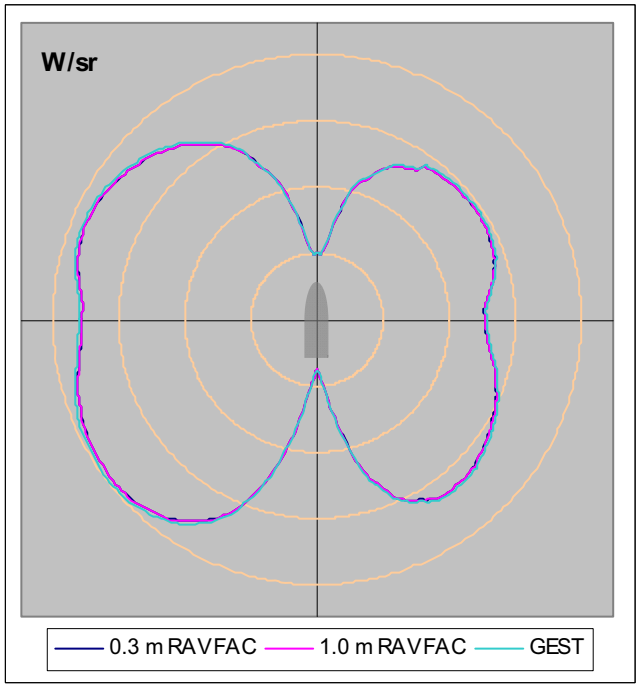

(b) Long-wave IR band

Figure A16 Background 2, 10 km viewing distance

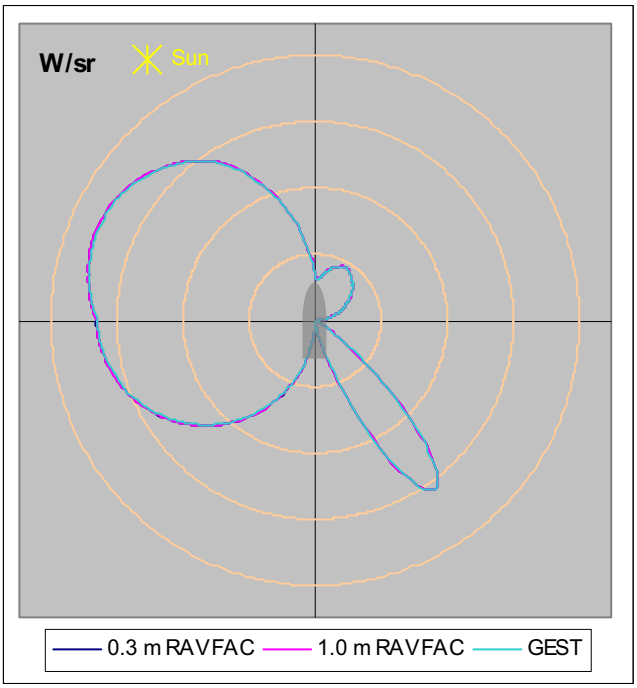

(a) Visible band

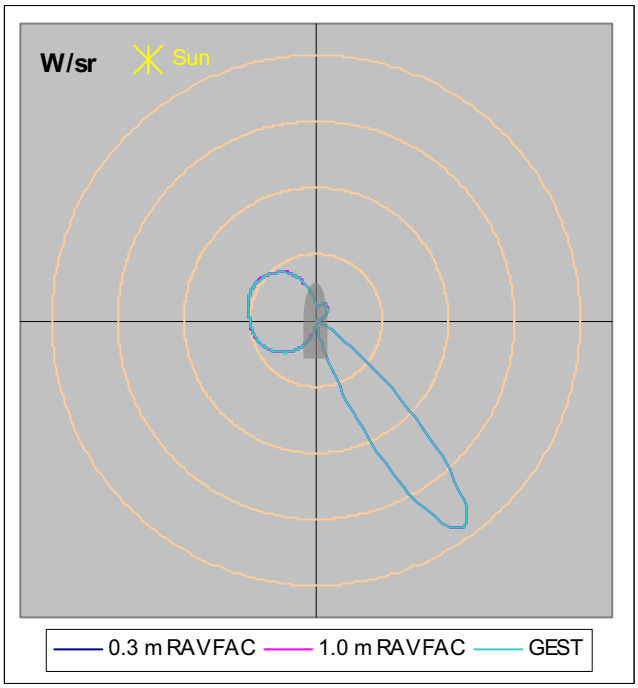

(b) Near-visible IR band

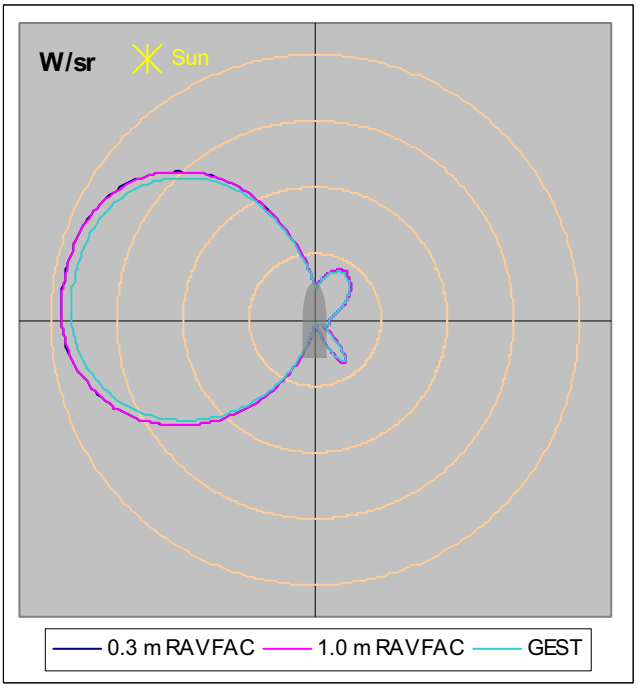

(c) Mid-wave IR band

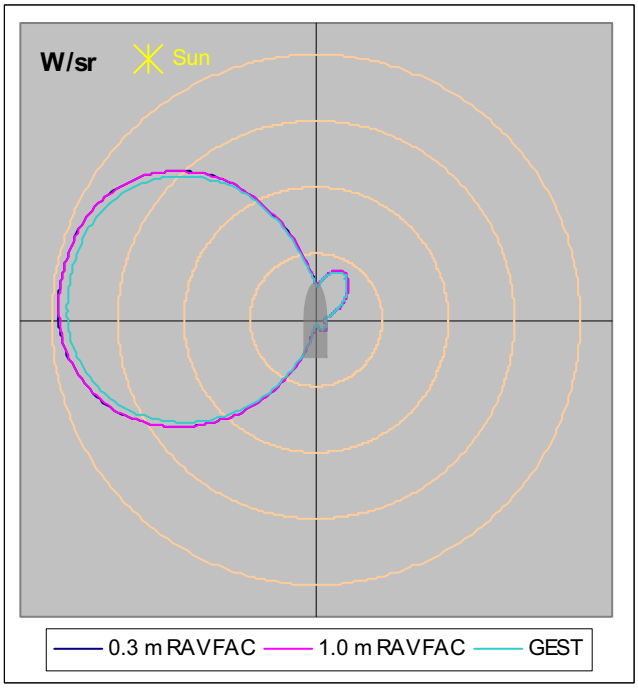

(d) Long-wave IR band

Figure A17 Background 3, 2 km viewing distance

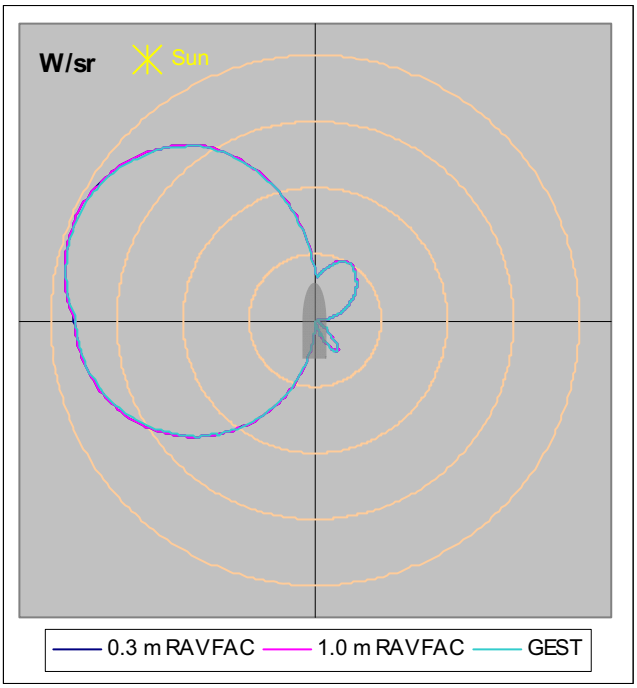

(a) Visible band

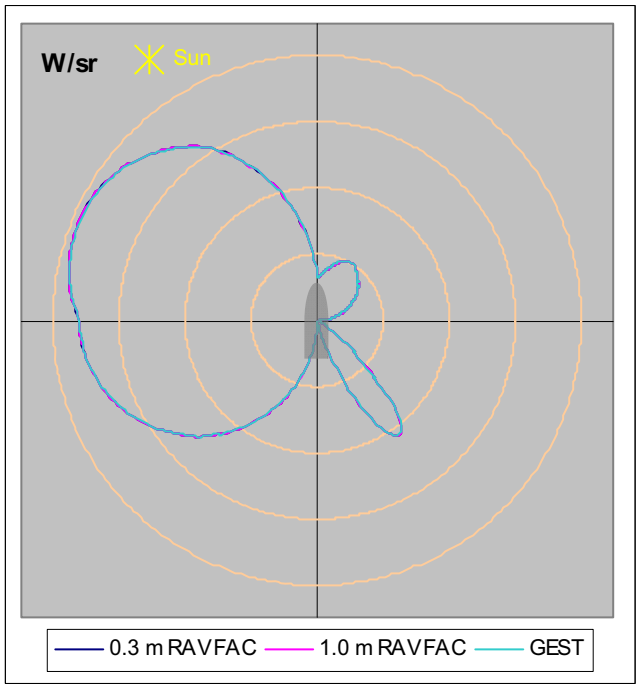

(b) Near-visible IR band

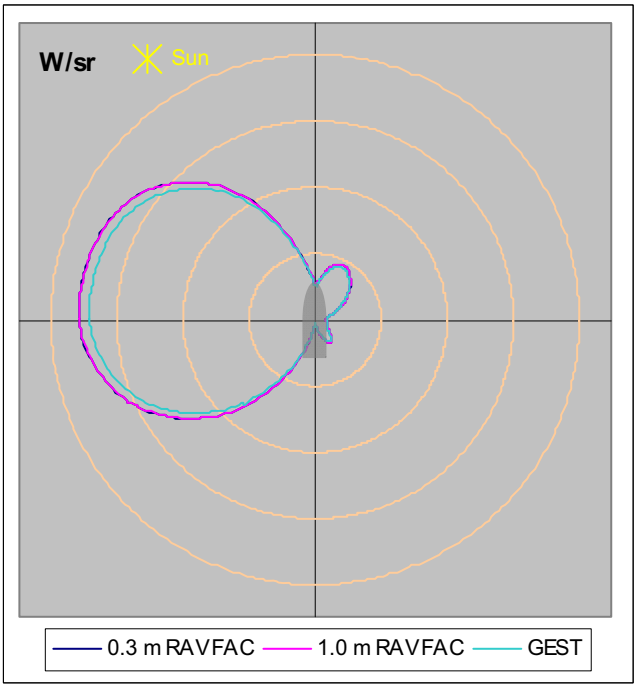

(c) Mid-wave IR band

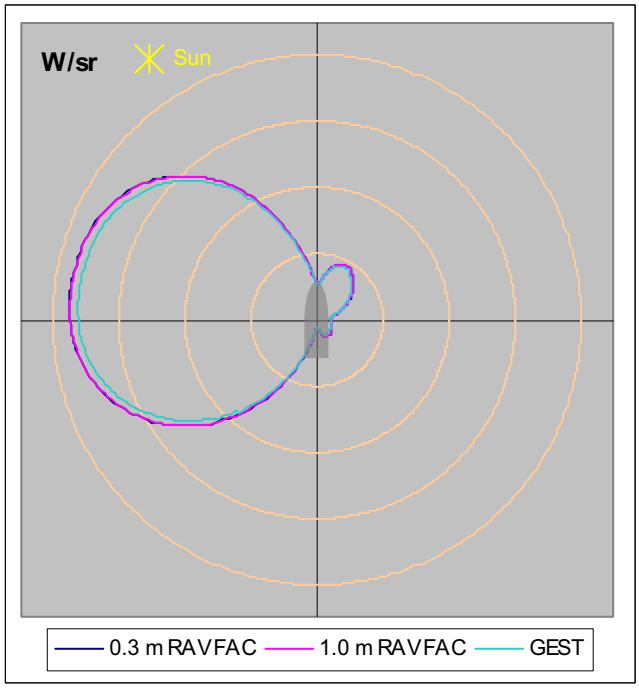

(d) Long-wave IR band

Figure A18 Background 3, 10 km viewing distance

Appendix B: OF contrast signature data — Complex wireframe model sub-processing

The following plots depict the apparent absolute contrast intensity data calculated for the model with the complex wireframe that was used in the investigation of model sub-processing. The plots are grouped into three sections: those comparing the results generated for the model with user-defined thermal boundary conditions and an exhaust plume; those comparing the results generated for the model with user-defined thermal boundary conditions but no exhaust plume; and those comparing the results generated for the model with no user-defined thermal boundary conditions or exhaust plume. It should be noted that no results are presented for Background 2 and the visible and near-visible IR bands as the platform is not detectable under these conditions. (For details of the backgrounds and the OF wavebands, refer to Section 3.)

B.1. Contrast signature plots for the complex wireframe model with user-defined thermal boundary conditions and an exhaust plume

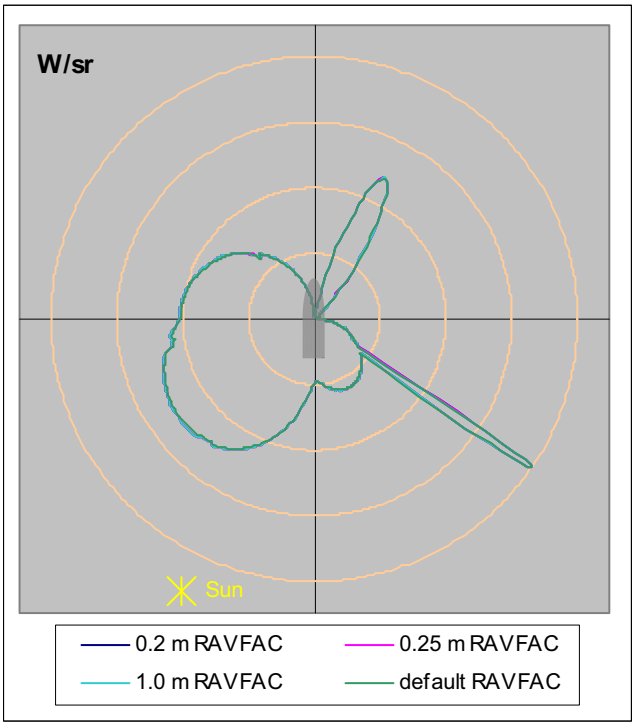

(a) Visible band

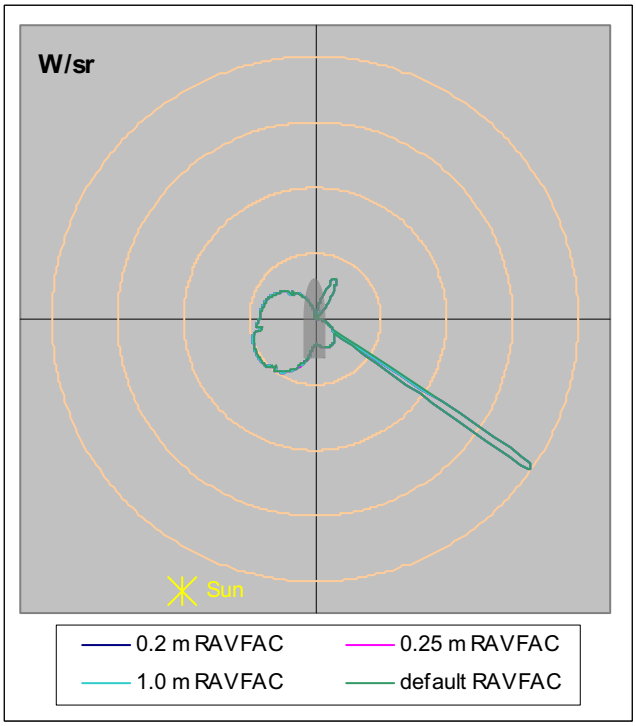

(b) Near-visible IR band

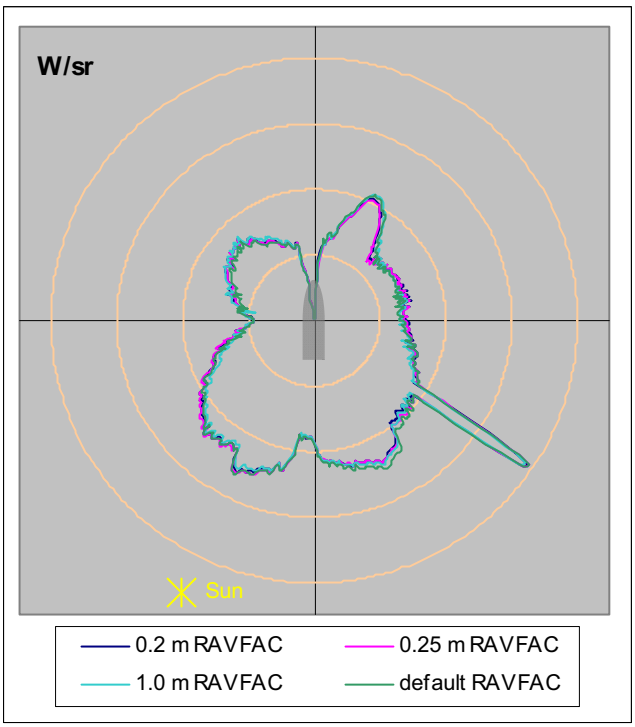

(c) Mid-wave IR band

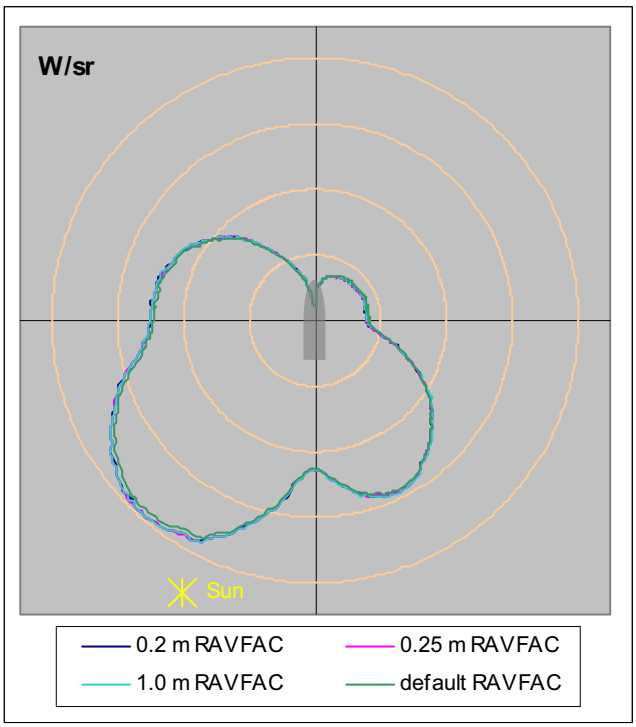

(d) Long-wave IR band

Figure B1 Background 1, 2 km viewing distance

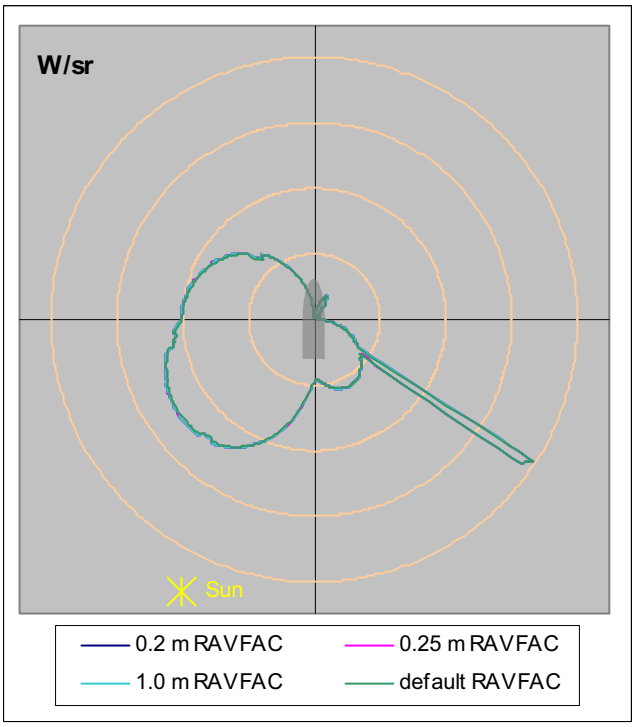

(a) Visible band

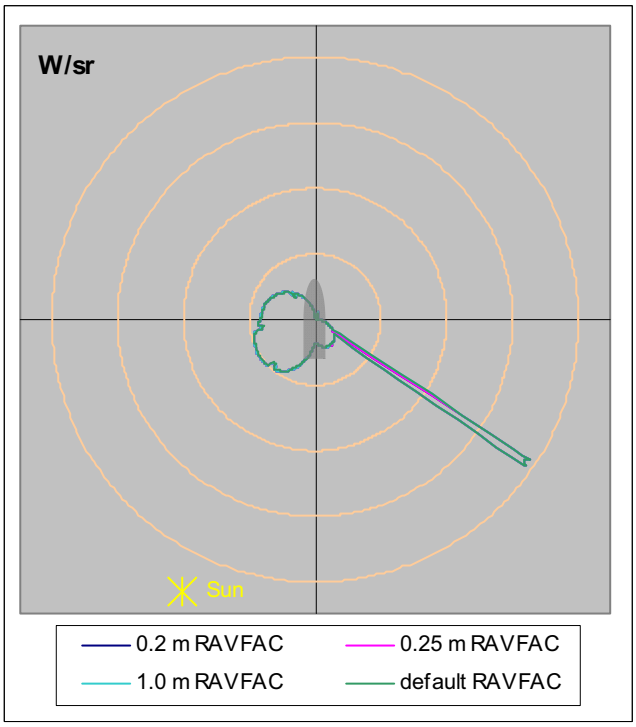

(b) Near-visible IR band

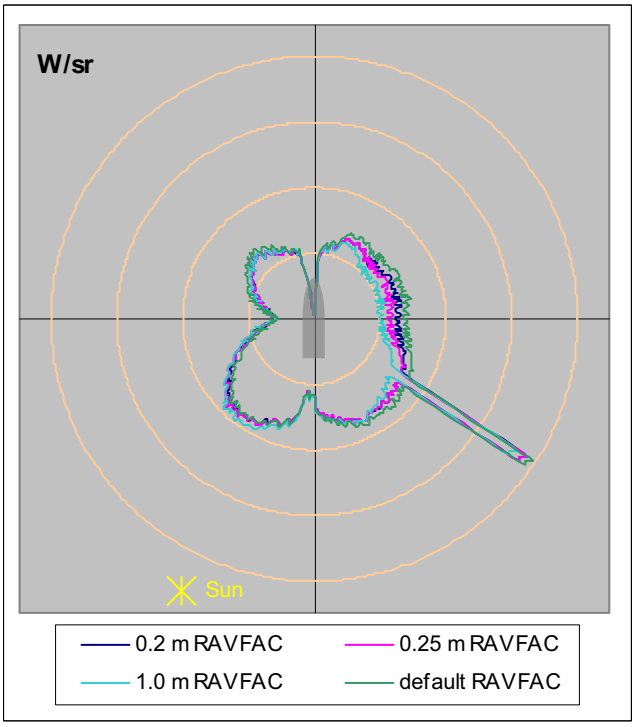

(c) Mid-wave IR band

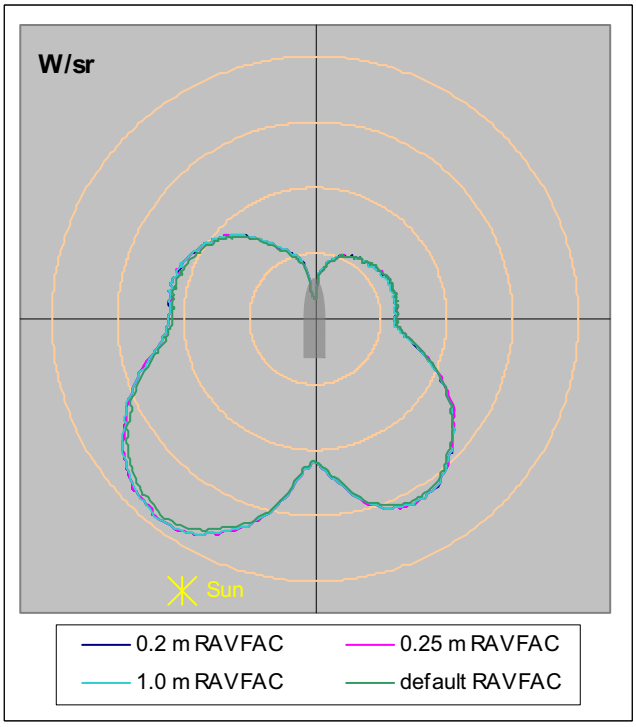

(d) Long-wave IR band

Figure B2 Background 1, 10 km viewing distance

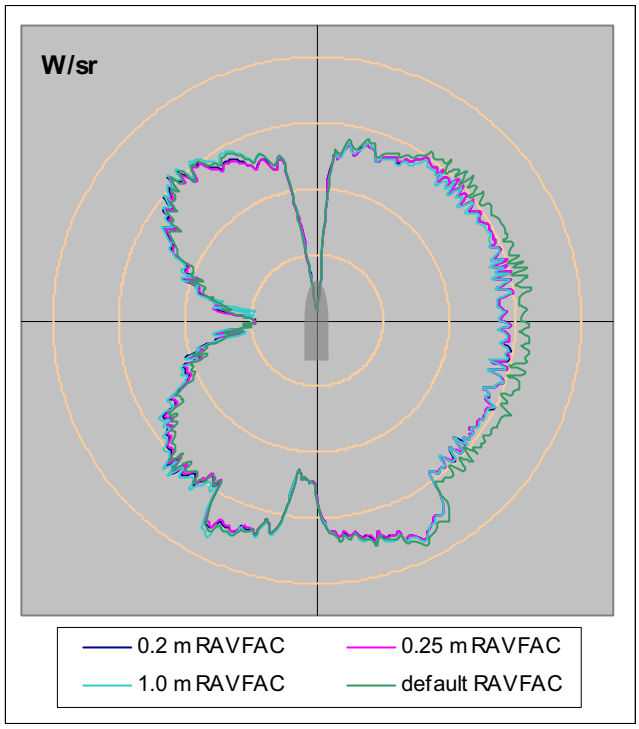

(a) Mid-wave IR band

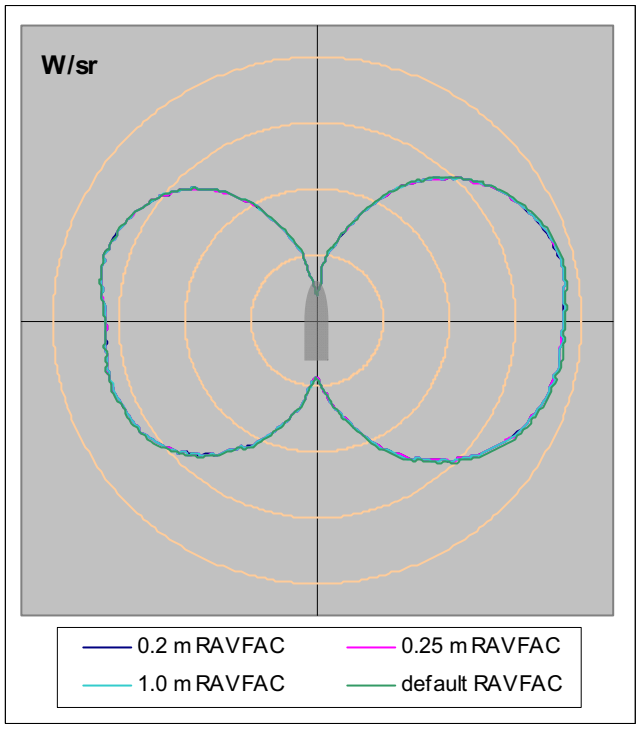

(b) Long-wave IR band

Figure B3 Background 2, 2 km viewing distance

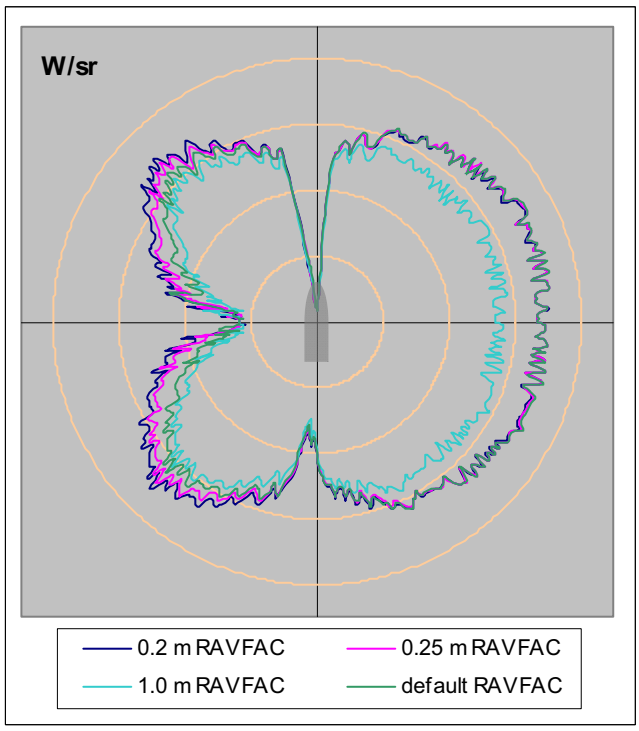

(a) Mid-wave IR band

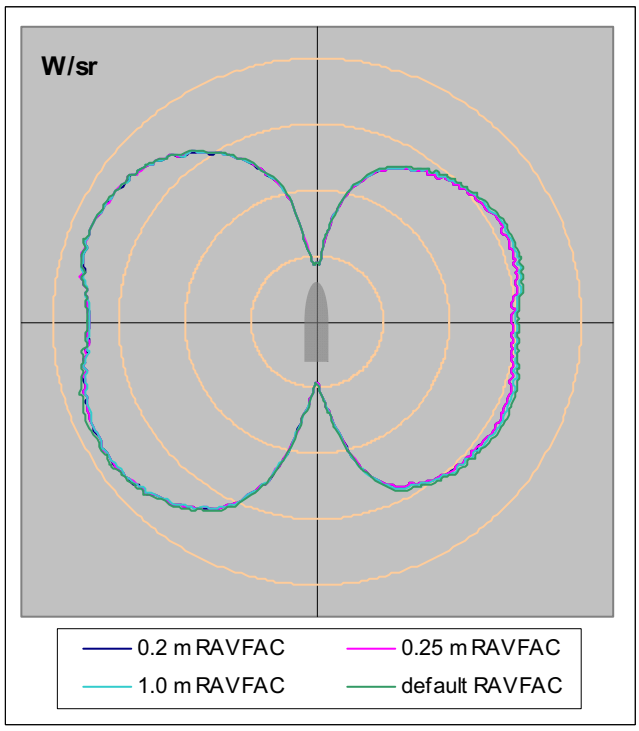

(b) Long-wave IR band

Figure B4 Background 2, 10 km viewing distance

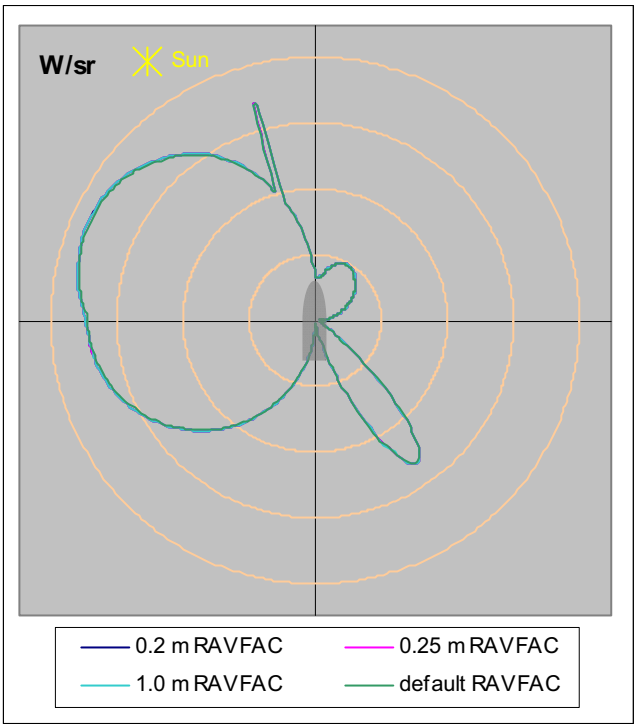

(a) Visible band

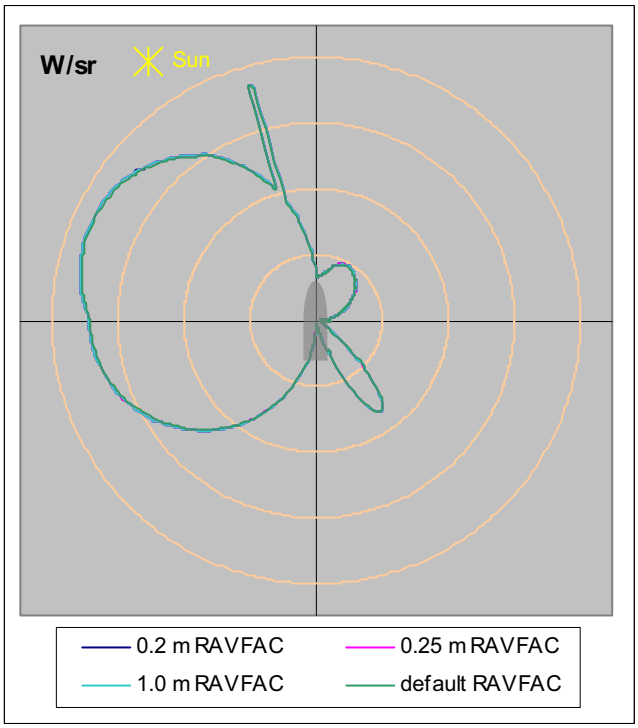

(b) Near-visible IR band

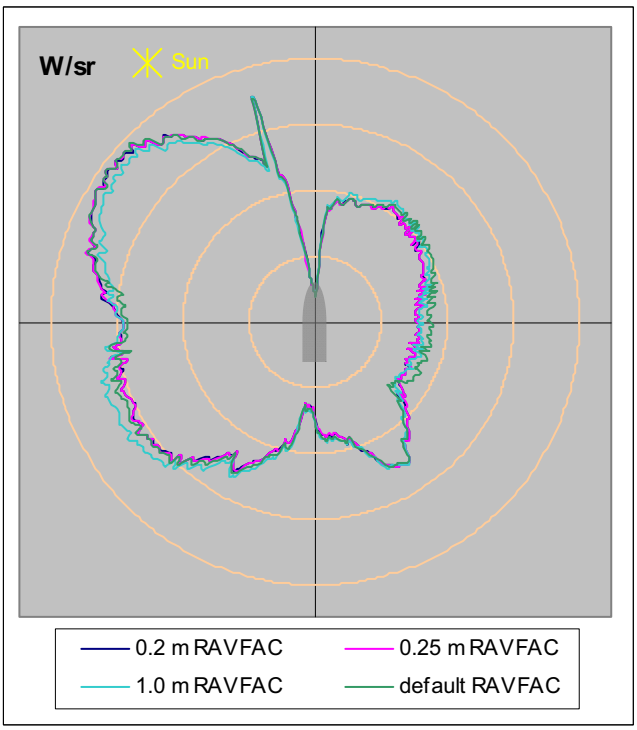

(c) Mid-wave IR band

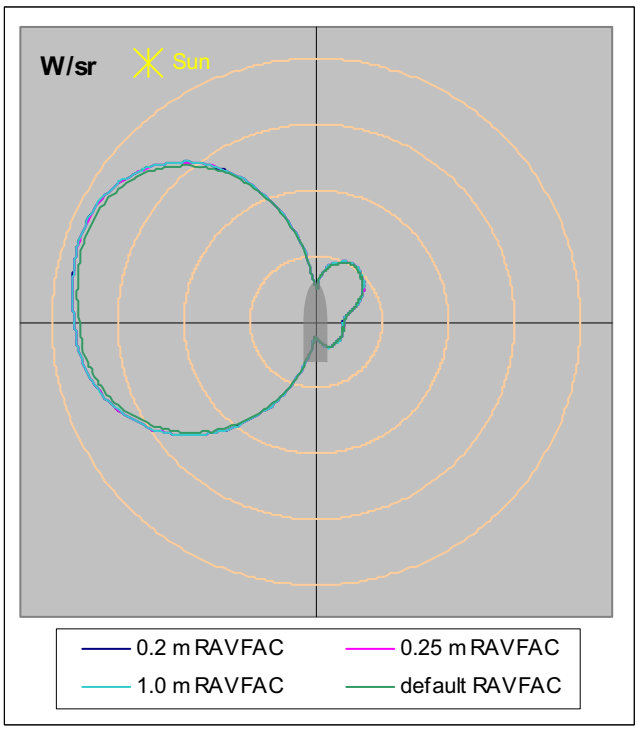

(d) Long-wave IR band

Figure B5 Background 3, 2 km viewing distance

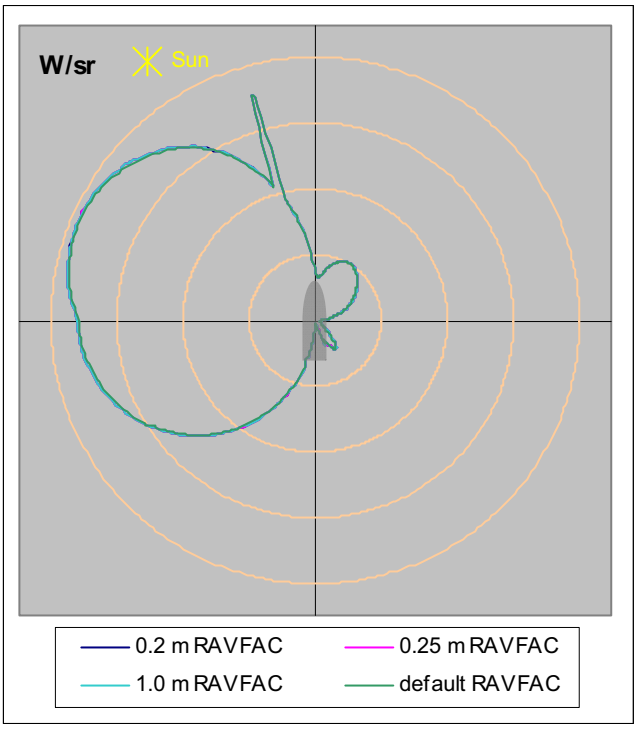

(a) Visible band

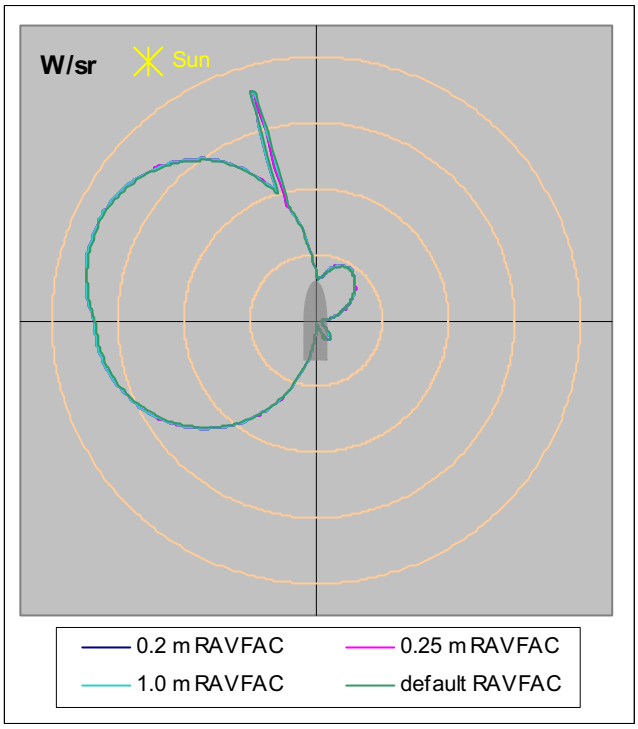

(b) Near-visible IR band

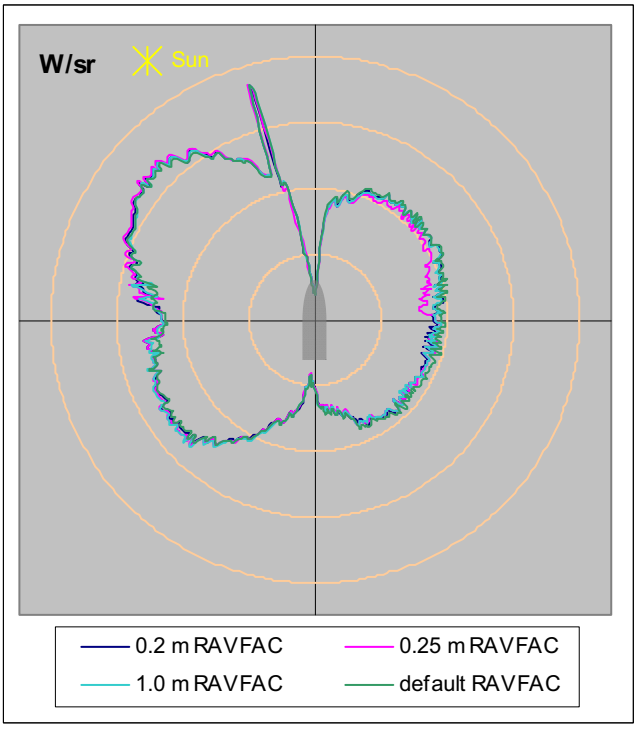

(c) Mid-wave IR band

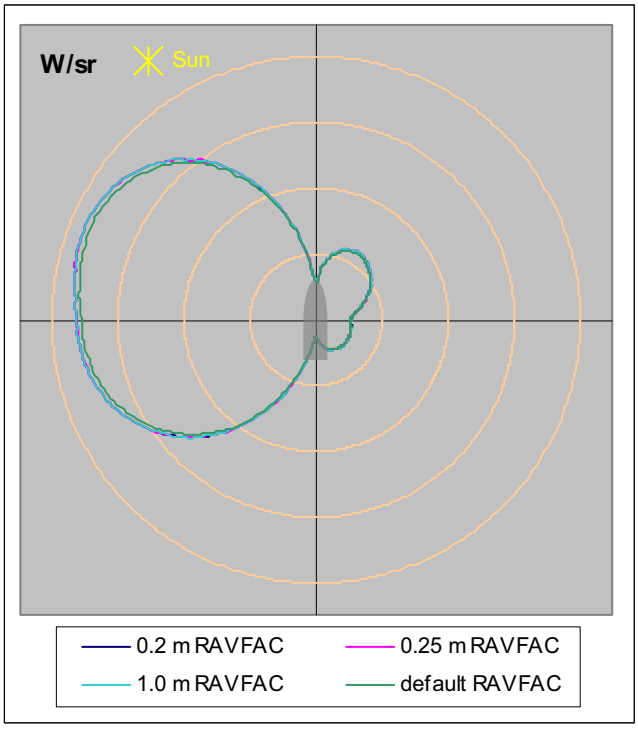

(d) Long-wave IR band

Figure B6 Background 3, 10 km viewing distance

B.2. Contrast signature plots for the complex wireframe model with user-defined thermal boundary conditions but no exhaust plume

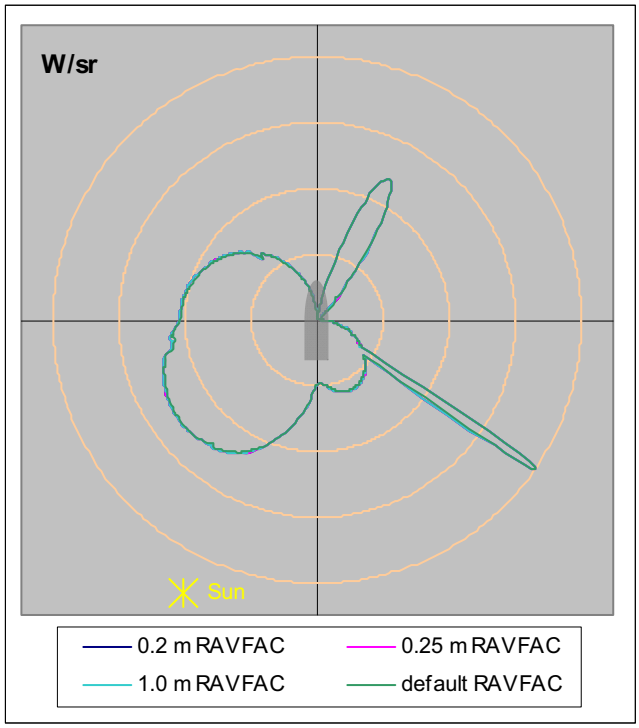

(a) Visible band

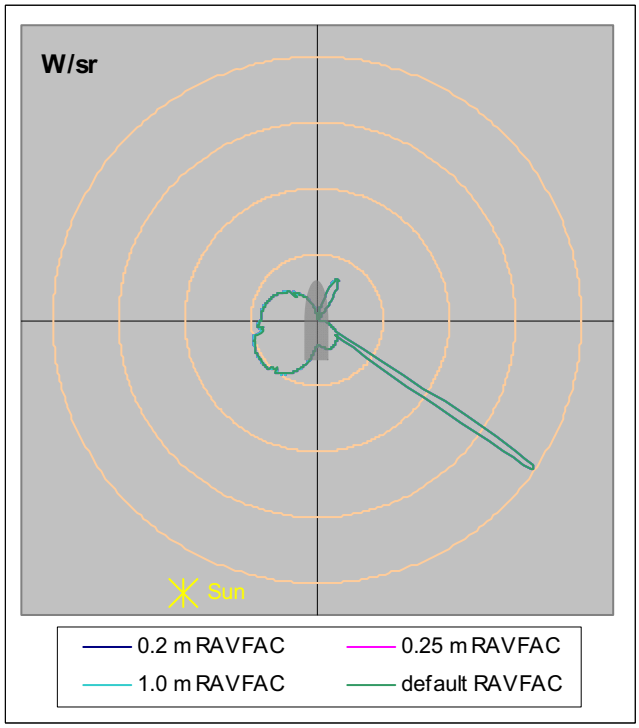

(b) Near-visible IR band

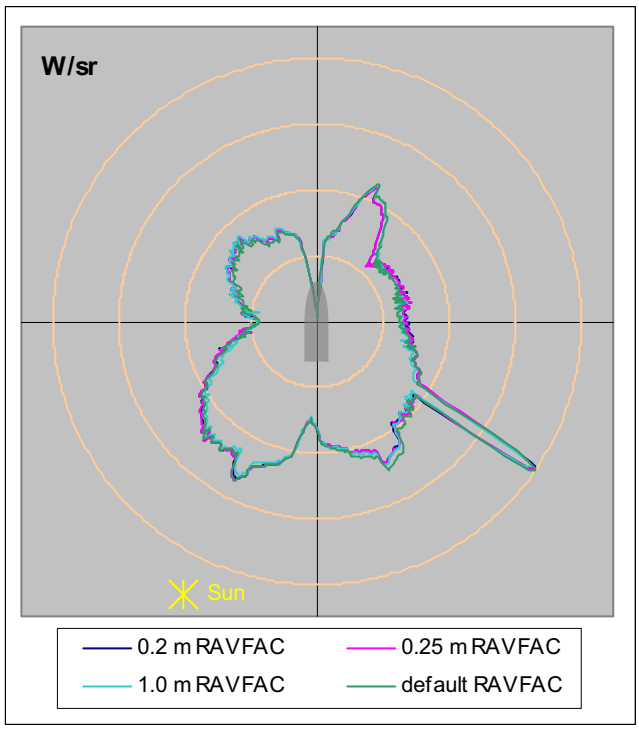

(c) Mid-wave IR band

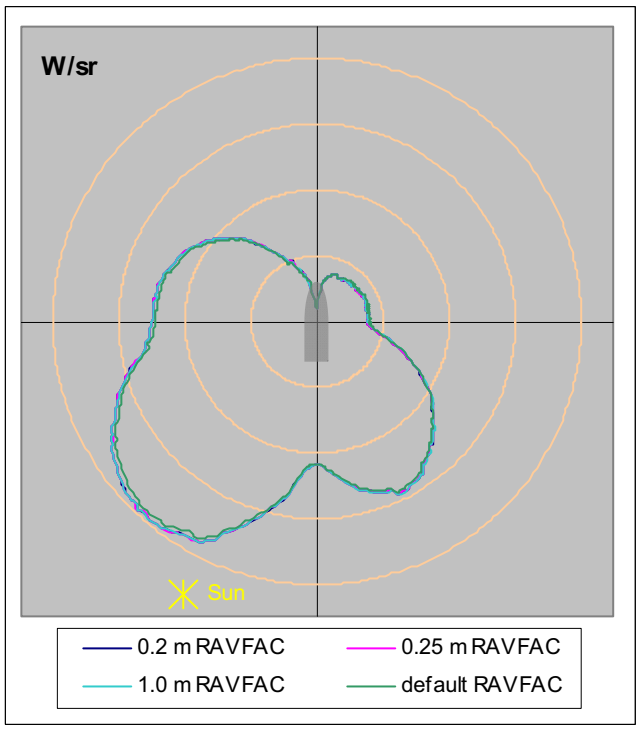

(d) Long-wave IR band

Figure B7 Background 1, 2 km viewing distance

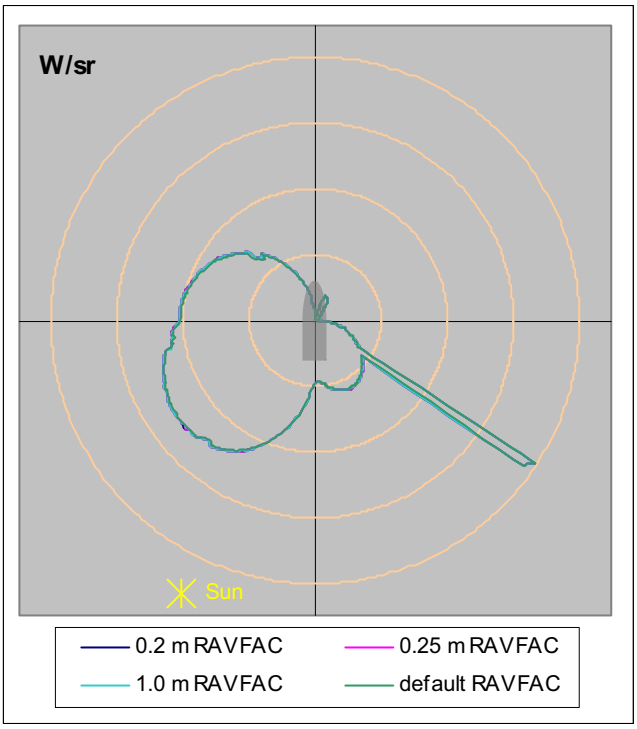

(a) Visible band

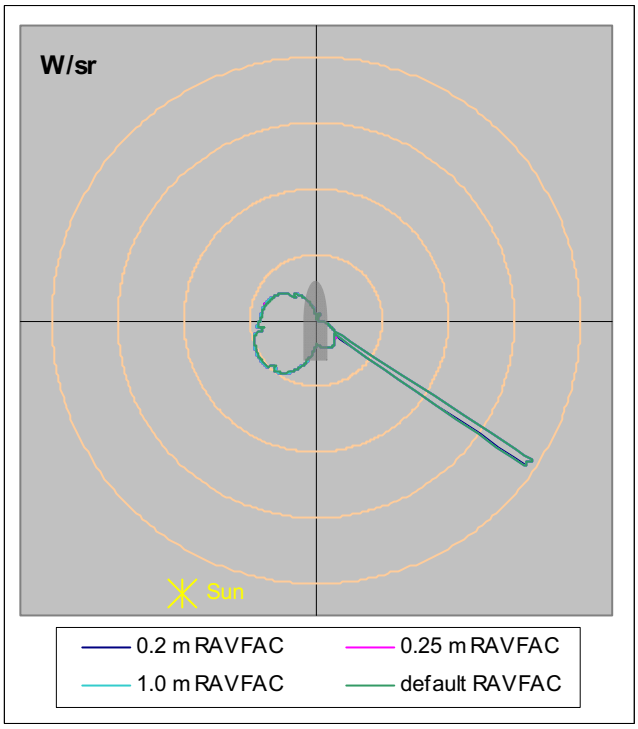

(b) Near-visible IR band

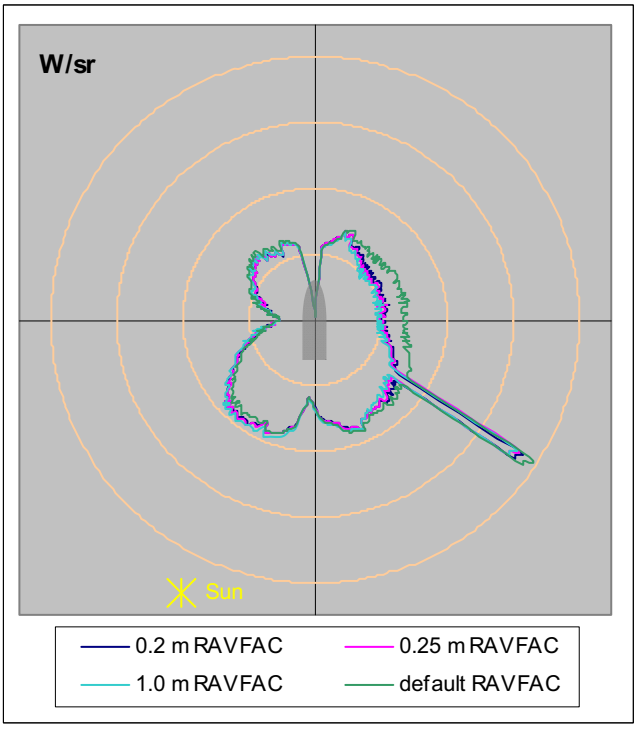

(c) Mid-wave IR band

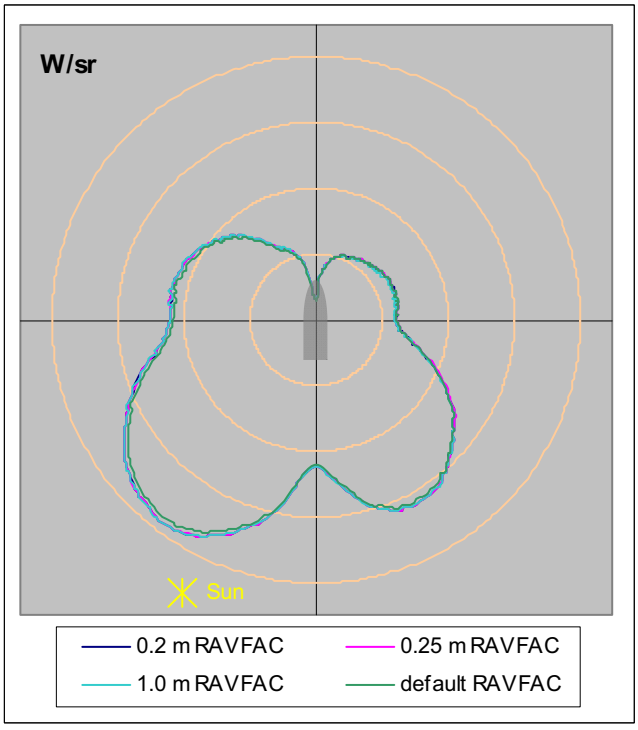

(d) Long-wave IR band

Figure B8 Background 1, 10 km viewing distance

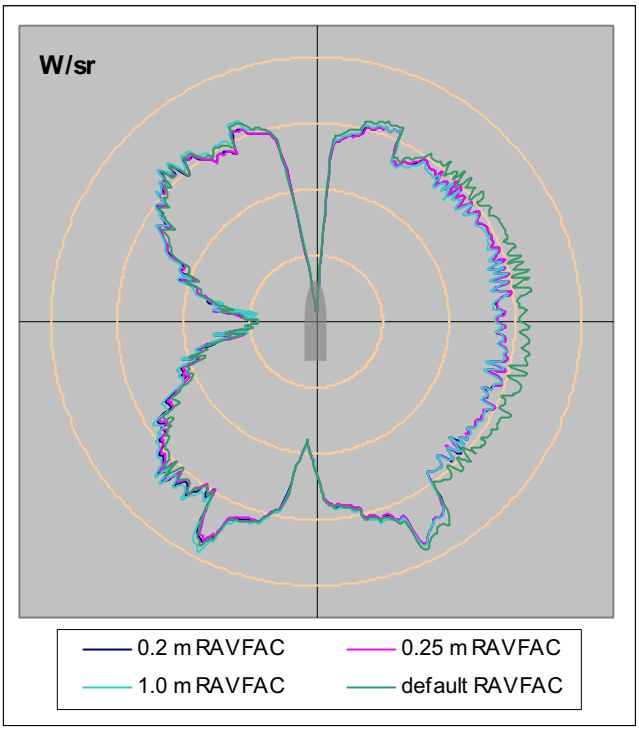

(a) Mid-wave IR band

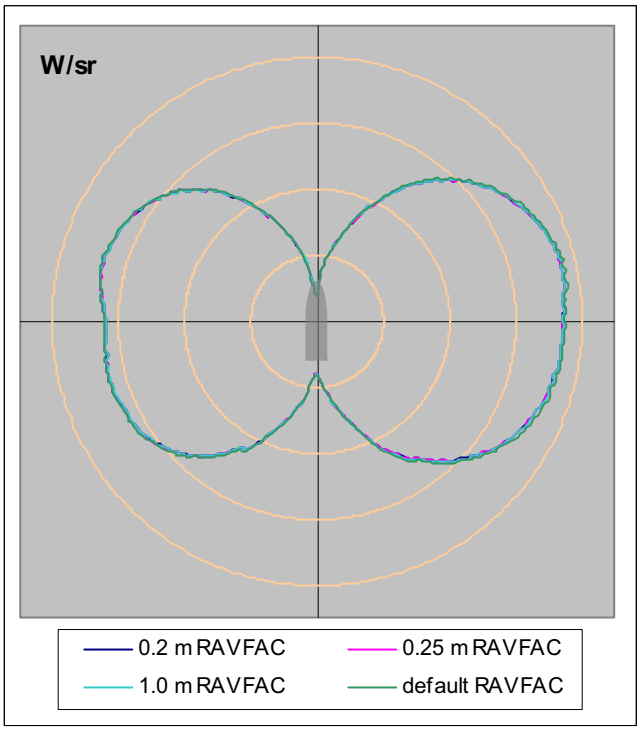

(b) Long-wave IR band

Figure B9 Background 2, 2 km viewing distance

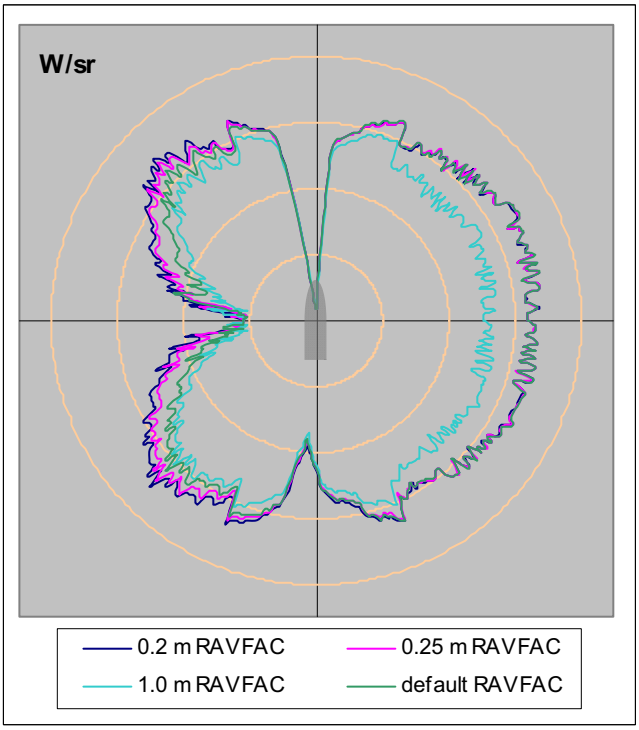

(a) Mid-wave IR band

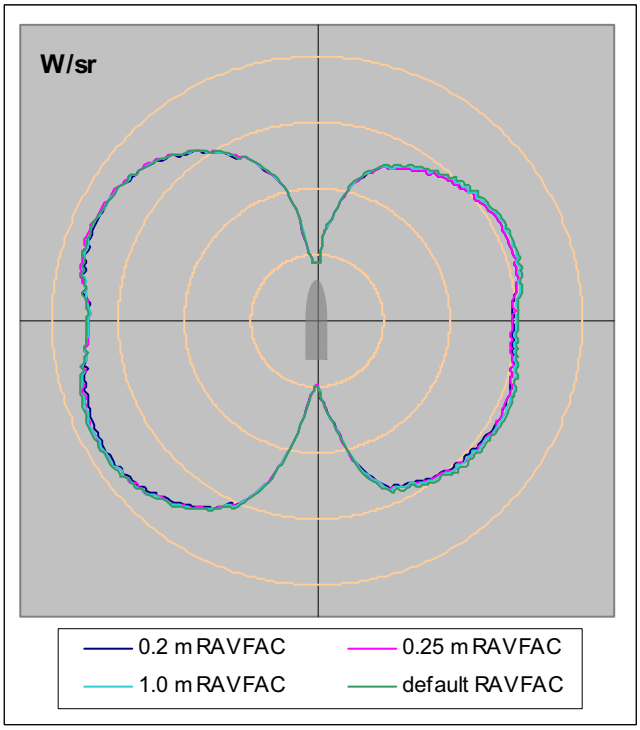

(b) Long-wave IR band

Figure B10 Background 2, 10 km viewing distance

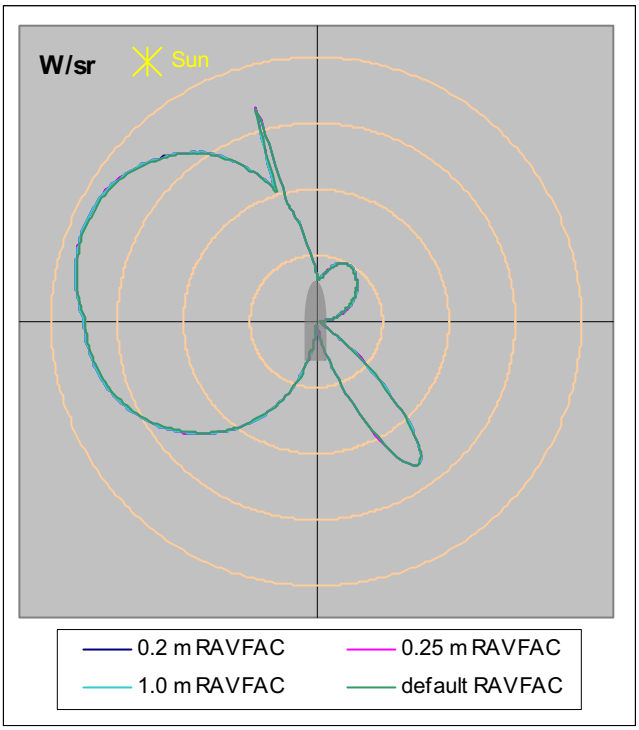

(a) Visible band

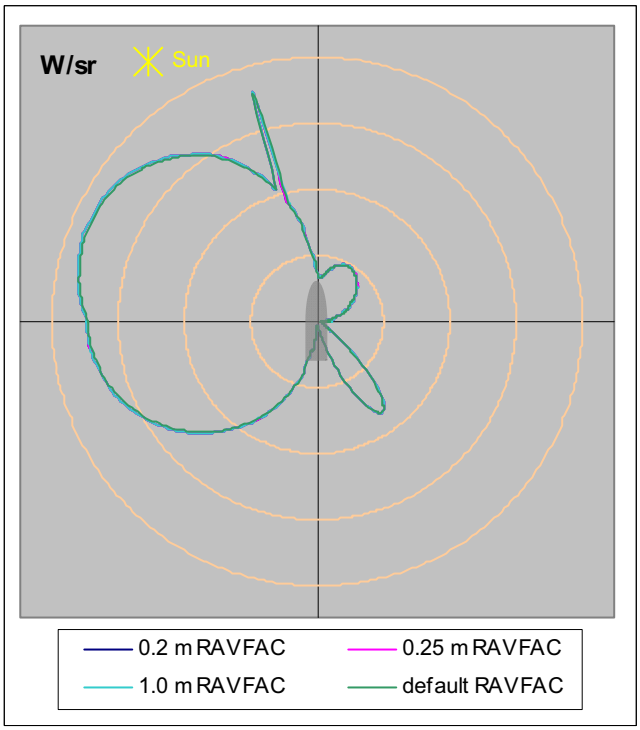

(b) Near-visible IR band

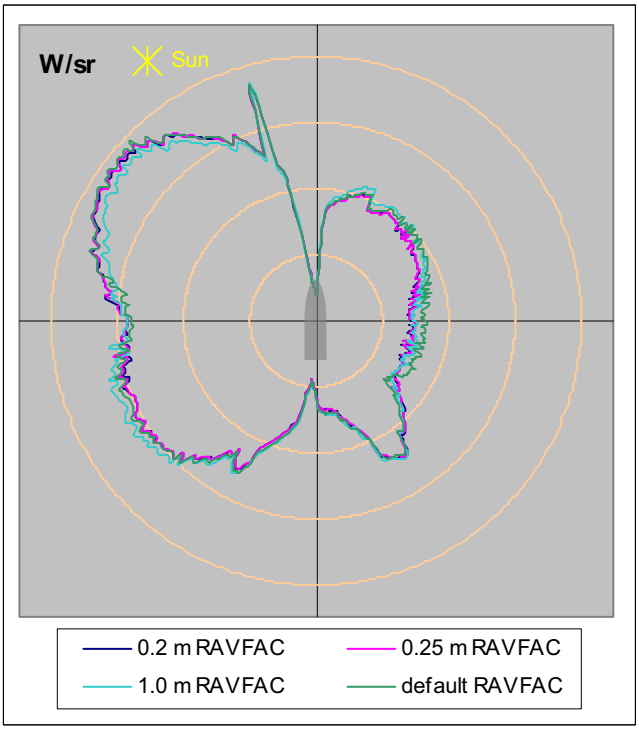

(c) Mid-wave IR band

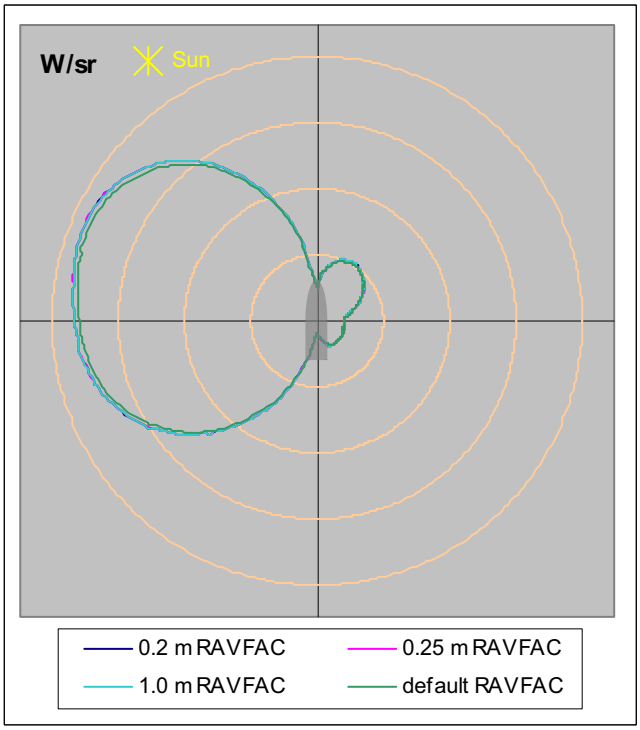

(d) Long-wave IR band

Figure B11 Background 3, 2 km viewing distance

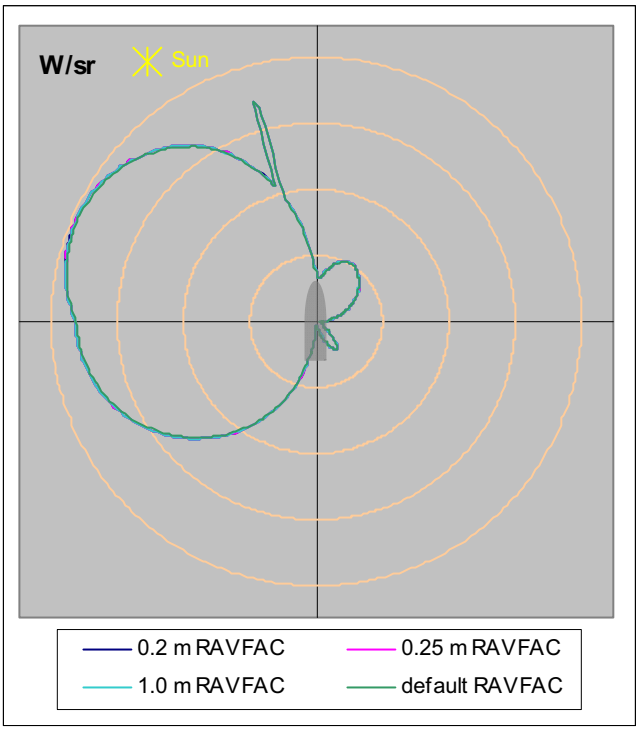

(a) Visible band

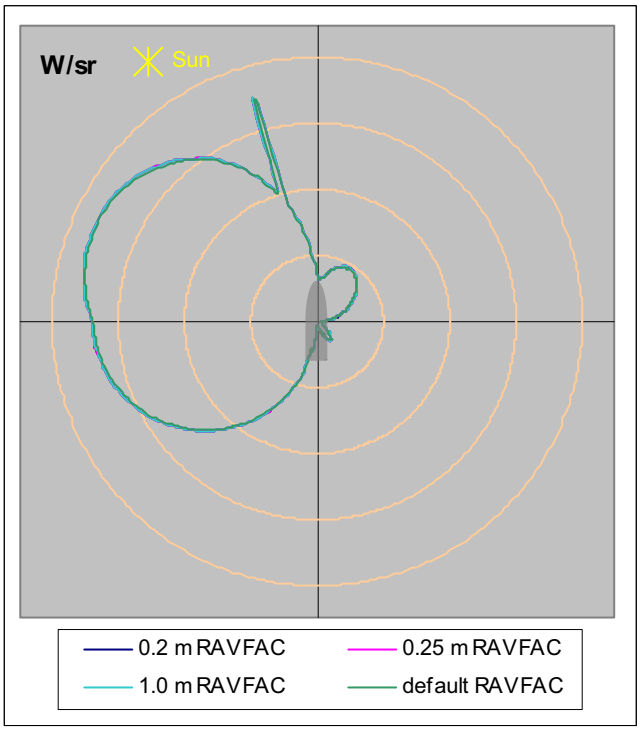

(b) Near-visible IR band

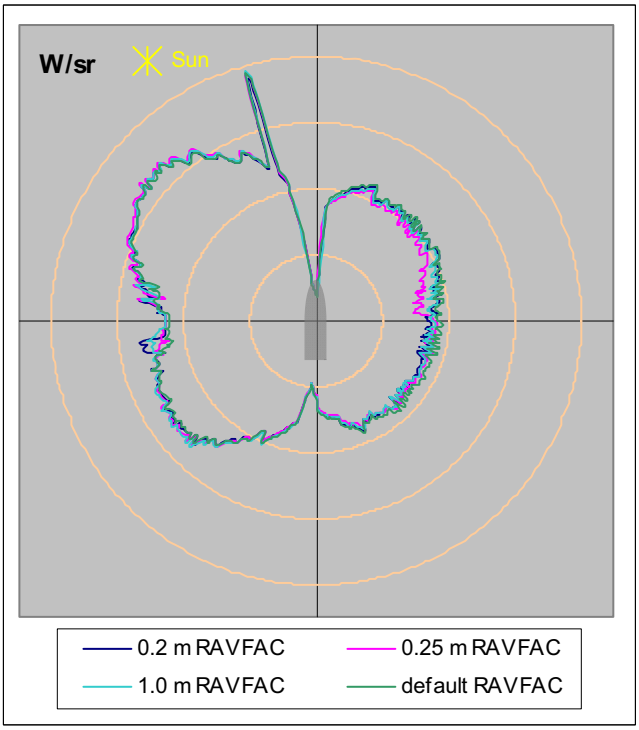

(c) Mid-wave IR band

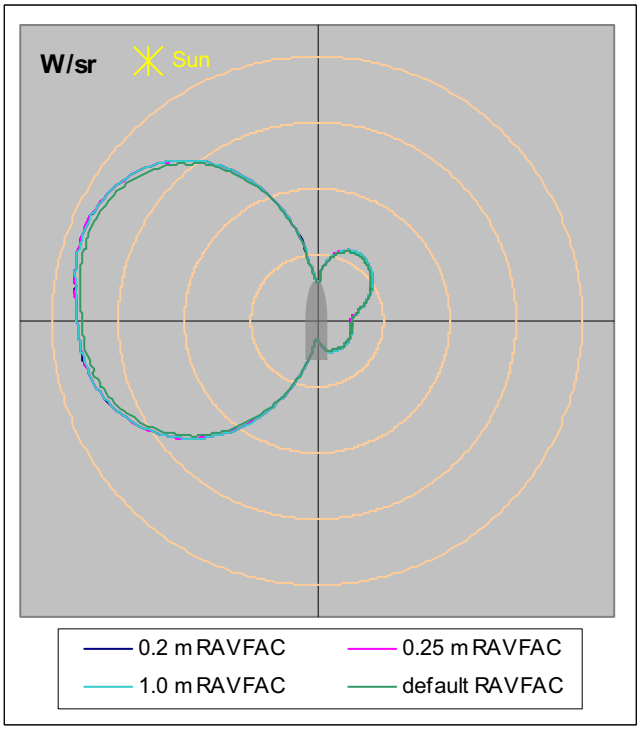

(d) Long-wave IR band

Figure B12 Background 3, 10 km viewing distance

B.3. Contrast signature plots for the complex wireframe model with no user-defined thermal boundary conditions or exhaust plume

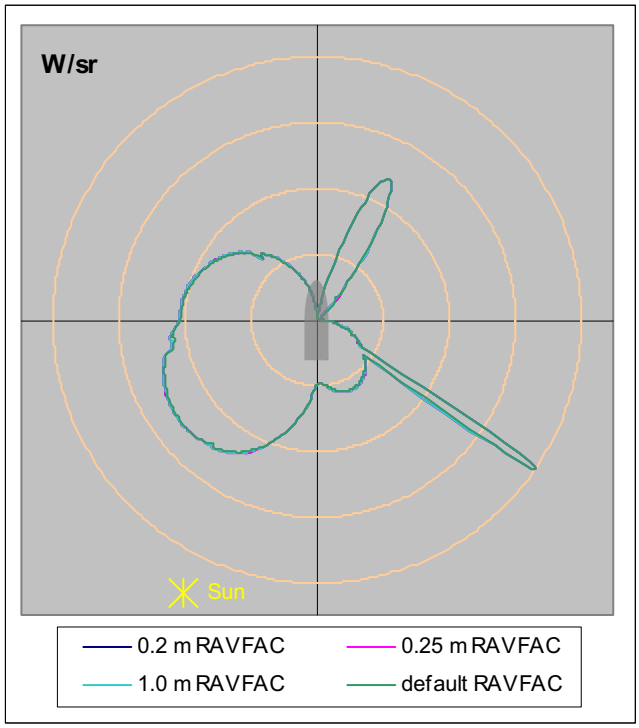

(a) Visible band

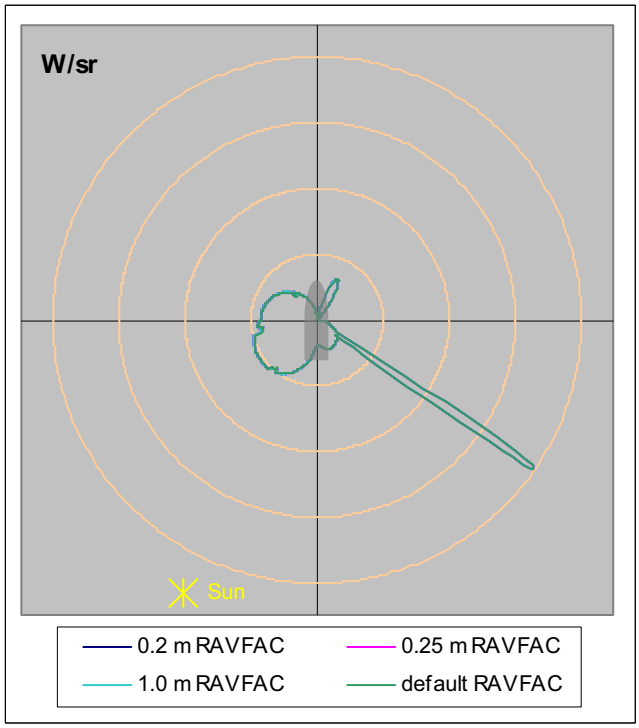

(b) Near-visible IR band

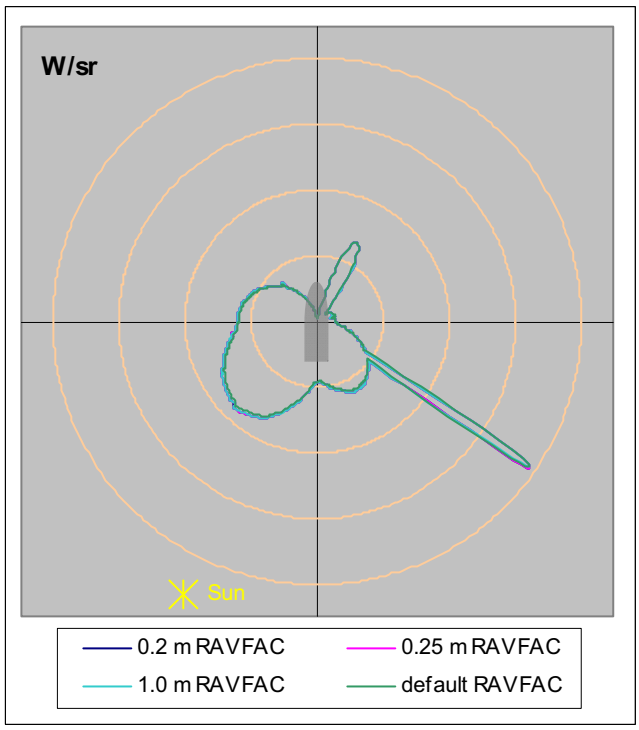

(c) Mid-wave IR band

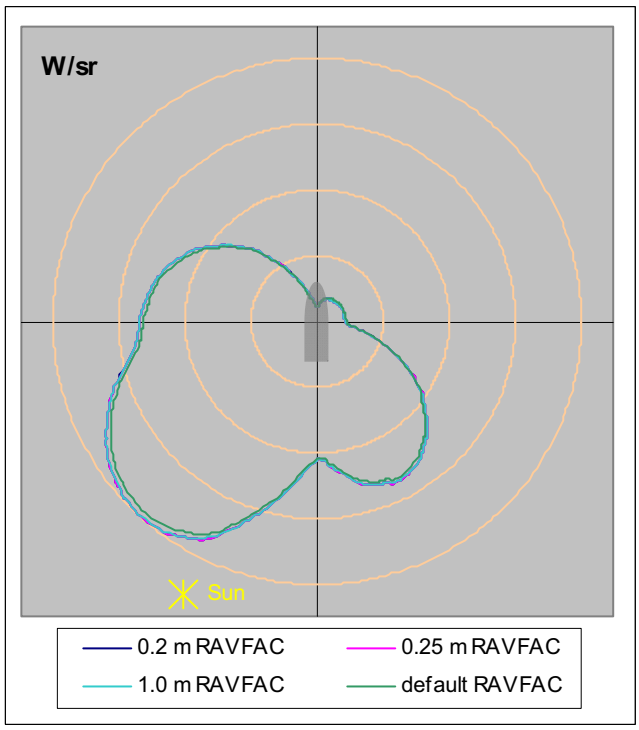

(d) Long-wave IR band

Figure B13 Background 1, 2 km viewing distance

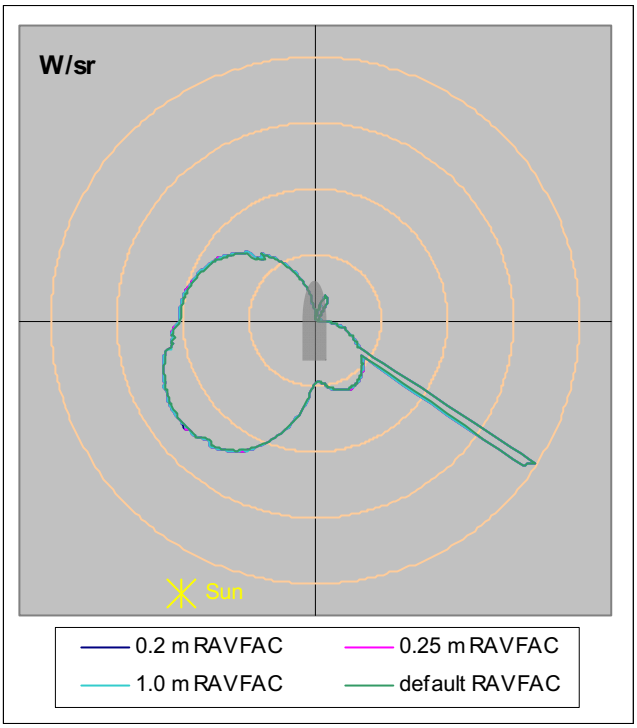

(a) Visible band

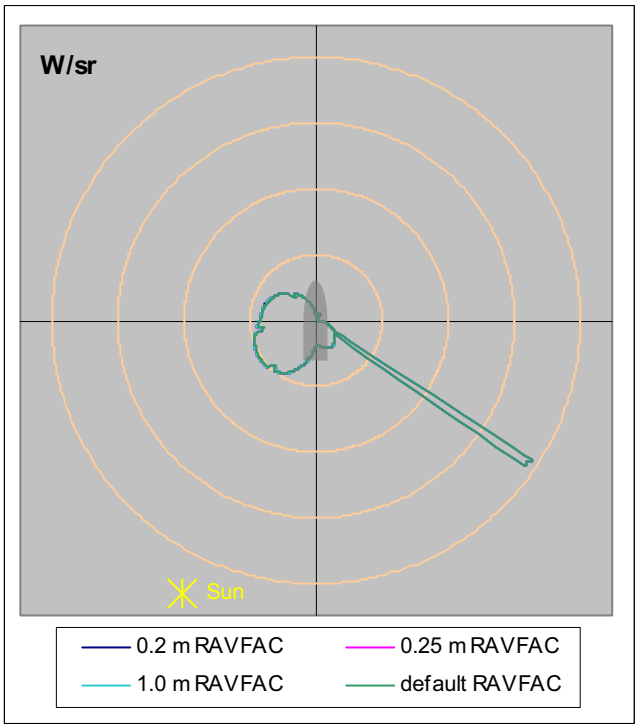

(b) Near-visible IR band

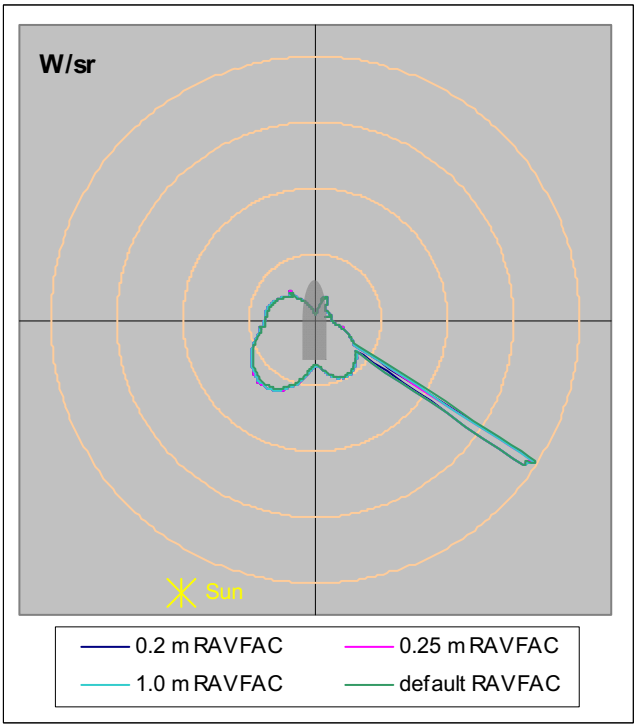

(c) Mid-wave IR band

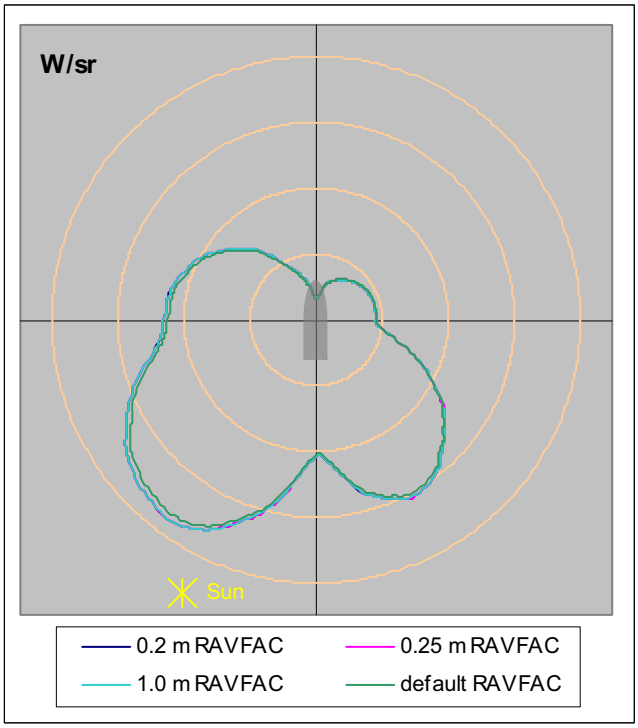

(d) Long-wave IR band

Figure B14 Background 1, 10 km viewing distance

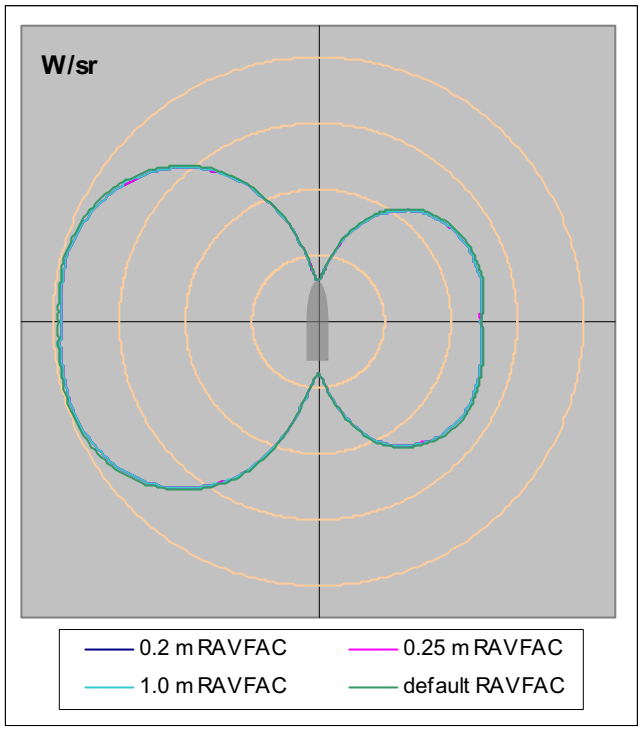

(a) Mid-wave IR band

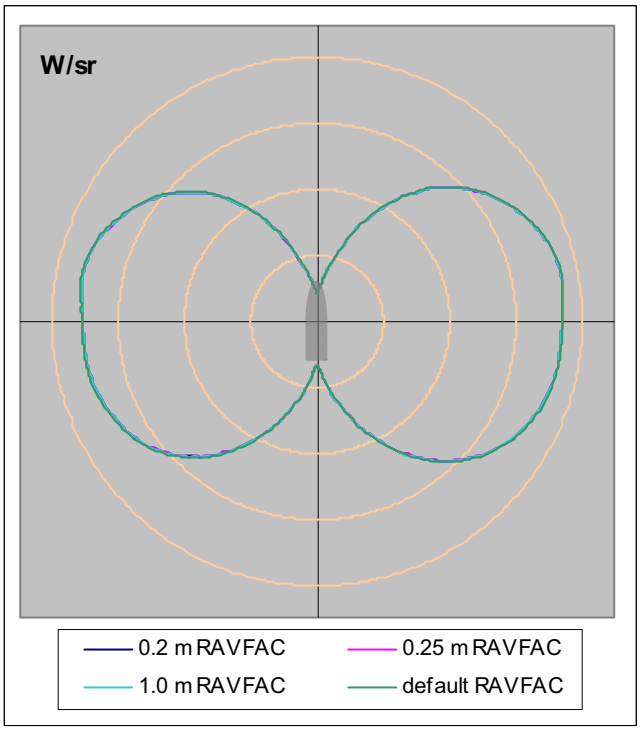

(b) Long-wave IR band

Figure B15 Background 2, 2 km viewing distance

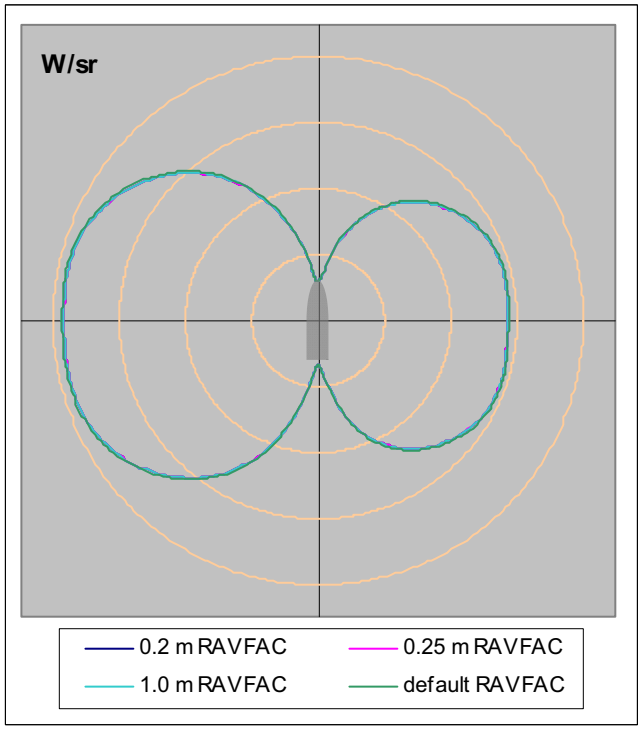

(a) Mid-wave IR band

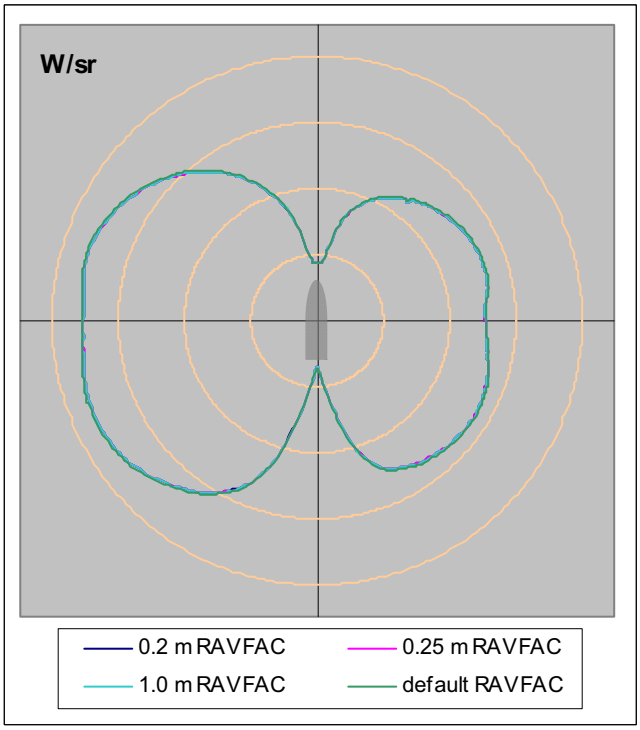

(b) Long-wave IR band

Figure B16 Background 2, 10 km viewing distance

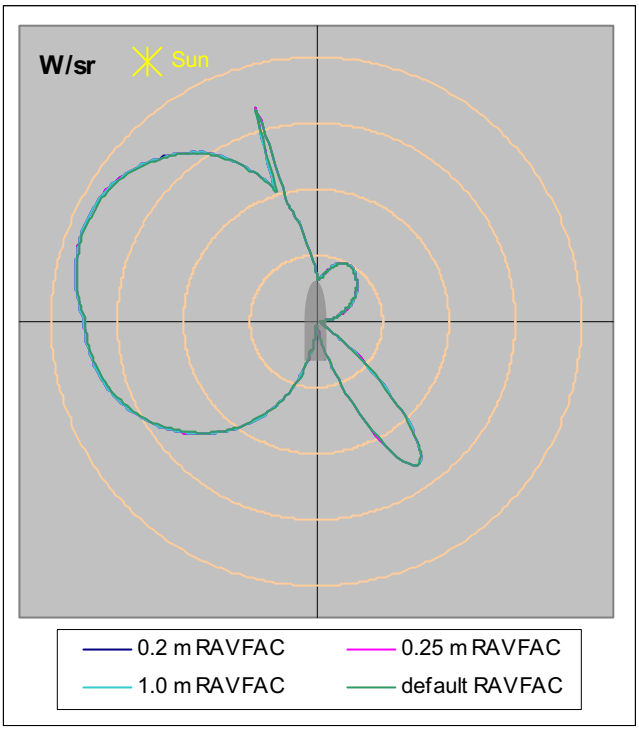

(a) Visible band

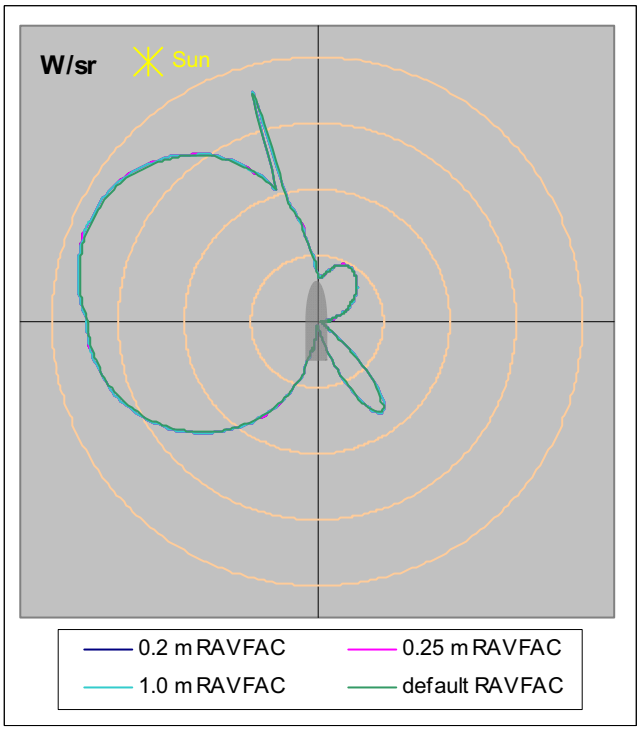

(b) Near-visible IR band

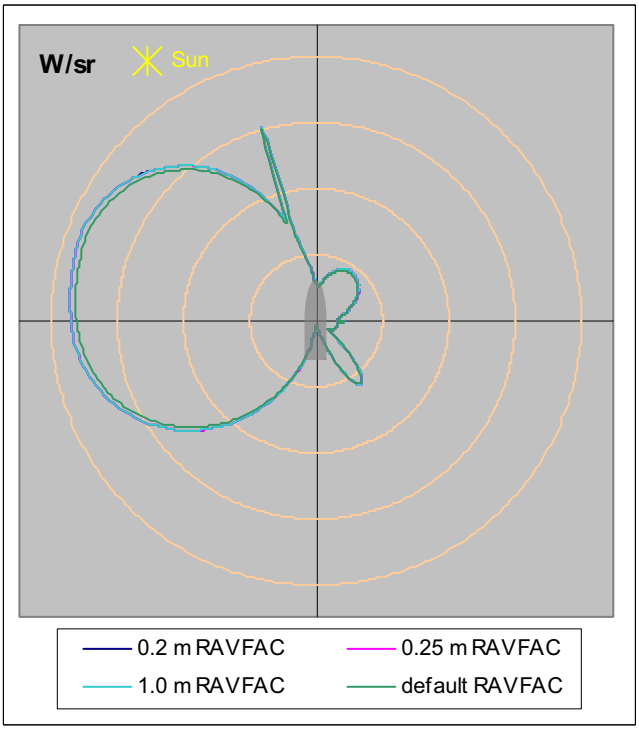

(c) Mid-wave IR band

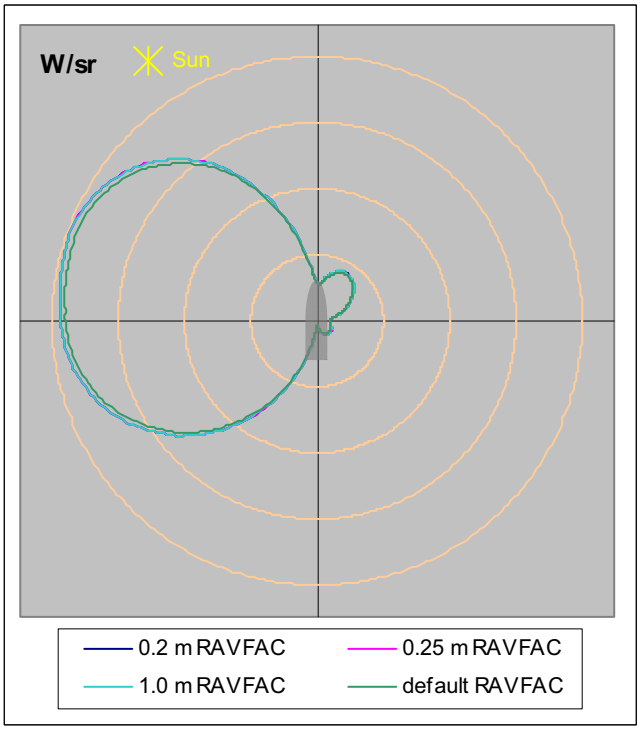

(d) Long-wave IR band

Figure B17 Background 3, 2 km viewing distance

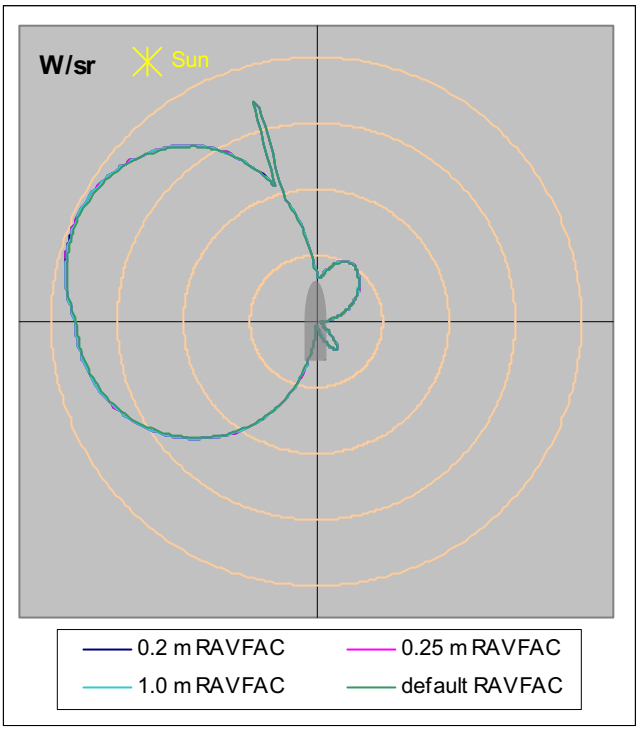

(a) Visible band

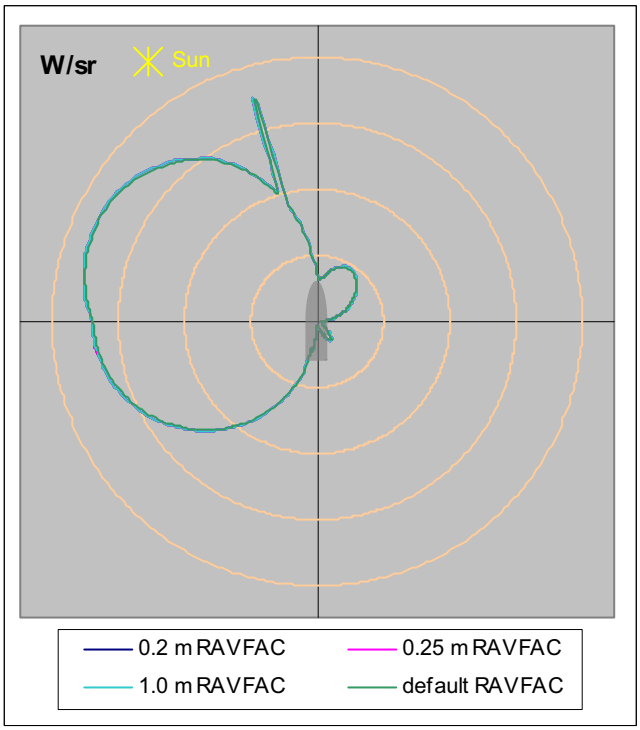

(b) Near-visible IR band

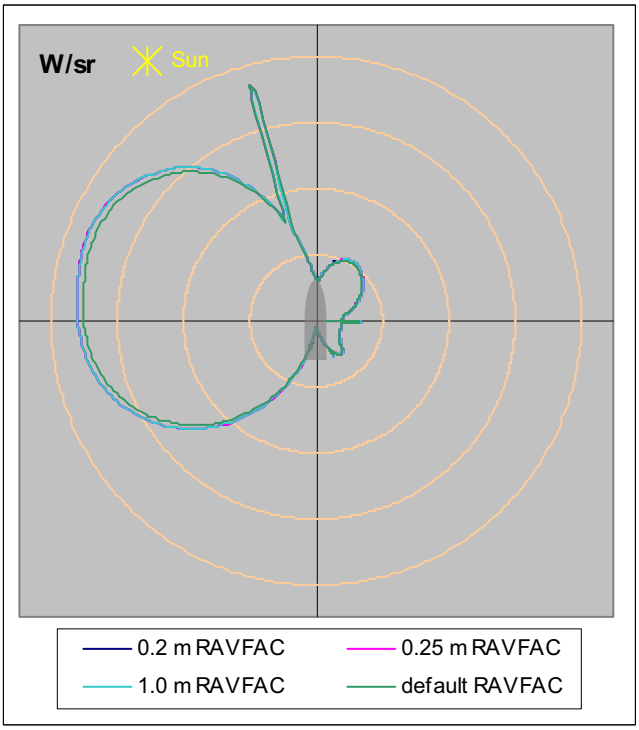

(c) Mid-wave IR band

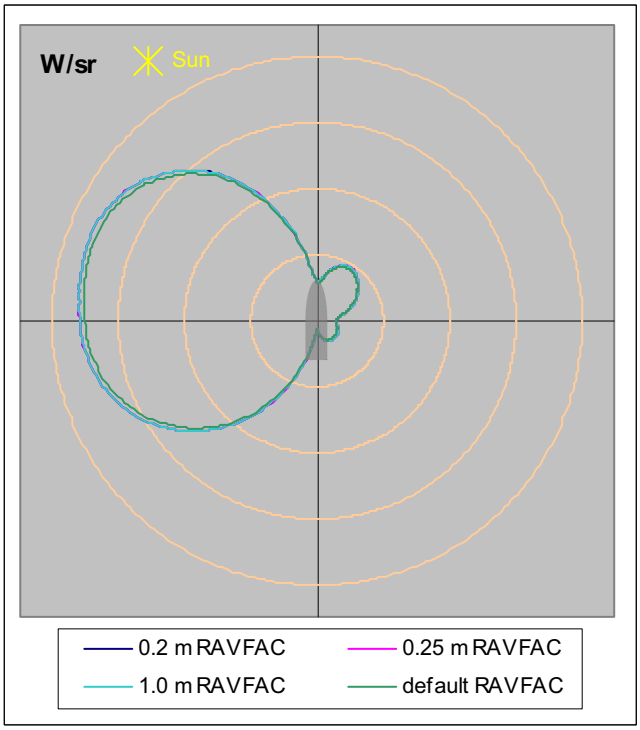

(d) Long-wave IR band

Figure B18 Background 3, 10 km viewing distance

Appendix C: OF contrast signature data — Simple wireframe versus complex wireframe, both with standard paints

The following plots depict the apparent absolute contrast intensity data calculated for the two models with standard paints that were used in the investigation of wireframe detail. The plots are grouped into three sections: those comparing the results generated for the models with user-defined thermal boundary conditions and an exhaust plume; those comparing the results generated for the models with user-defined thermal boundary conditions but no exhaust plume; and those comparing the results generated for the models with no user-defined thermal boundary conditions or exhaust plume. It should be noted that no results are presented for Background 2 and the visible and near-visible IR bands as the platform is not detectable under these conditions. (For details of the backgrounds and the OF wavebands, refer to Section 3.)

C.1. Contrast signature plots for the two models, both with user-defined thermal boundary conditions and an exhaust plume

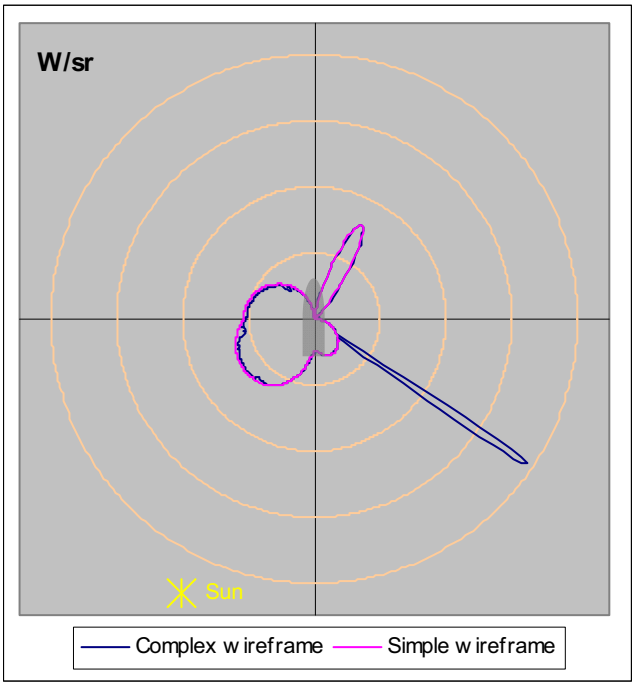

(a) Visible band

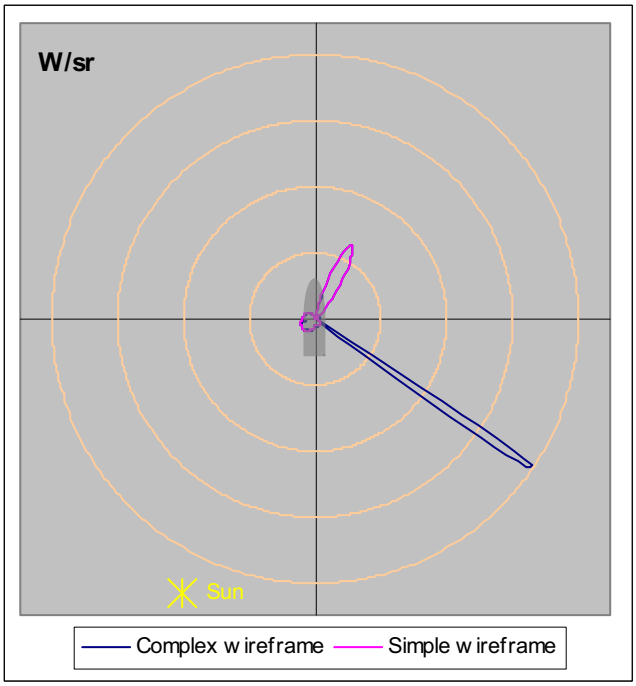

(b) Near-visible IR band

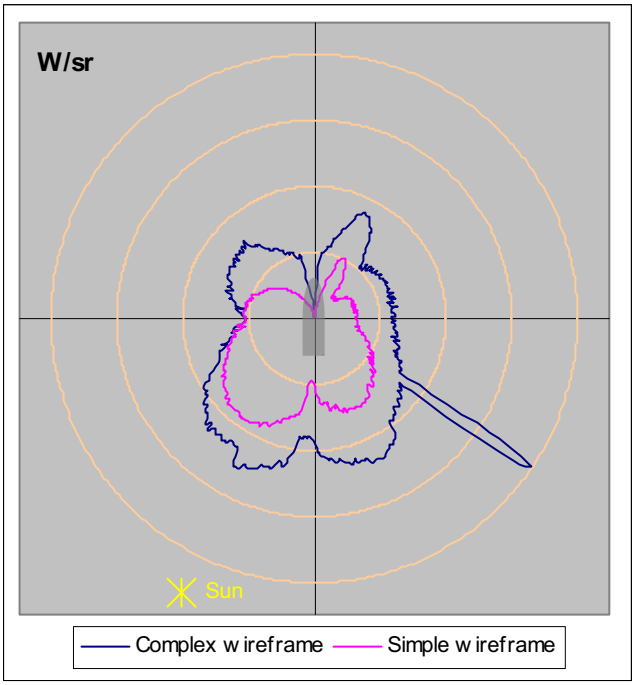

(c) Mid-wave IR band

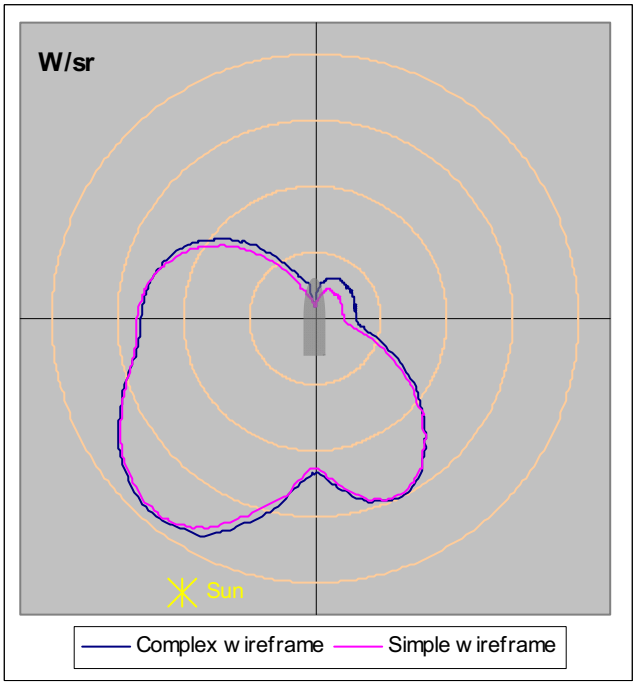

(d) Long-wave IR band

Figure C1 Background 1, 2 km viewing distance

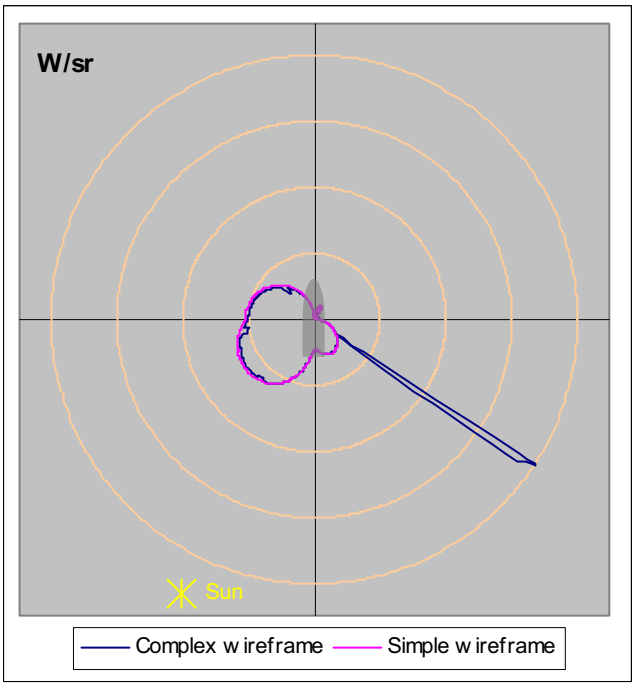

(a) Visible band

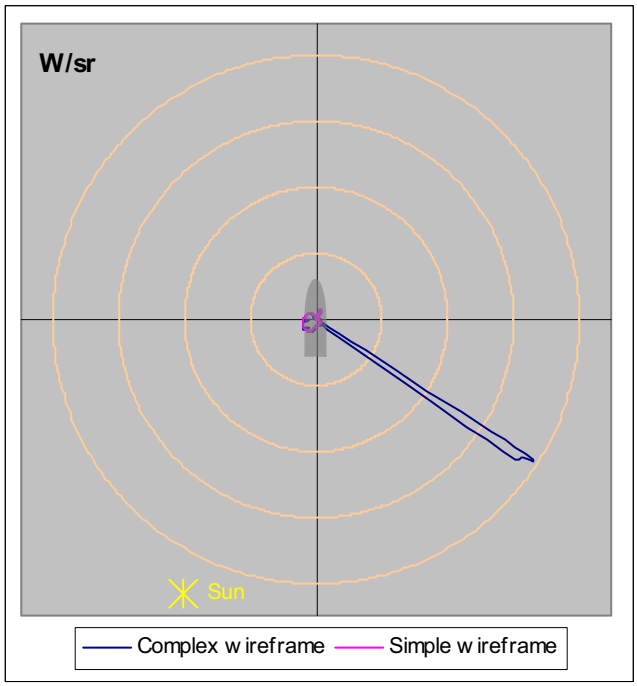

(b) Near-visible IR band

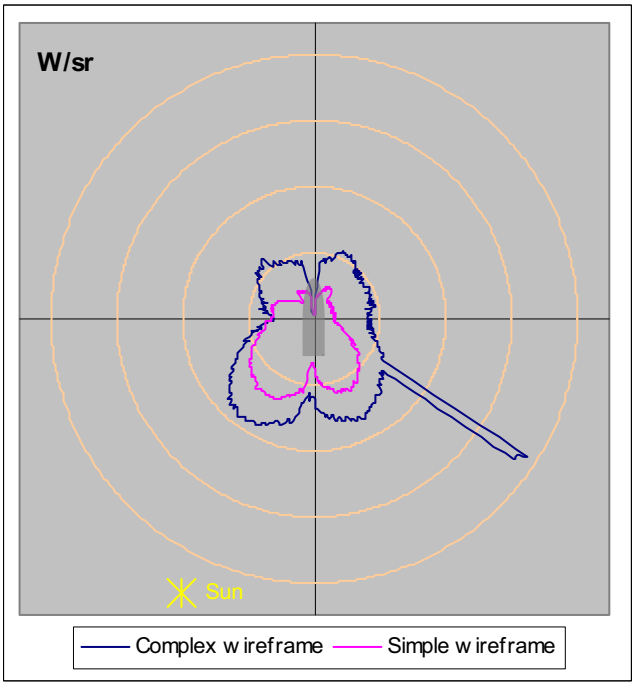

(c) Mid-wave IR band

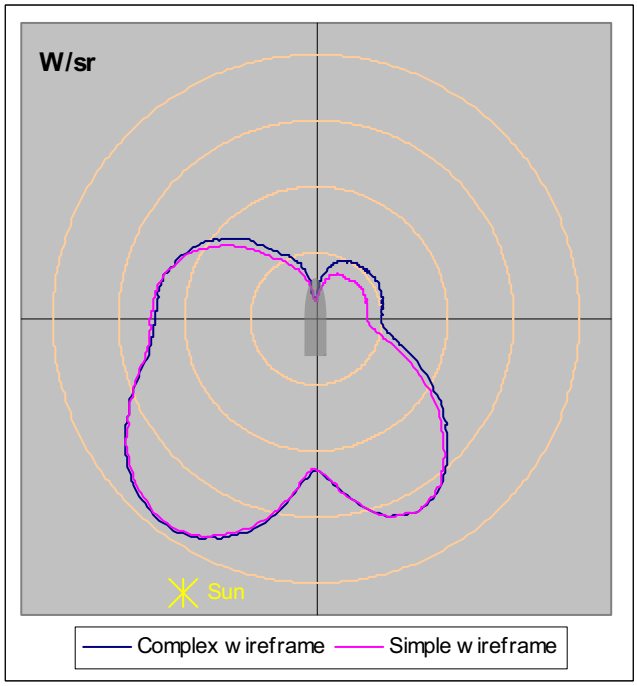

(d) Long-wave IR band

Figure C2 Background 1, 10 km viewing distance

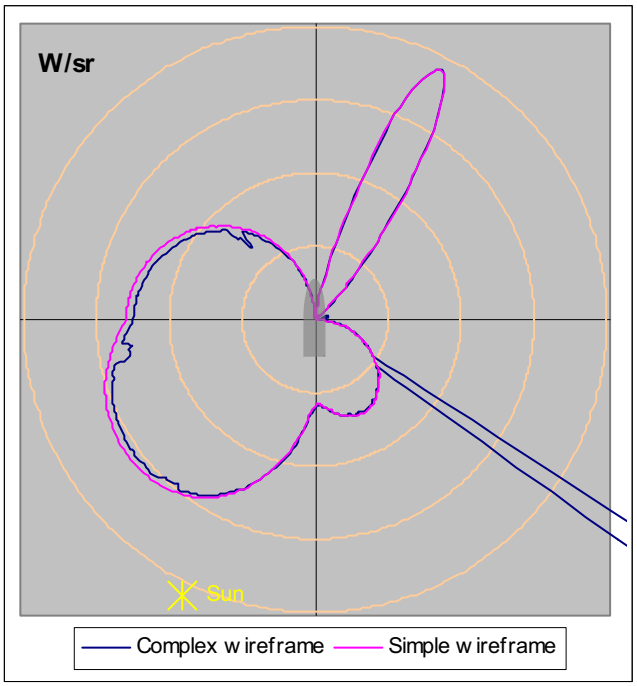

(a) Visible band

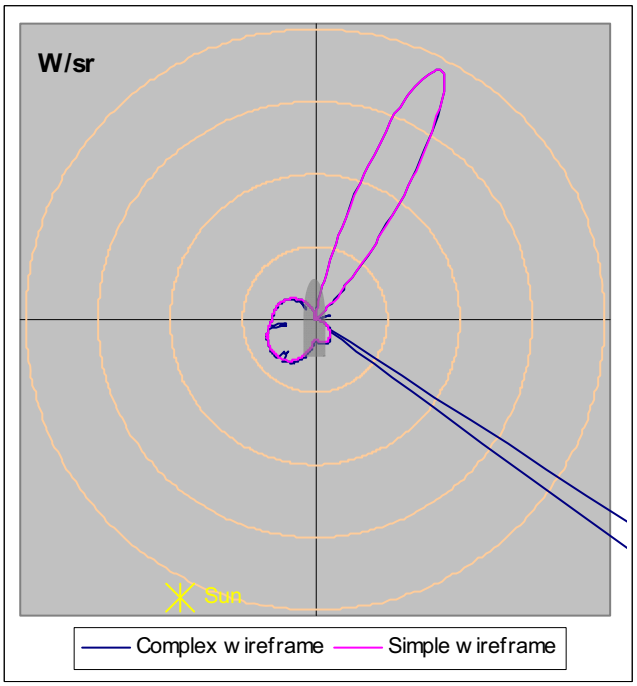

(b) Near-visible IR band

Figure C3 Background 1, 2 km viewing distance, reduced scale

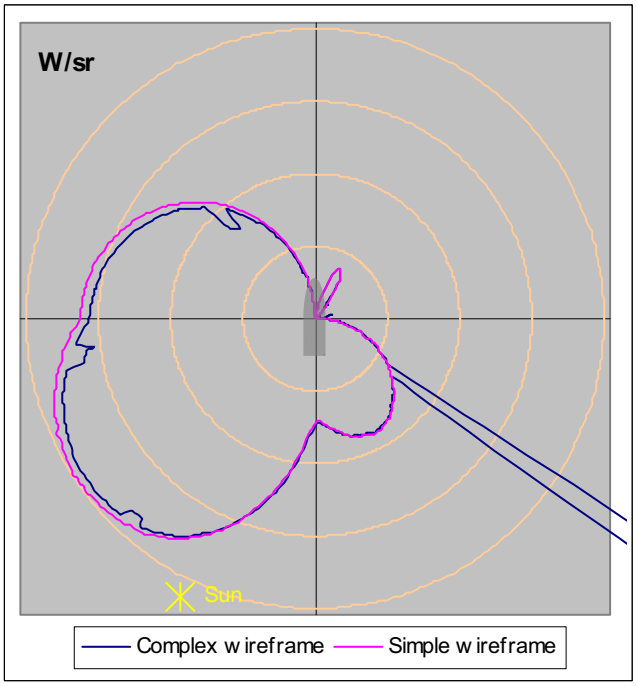

(a) Visible band

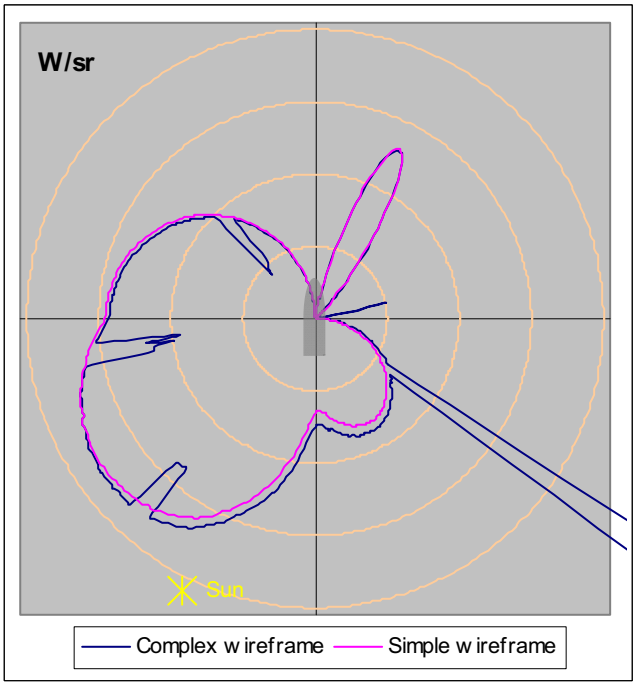

(b) Near-visible IR band

Figure C4 Background 1, 10 km viewing distance, reduced scale

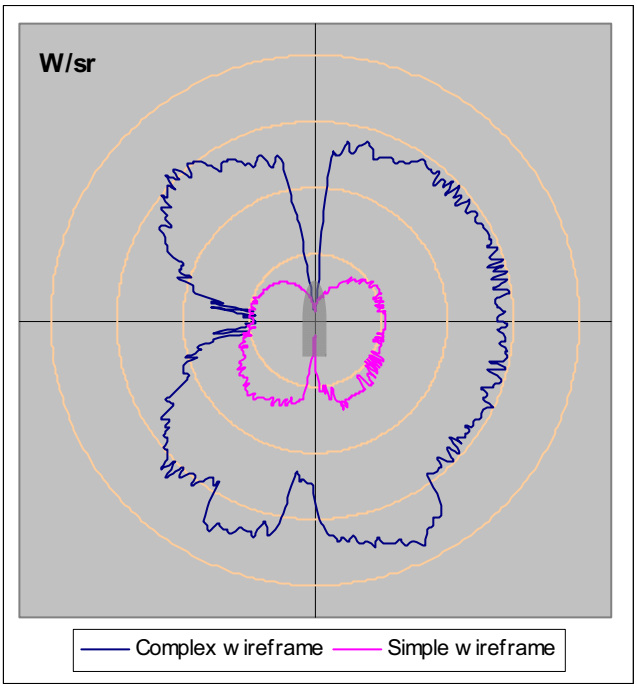

(a) Mid-wave IR band

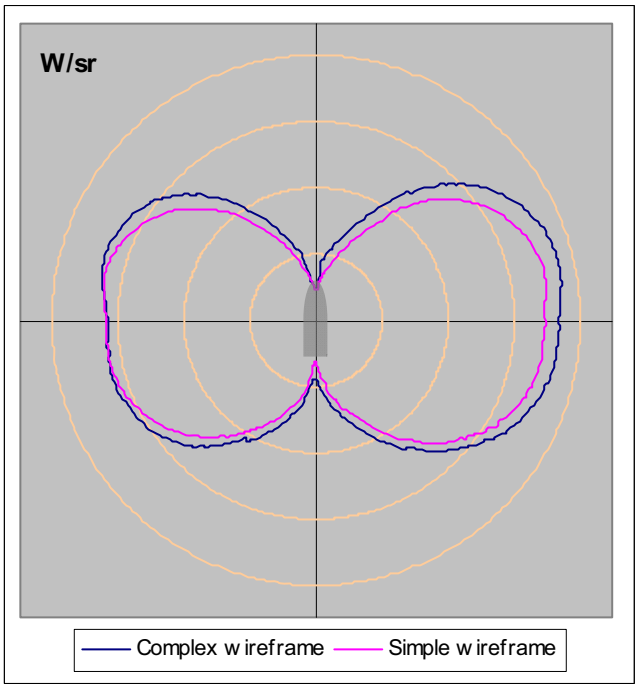

(b) Long-wave IR band

Figure C5 Background 2, 2 km viewing distance

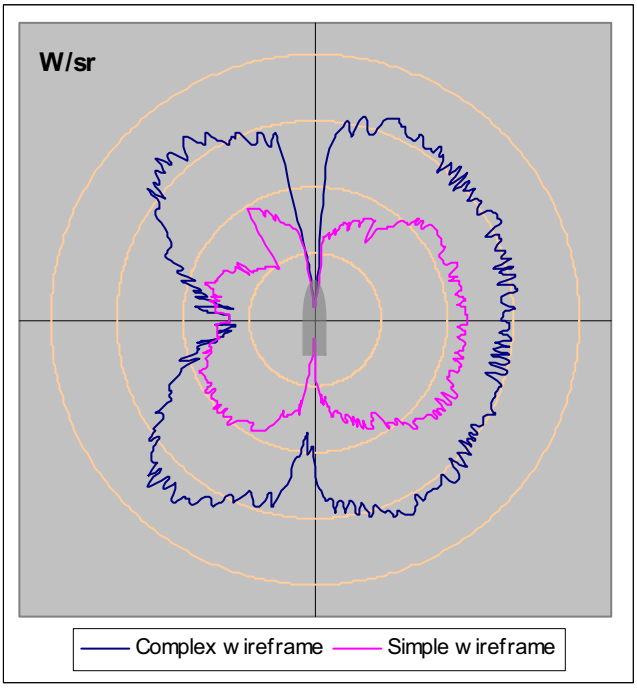

(a) Mid-wave IR band

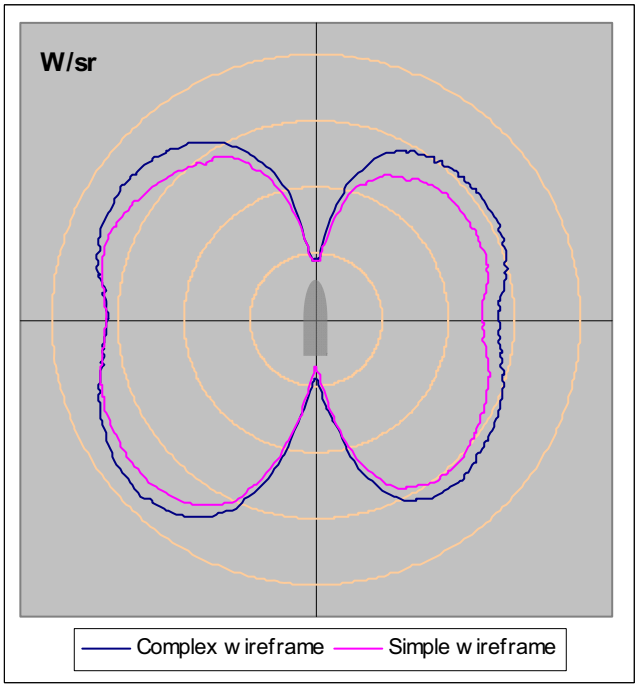

(b) Long-wave IR band

Figure C6 Background 2, 10 km viewing distance

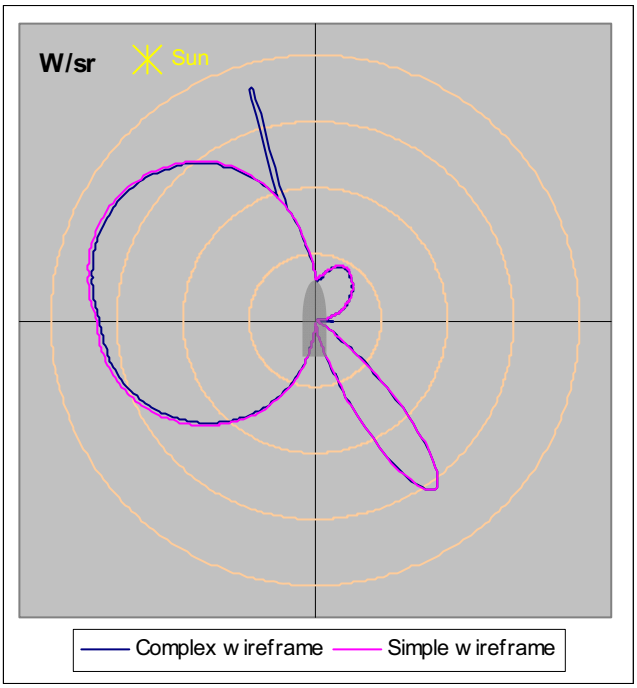

(a) Visible band

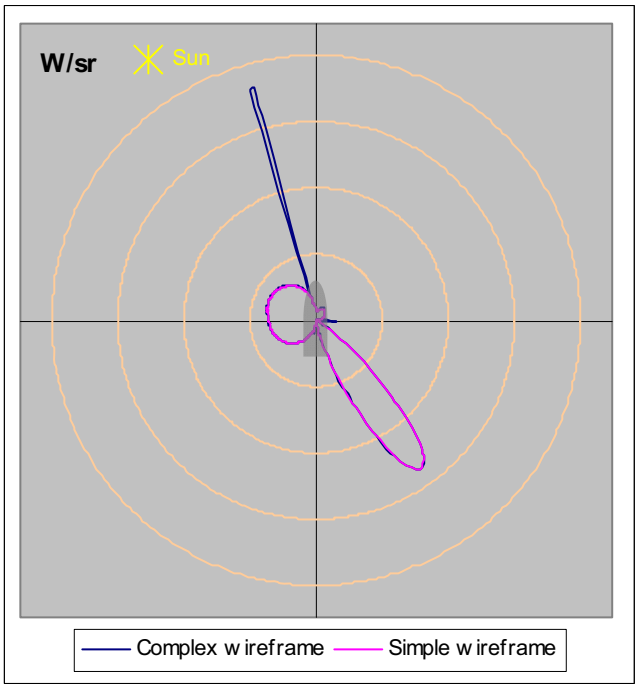

(b) Near-visible IR band

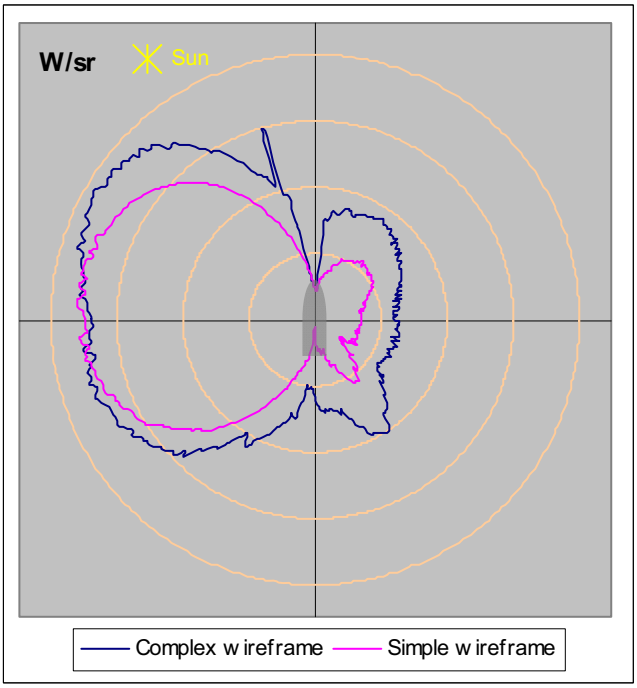

(c) Mid-wave IR band

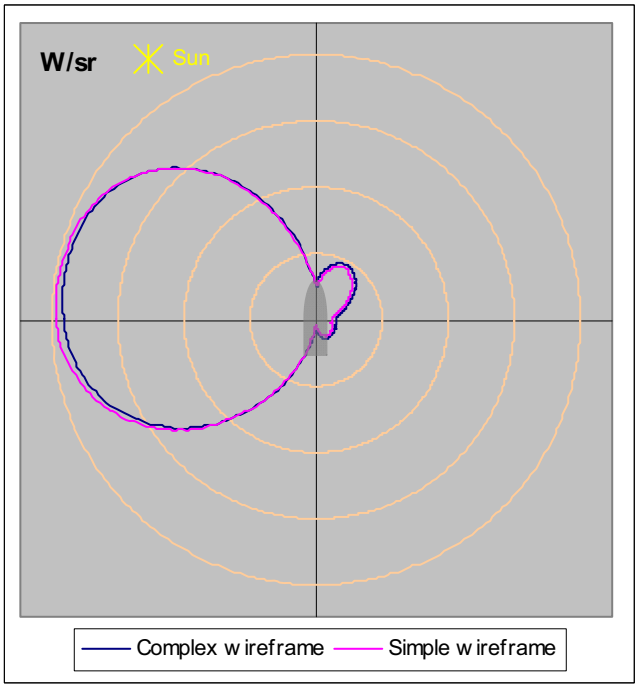

(d) Long-wave IR band

Figure C7 Background 3, 2 km viewing distance

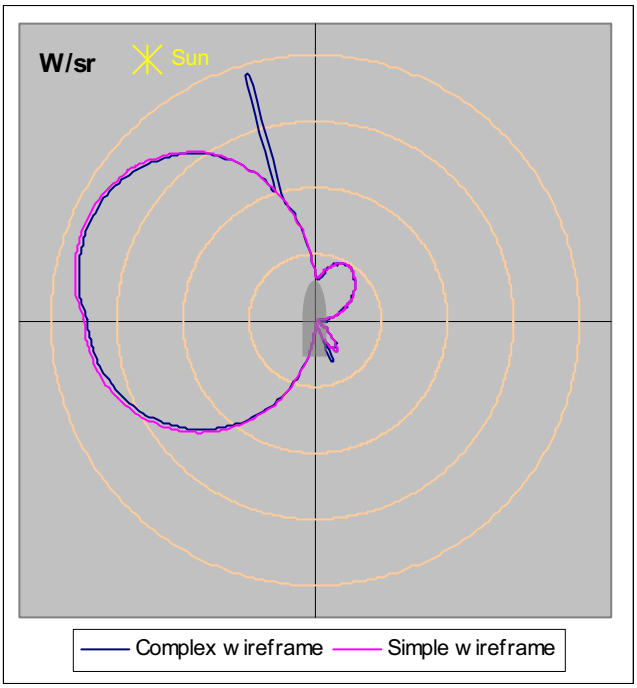

(a) Visible band

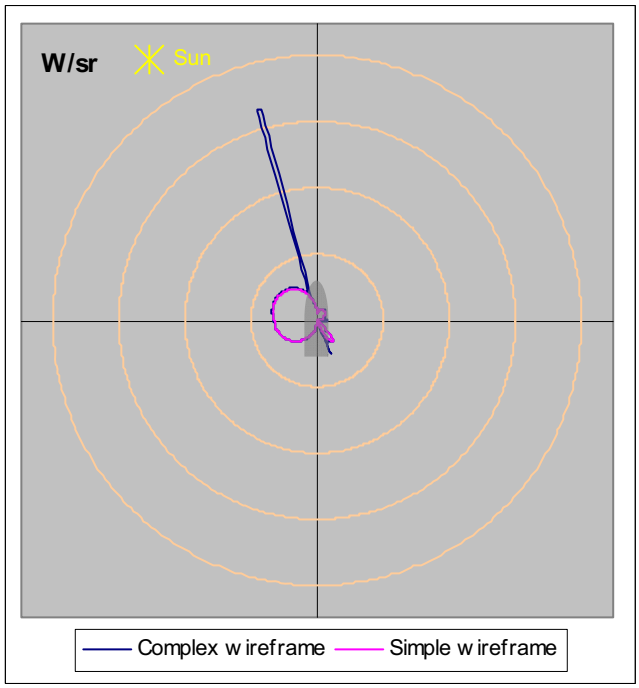

(b) Near-visible IR band

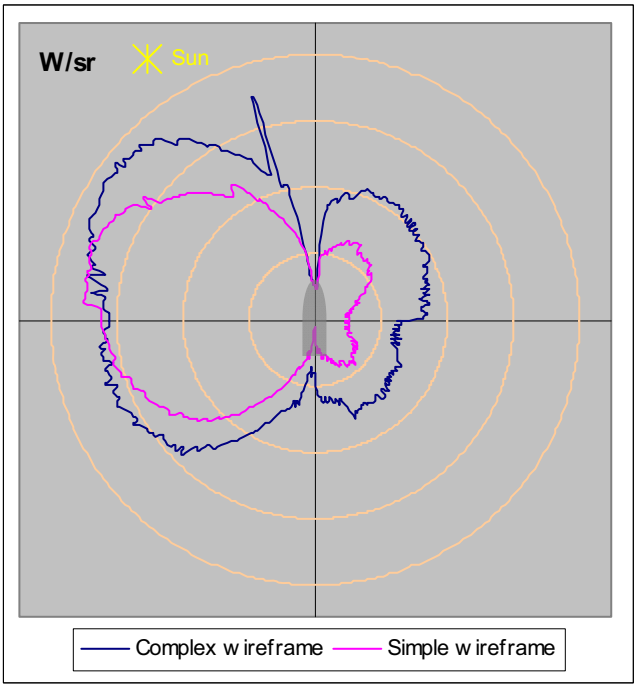

(c) Mid-wave IR band

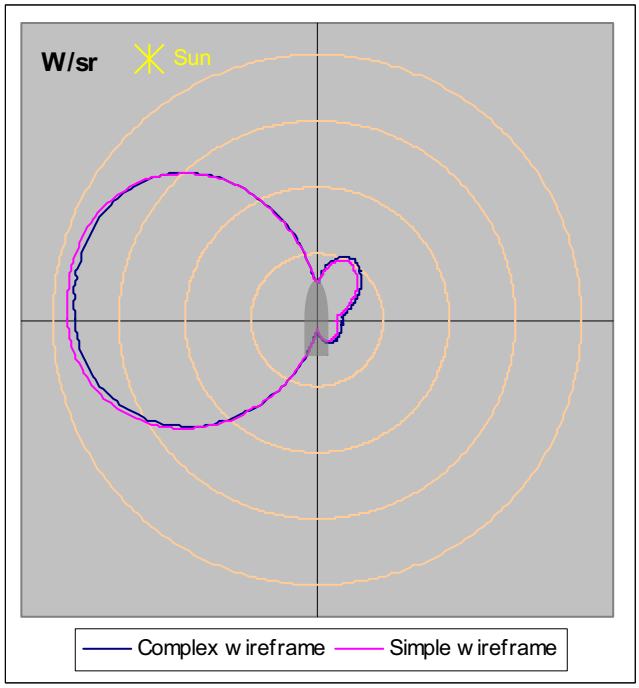

(d) Long-wave IR band

Figure C8 Background 3, 10 km viewing distance

C.2. Contrast signature plots for the two models, both with user-defined thermal boundary conditions but no exhaust plume

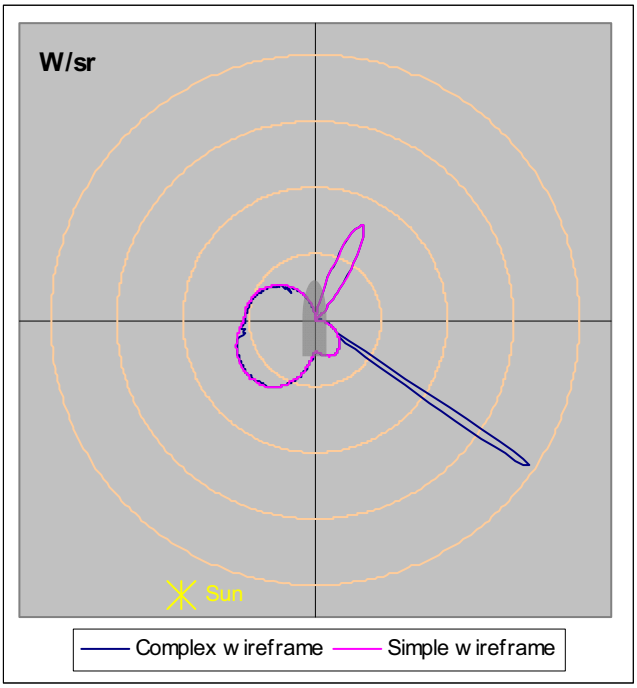

(a) Visible band

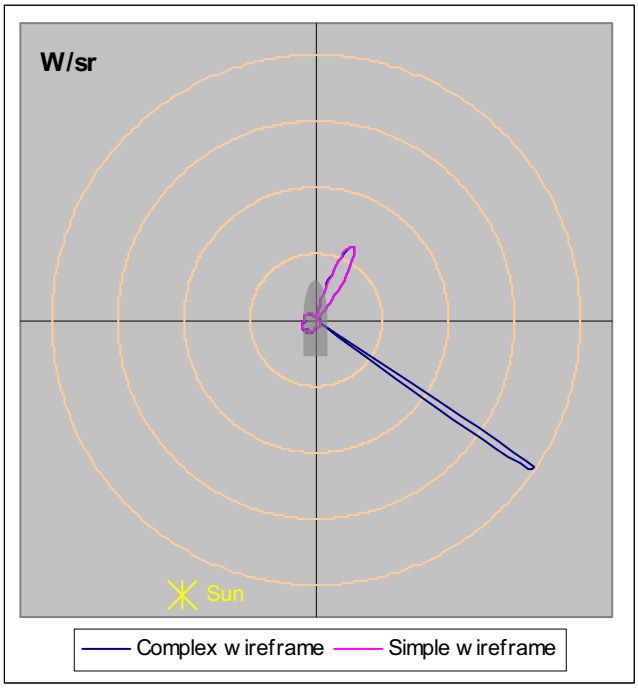

(b) Near-visible IR band

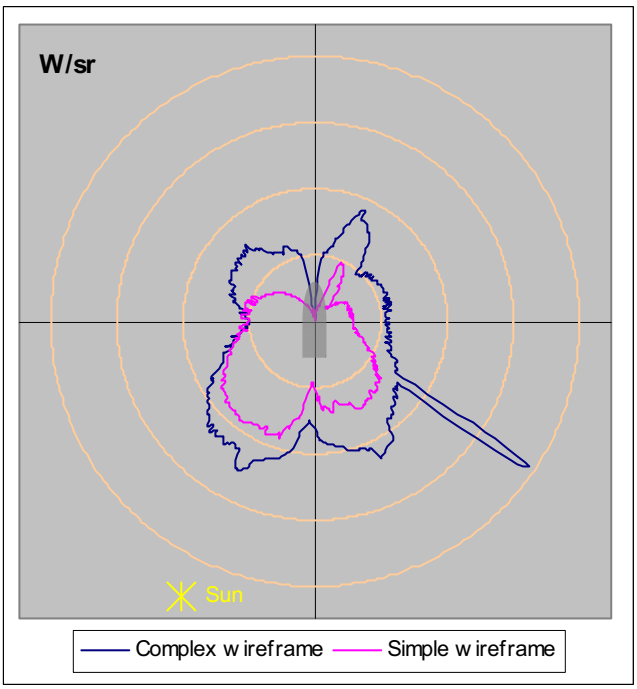

(c) Mid-wave IR band

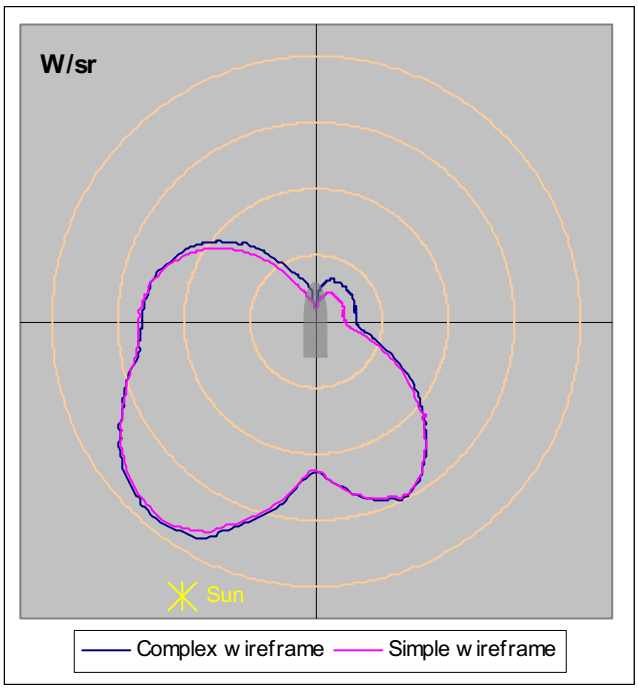

(d) Long-wave IR band

Figure C9 Background 1, 2 km viewing distance

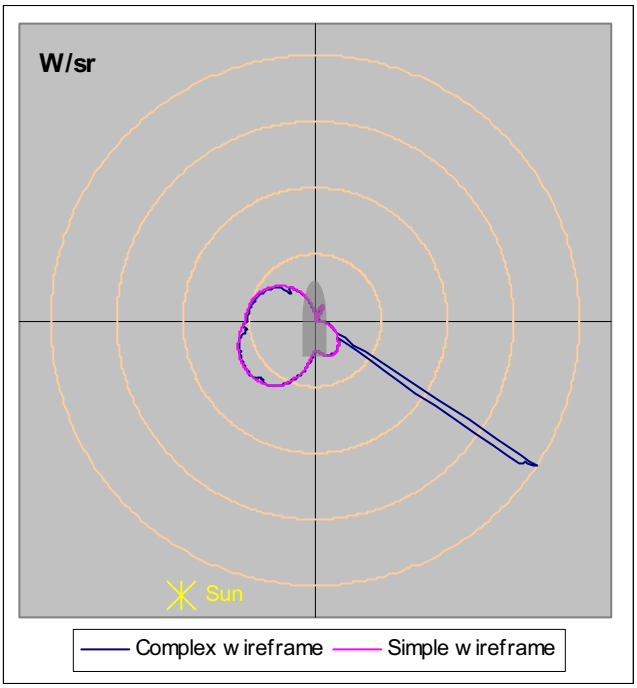

(a) Visible band

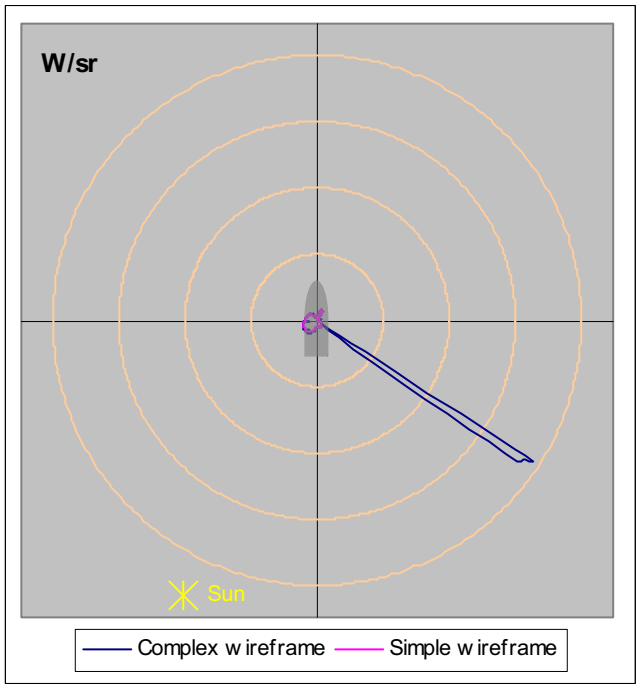

(b) Near-visible IR band

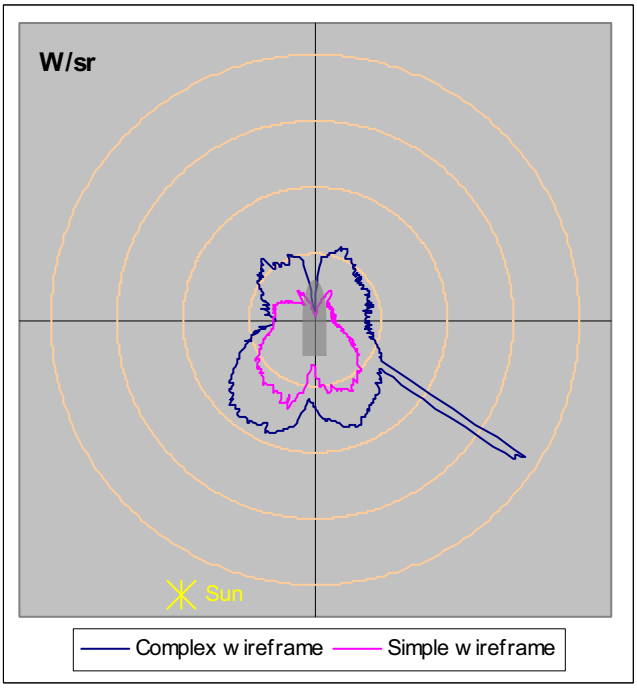

(c) Mid-wave IR band

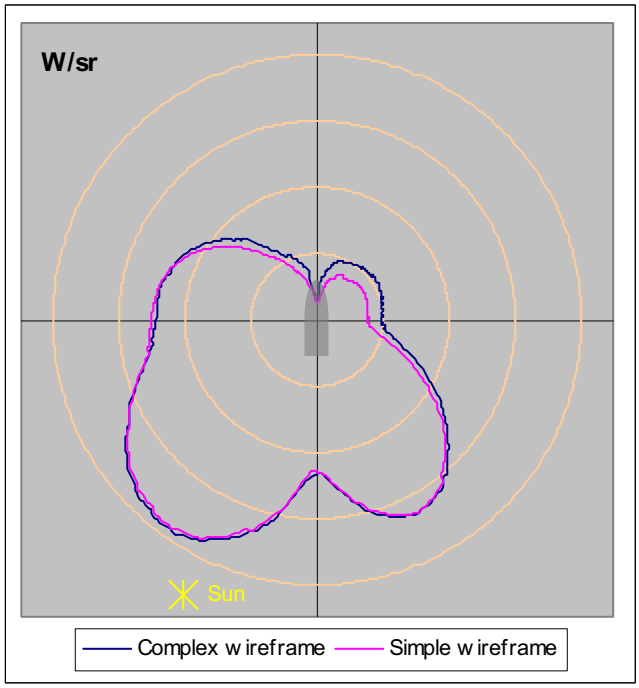

(d) Long-wave IR band

Figure C10 Background 1, 10 km viewing distance

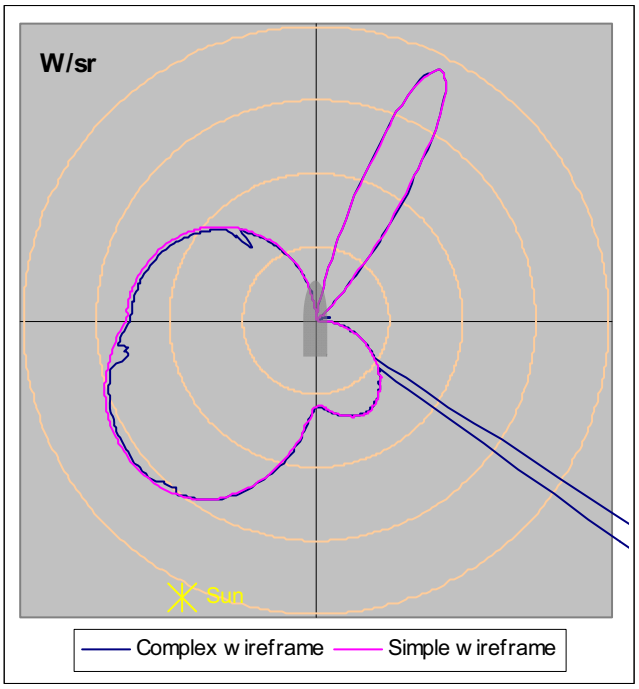

(a) Visible band

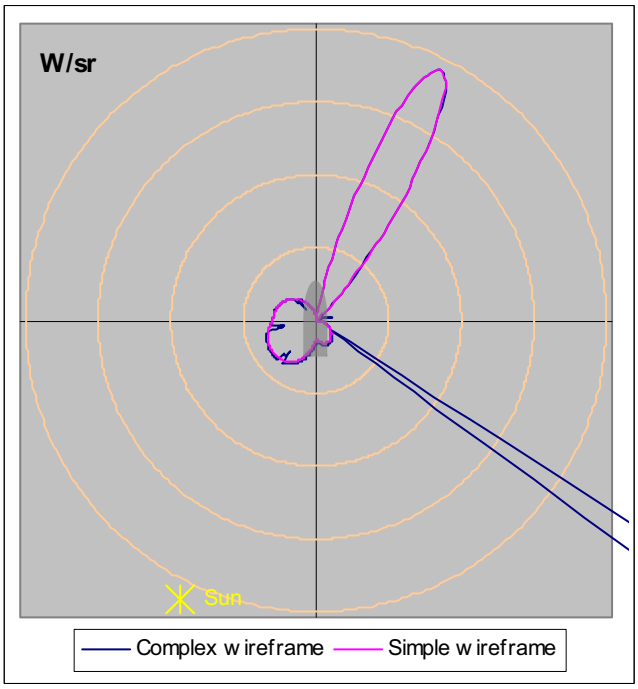

(b) Near-visible IR band

Figure C11 Background 1, 2 km viewing distance, reduced scale

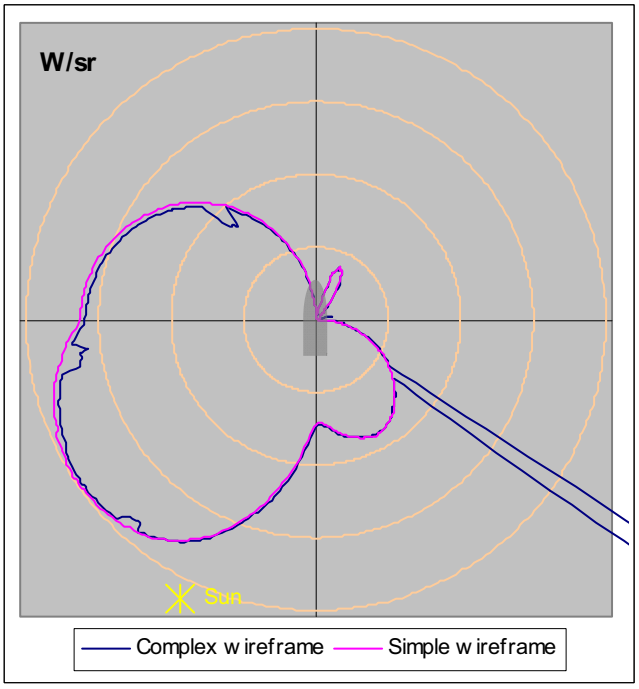

(a) Visible band

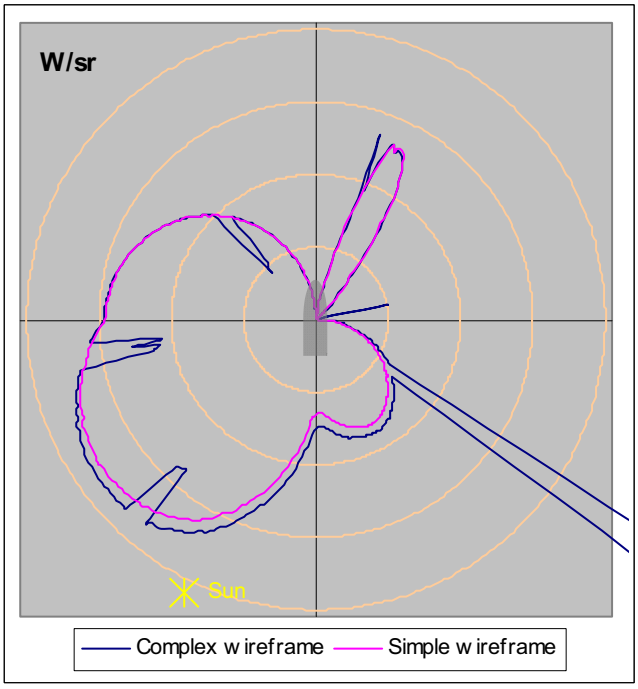

(b) Near-visible IR band

Figure C12 Background 1, 10 km viewing distance, reduced scale

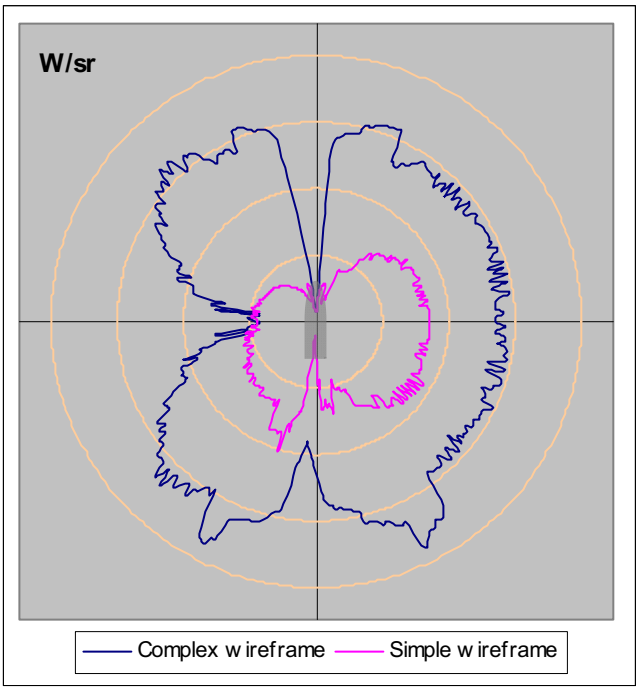

(a) Mid-wave IR band

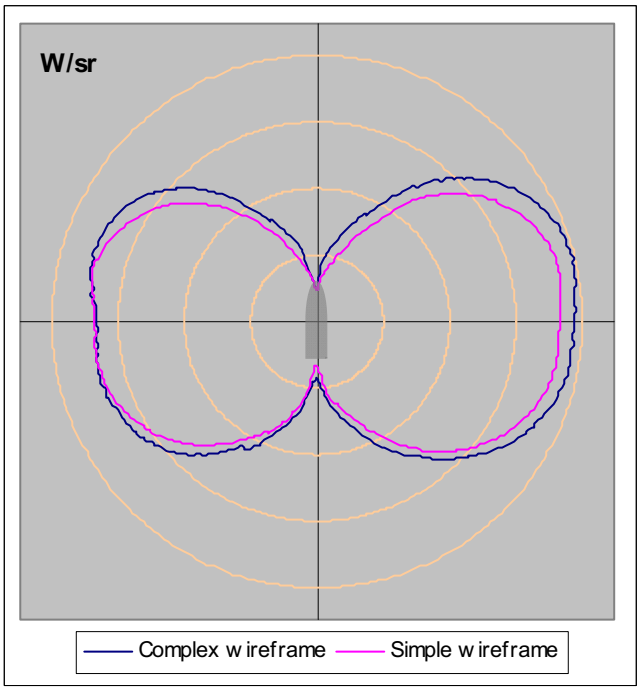

(b) Long-wave IR band

Figure C13 Background 2, 2 km viewing distance

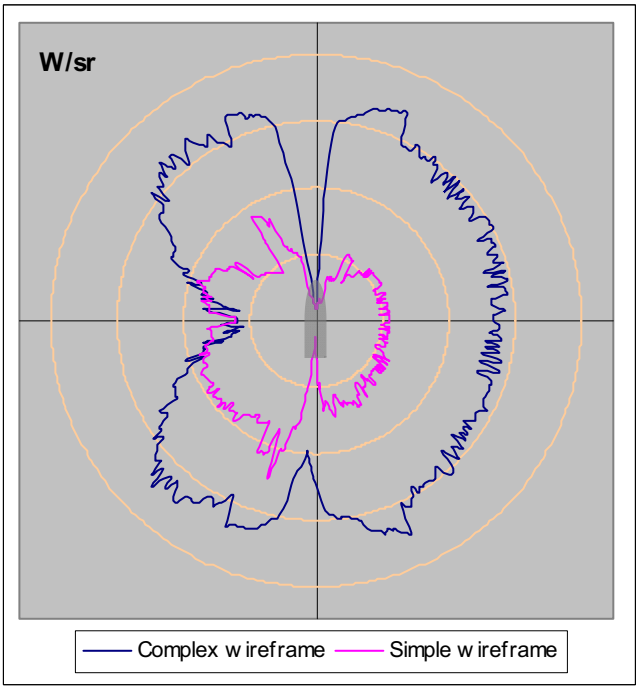

(a) Mid-wave IR band

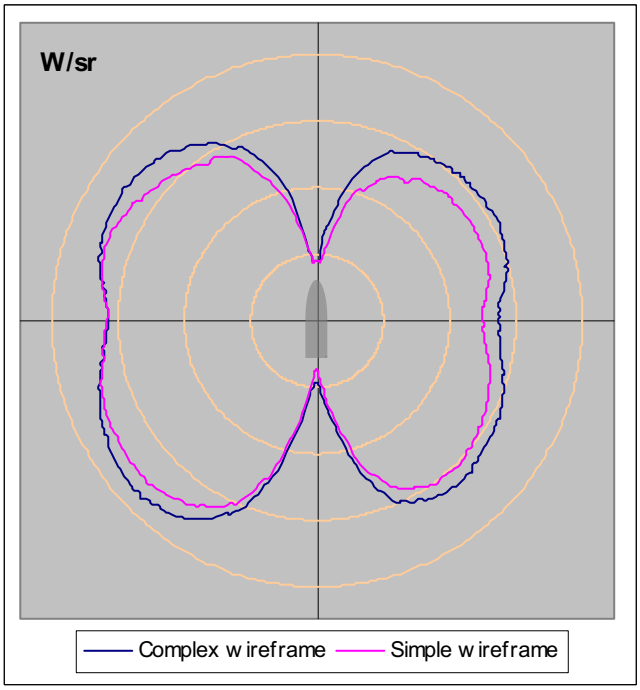

(b) Long-wave IR band

Figure C14 Background 2, 10 km viewing distance

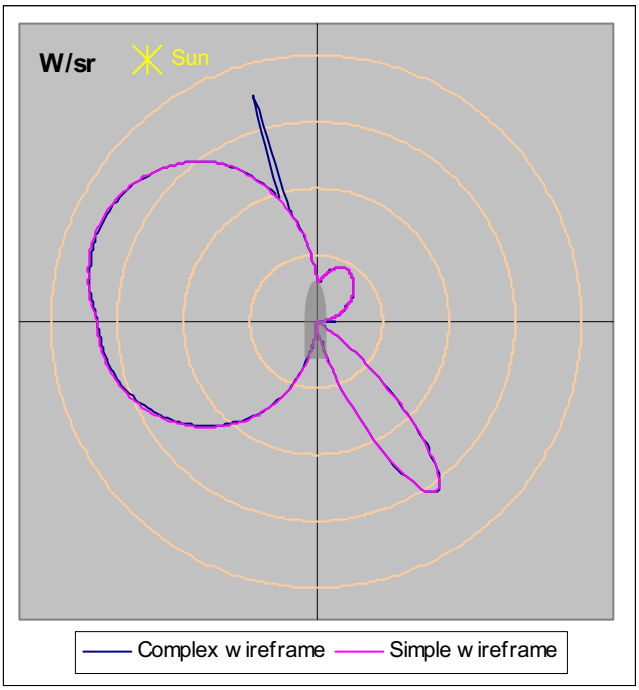

(a) Visible band

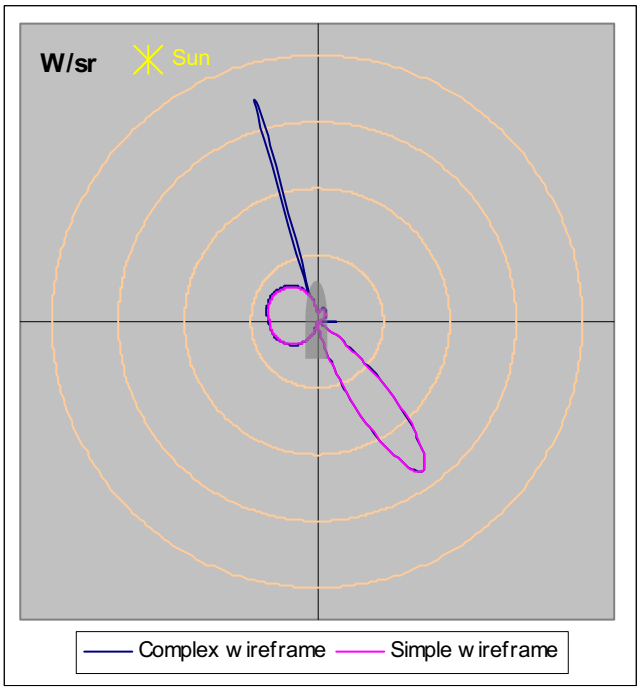

(b) Near-visible IR band

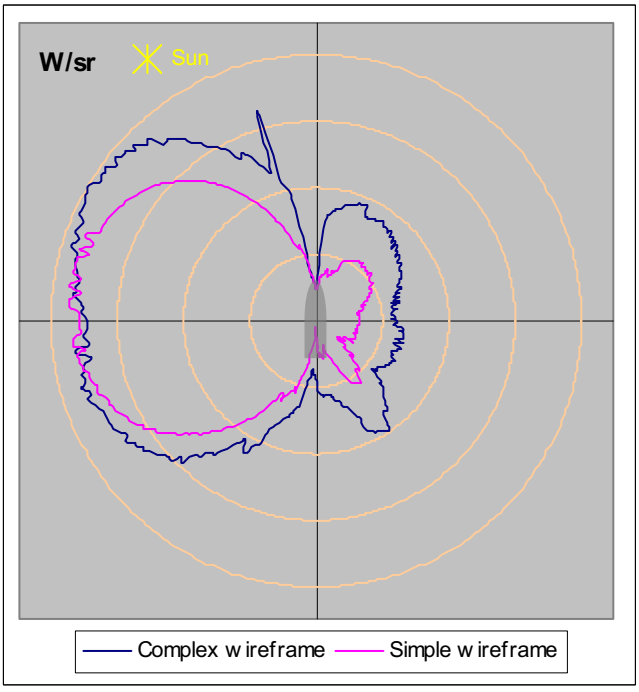

(c) Mid-wave IR band

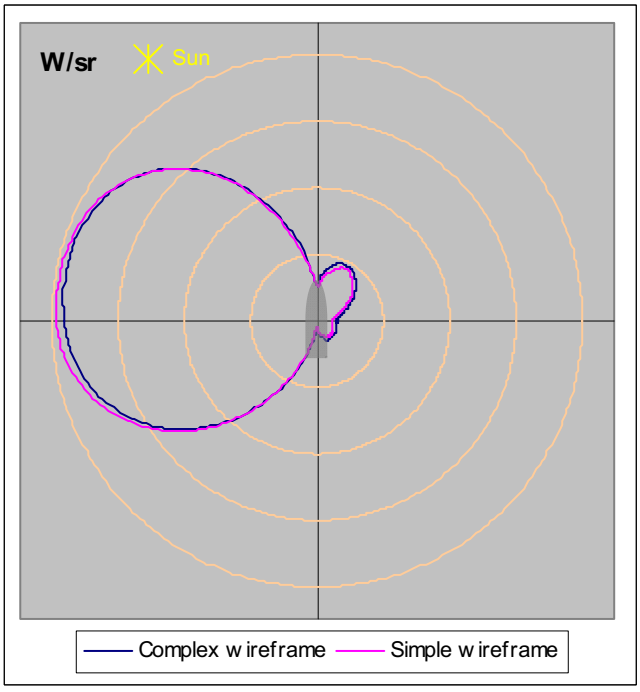

(d) Long-wave IR band

Figure C15 Background 3, 2 km viewing distance

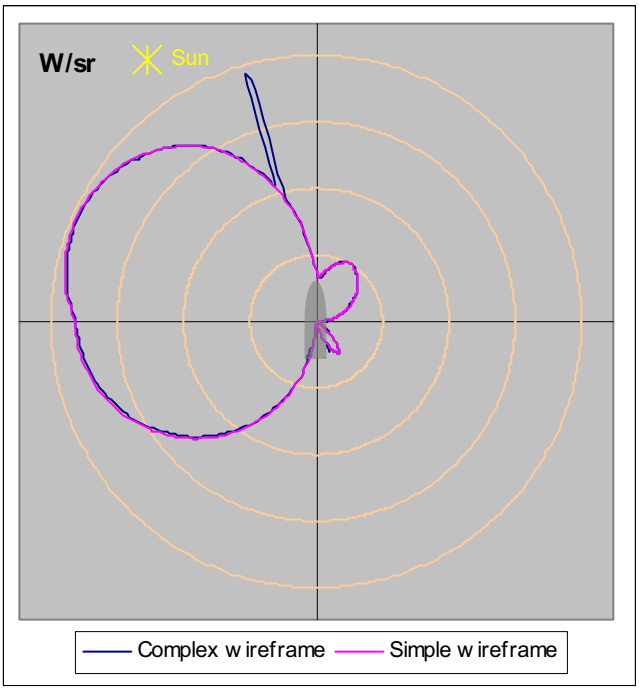

(a) Visible band

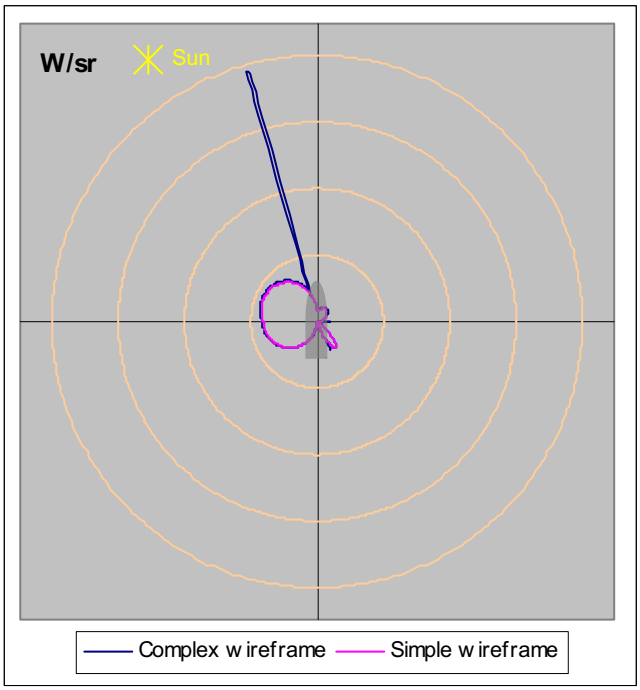

(b) Near-visible IR band

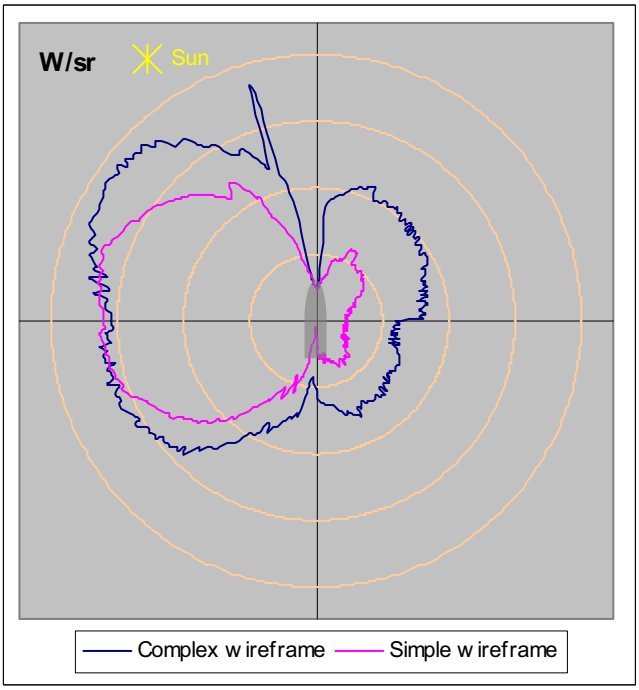

(c) Mid-wave IR band

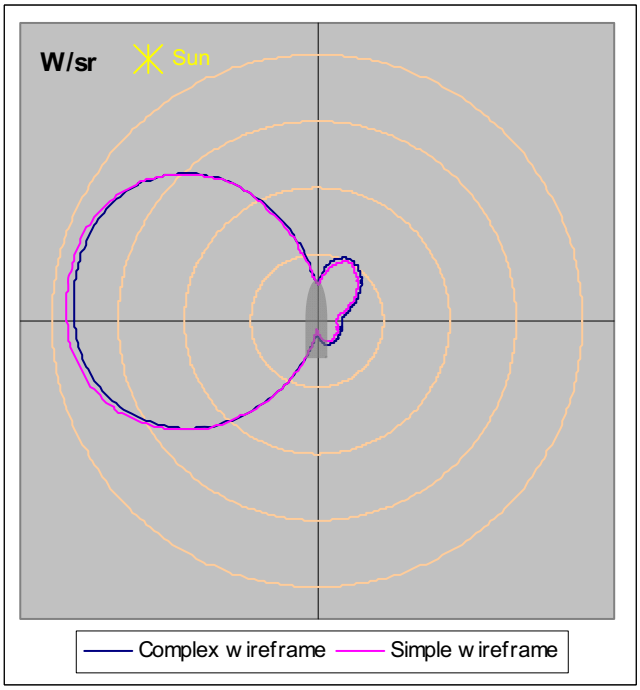

(d) Long-wave IR band

Figure C16 Background 3, 10 km viewing distance

C.3. Contrast signature plots for the two models, both with no user-defined thermal boundary conditions or exhaust plume

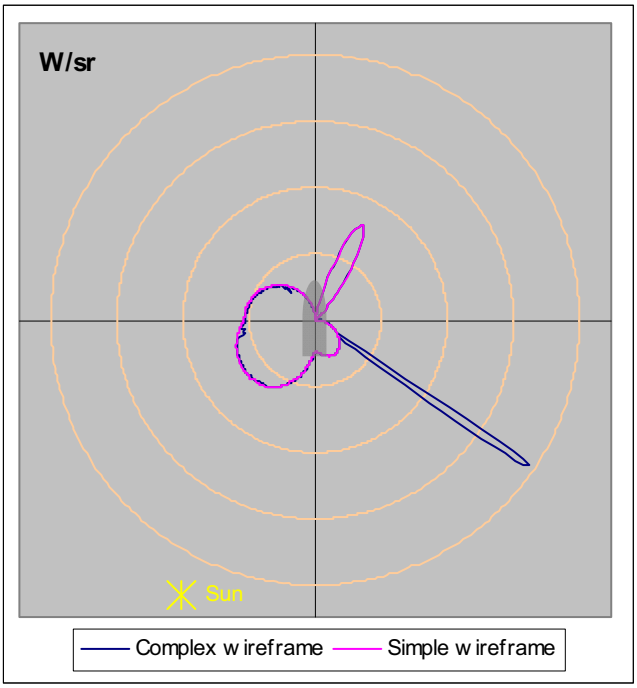

(a) Visible band

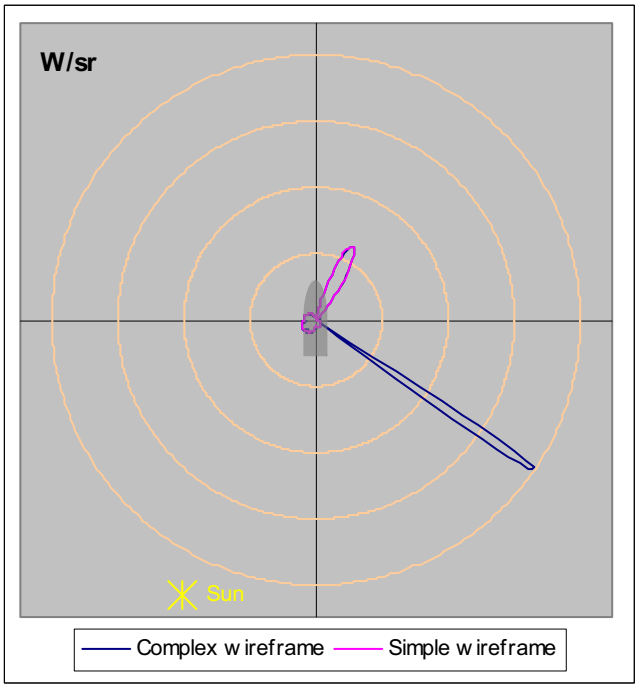

(b) Near-visible IR band

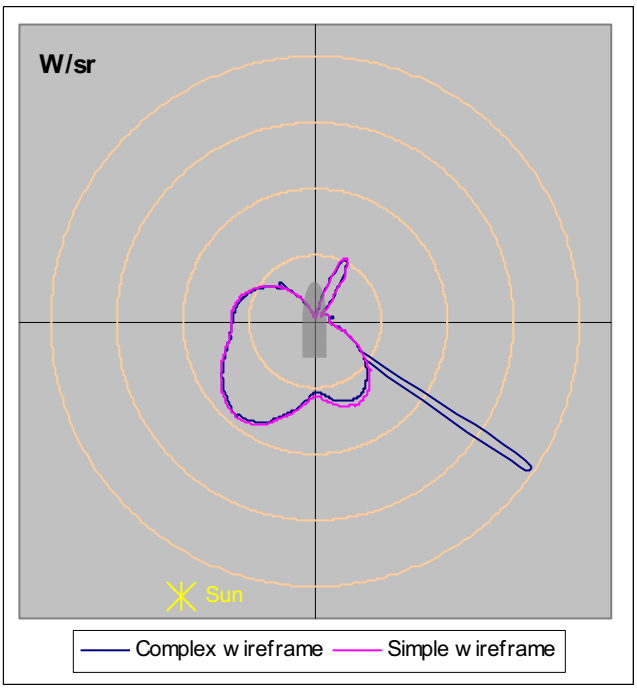

(c) Mid-wave IR band

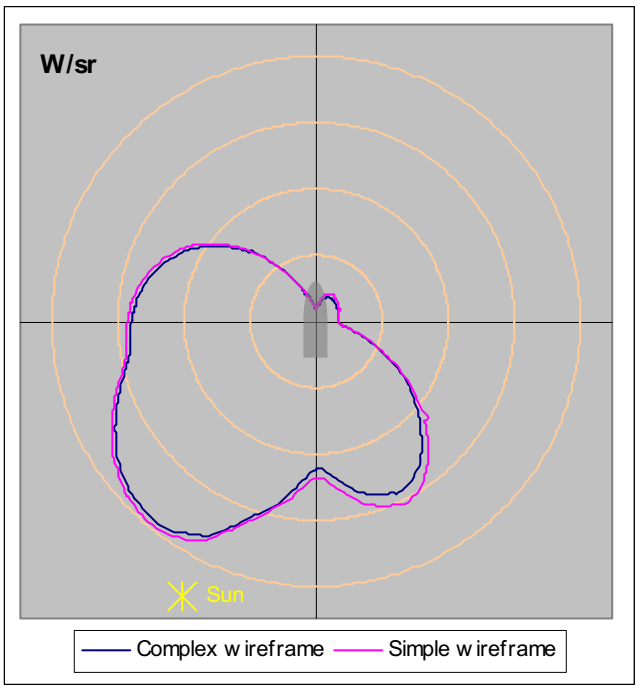

(d) Long-wave IR band

Figure C17 Background 1, 2 km viewing distance

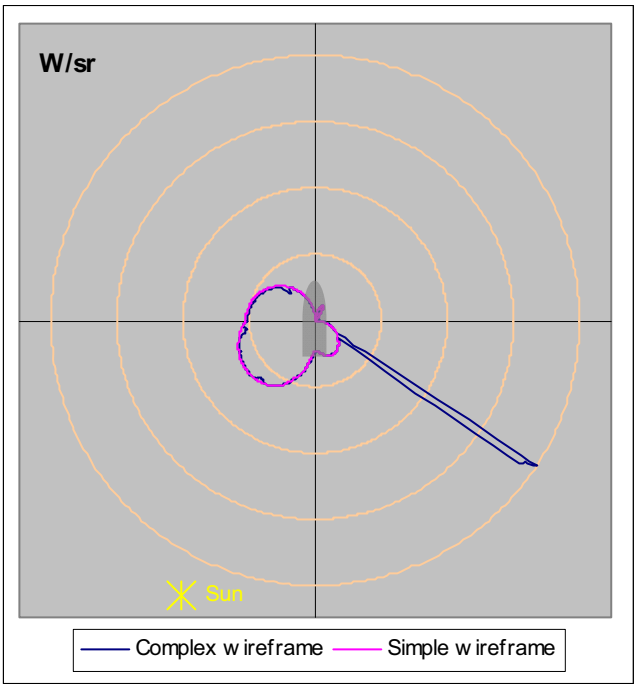

(a) Visible band

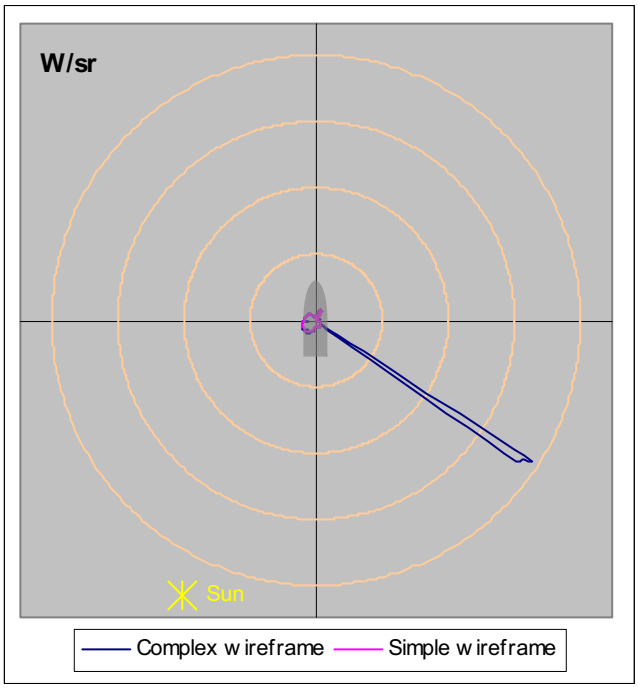

(b) Near-visible IR band

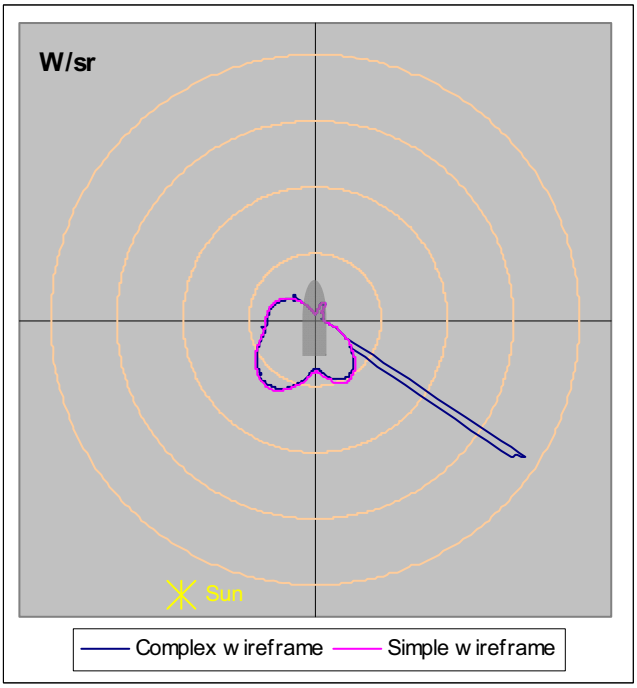

(c) Mid-wave IR band

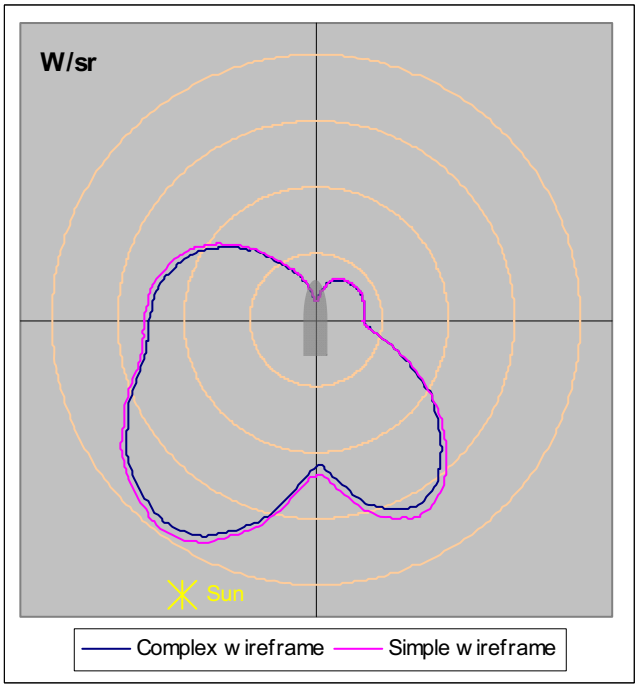

(d) Long-wave IR band

Figure C18 Background 1, 10 km viewing distance

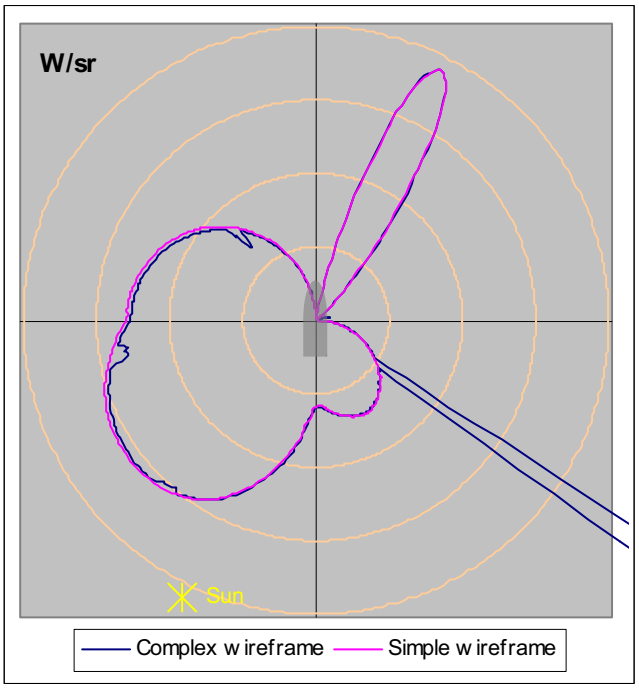

(a) Visible band

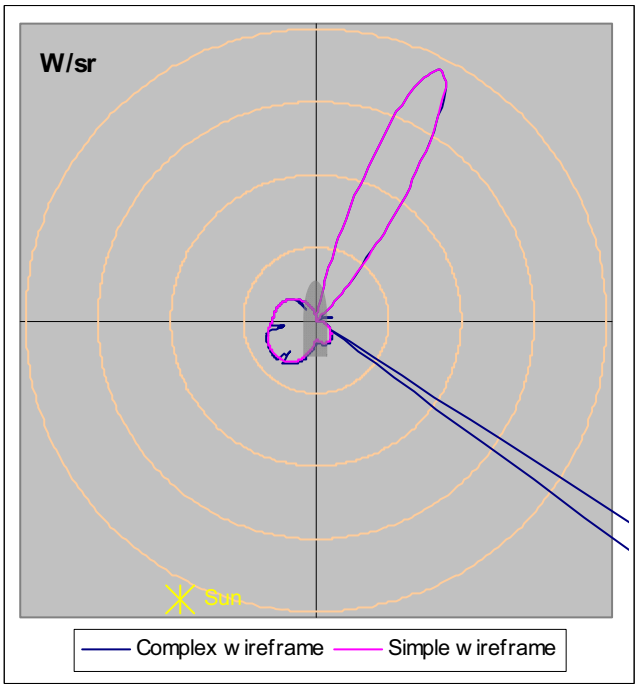

(b) Near-visible IR band

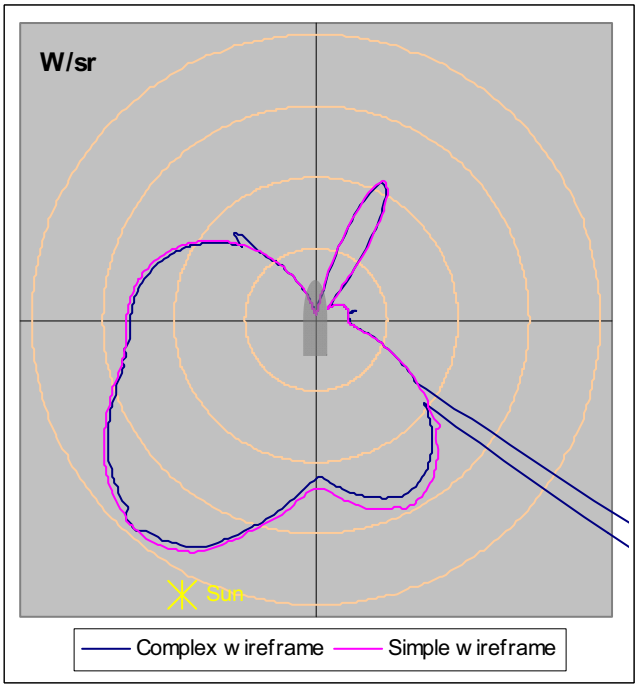

(c) Mid-wave IR band

Figure C19 Background 1, 2 km viewing distance, reduced scale

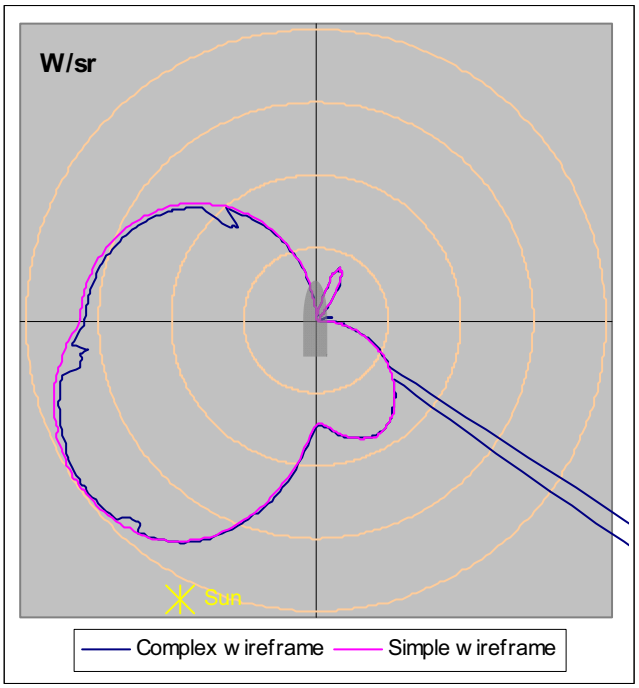

(a) Visible band

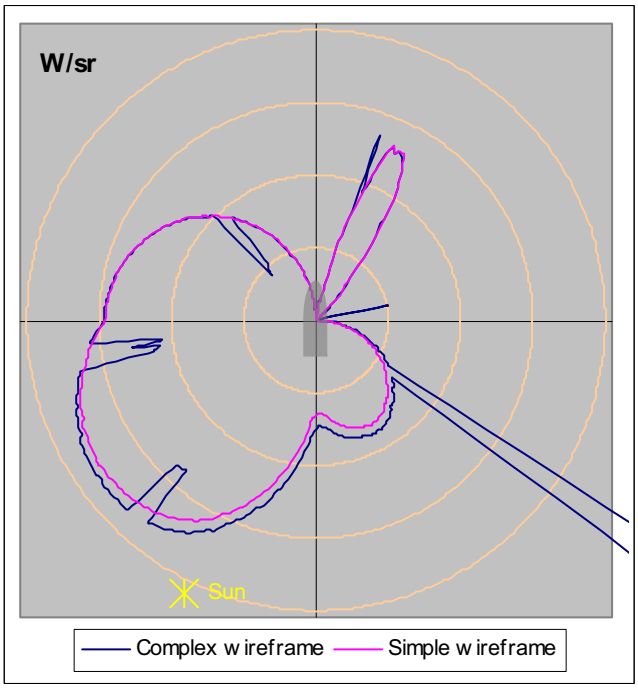

(b) Near-visible IR band

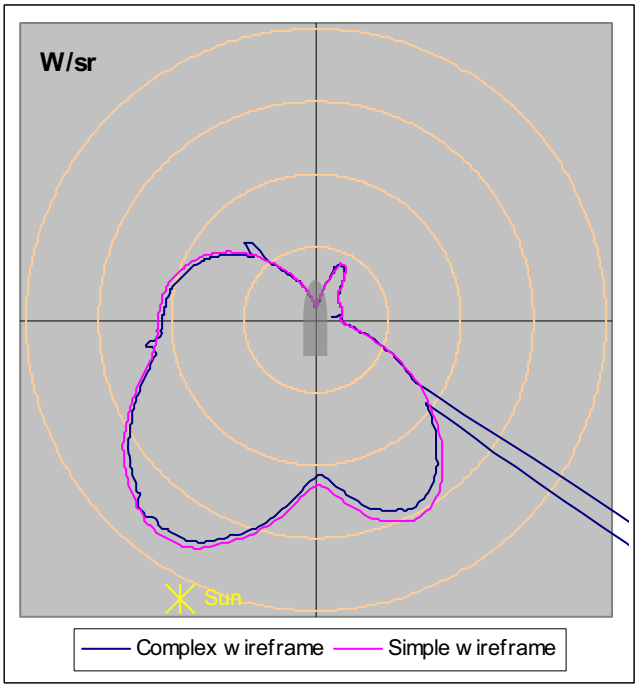

(c) Mid-wave IR band

Figure C20 Background 1, 10 km viewing distance, reduced scale

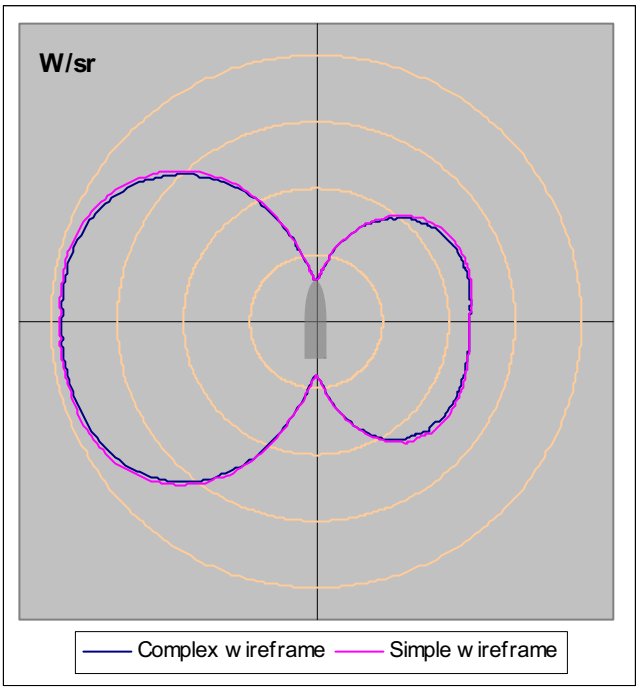

(a) Mid-wave IR band

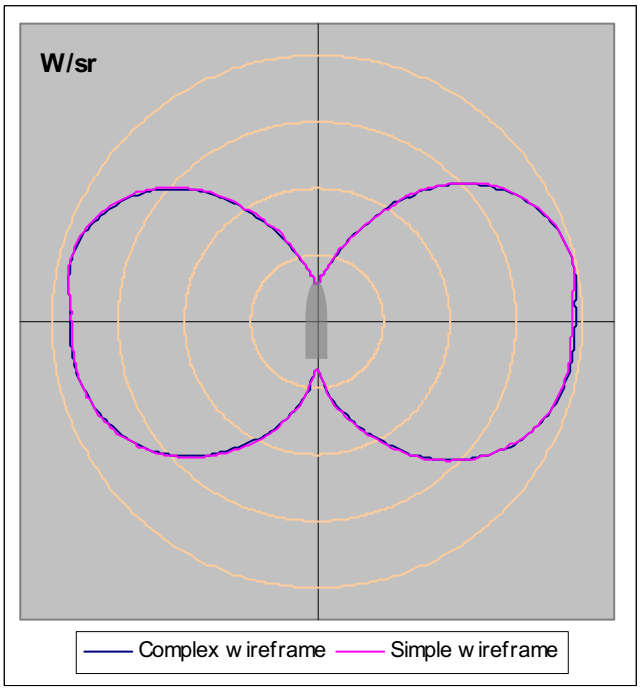

(b) Long-wave IR band

Figure C21 Background 2, 2 km viewing distance

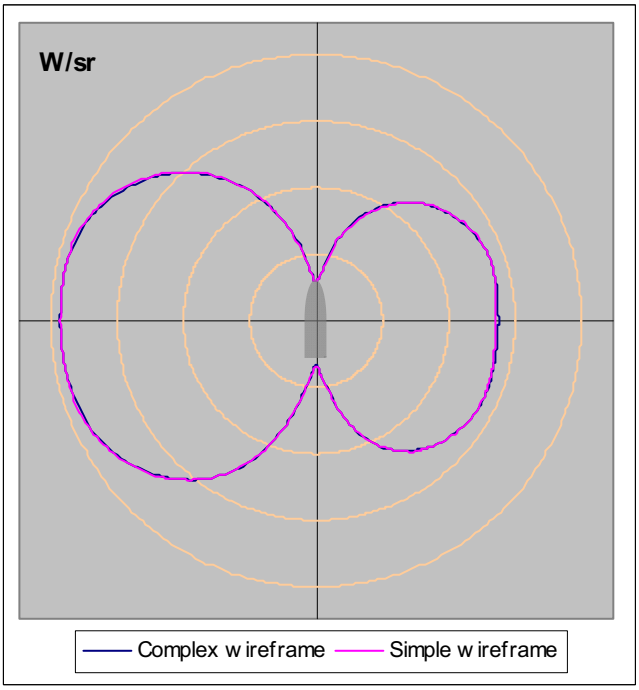

(a) Mid-wave IR band

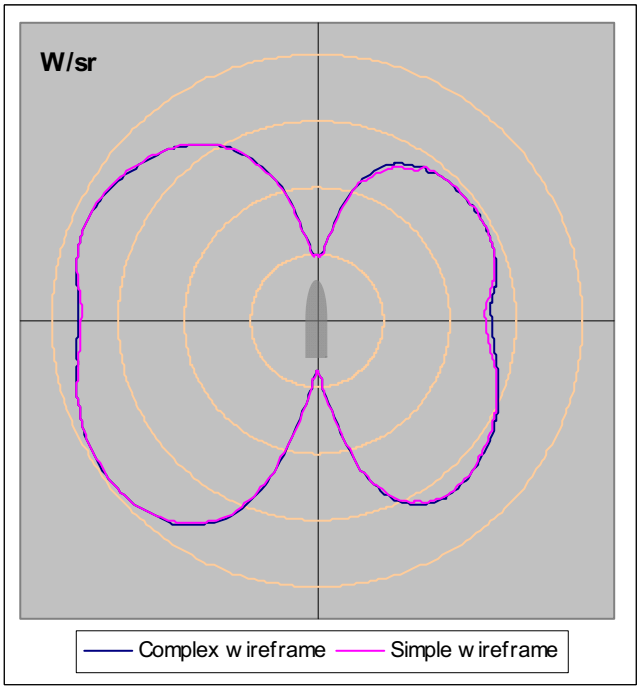

(b) Long-wave IR band

Figure C22 Background 2, 10 km viewing distance

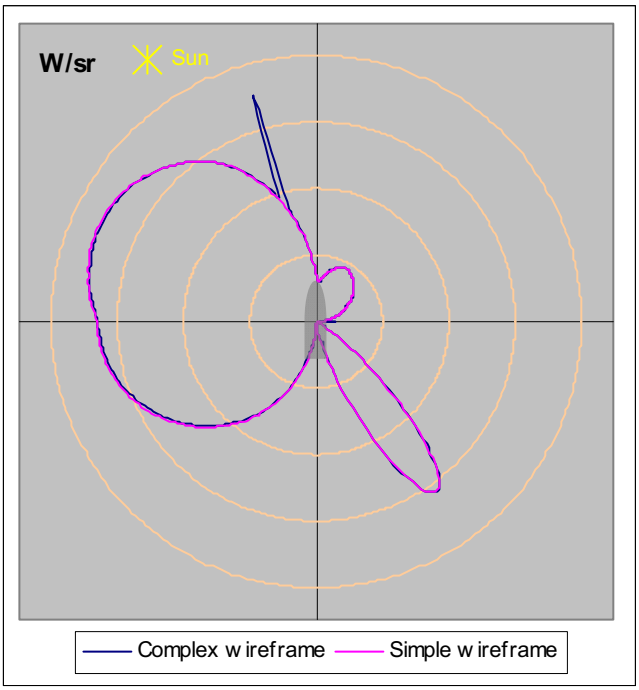

(a) Visible band

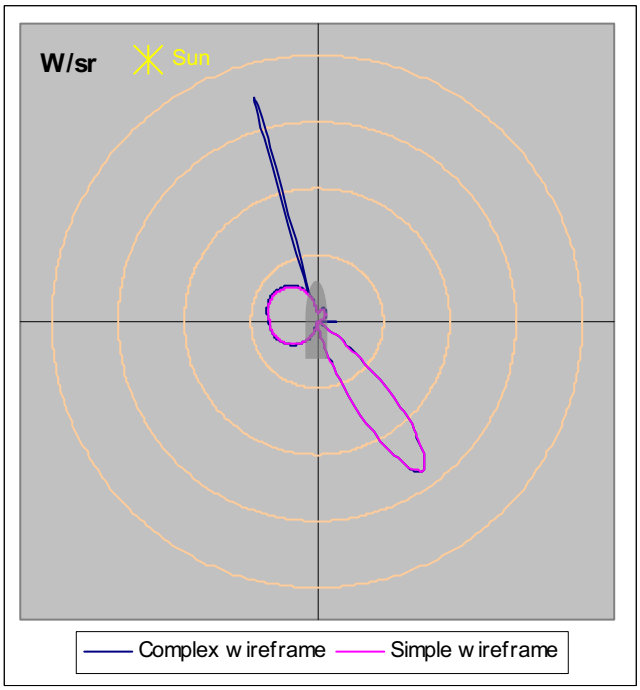

(b) Near-visible IR band

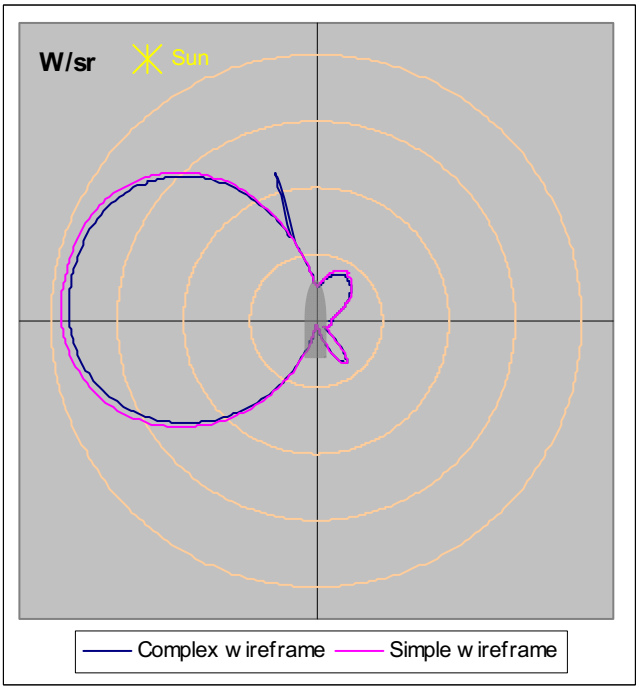

(c) Mid-wave IR band

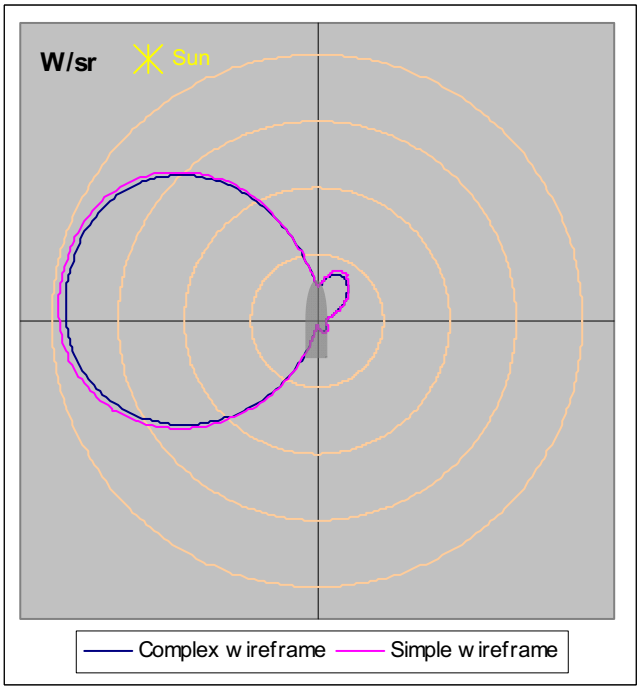

(d) Long-wave IR band

Figure C23 Background 3, 2 km viewing distance

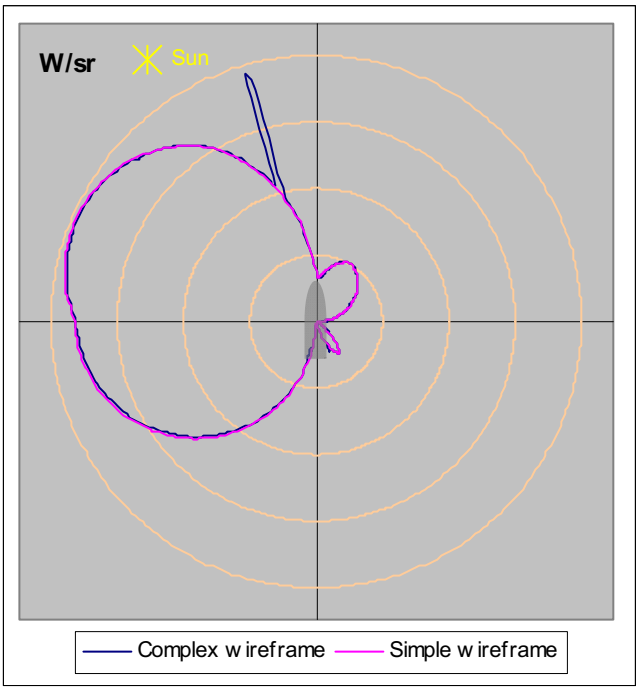

(a) Visible band

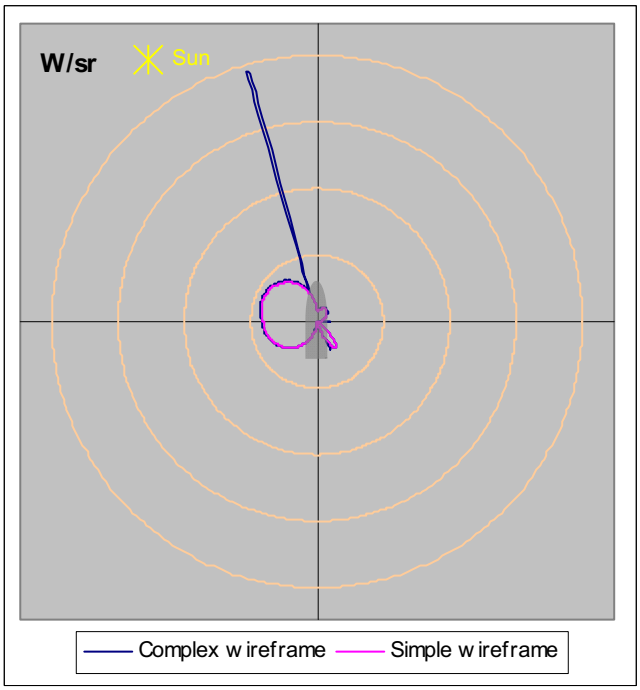

(b) Near-visible IR band

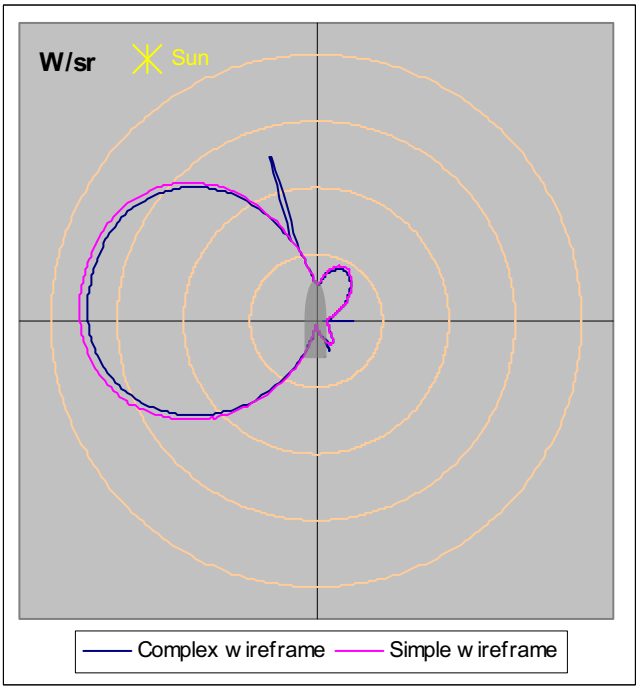

(c) Mid-wave IR band

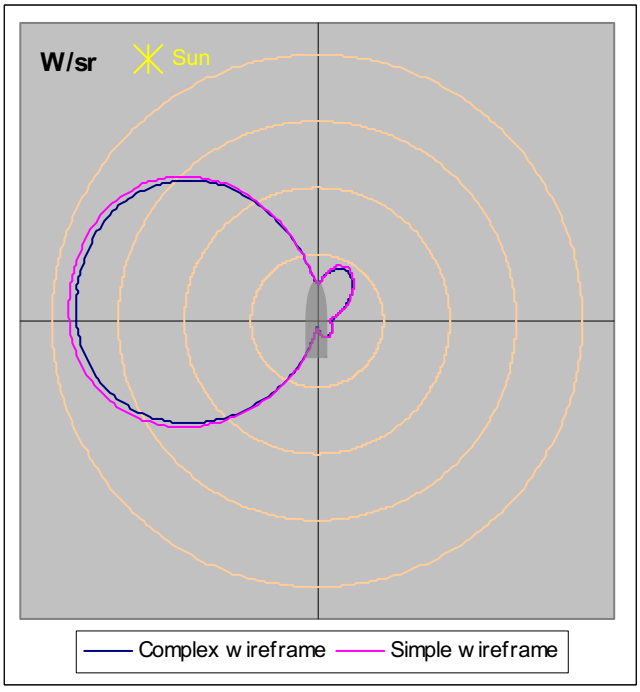

(d) Long-wave IR band

Figure C24 Background 3, 10 km viewing distance

Appendix D: OF contrast signature data —Simple wireframe versus complex wireframe, both with near-infrared reflecting paints (NIRR)

The following plots depict the apparent absolute contrast intensity data calculated for the two models with NIRR paints that were used in the investigation of wireframe detail. The plots are grouped into three sections: those comparing the results generated for the models with user-defined thermal boundary conditions and an exhaust plume; those comparing the results generated for the models with user-defined thermal boundary conditions but no exhaust plume; and those comparing the results generated for the models with no user-defined thermal boundary conditions or exhaust plume. It should be noted that no results are presented for Background 2 and the visible and near-visible IR bands as the platform is not detectable under these conditions. (For details of the backgrounds and the OF wavebands, refer to Section 3.)

D.1. Contrast signature plots for the two models, both with user-defined thermal boundary conditions and an exhaust plume

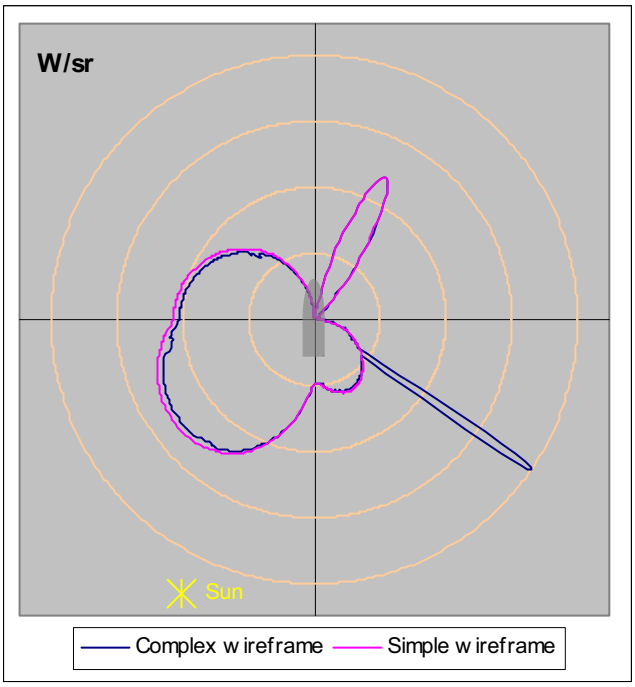

(a) Visible band

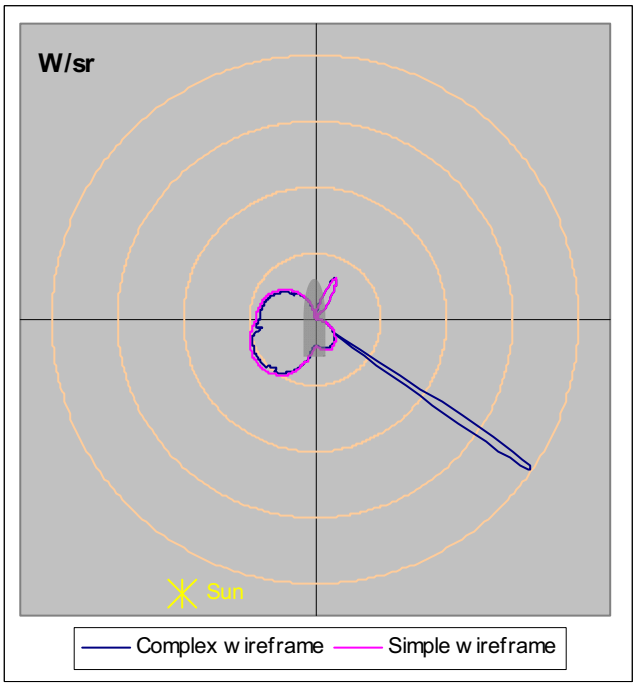

(b) Near-visible IR band

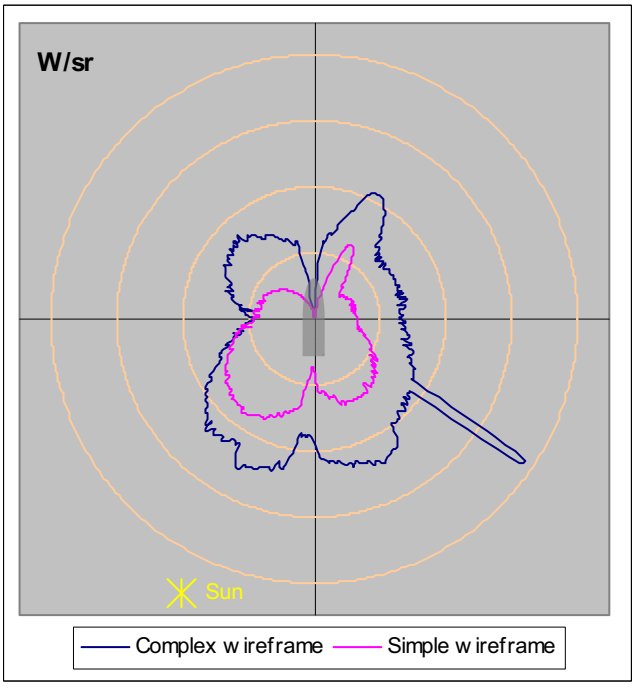

(c) Mid-wave IR band

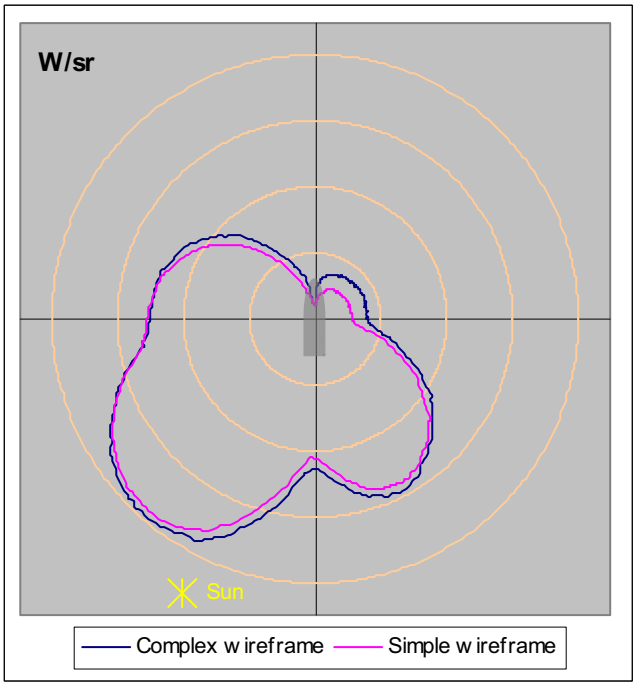

(d) Long-wave IR band

Figure D1 Background 1, 2 km viewing distance

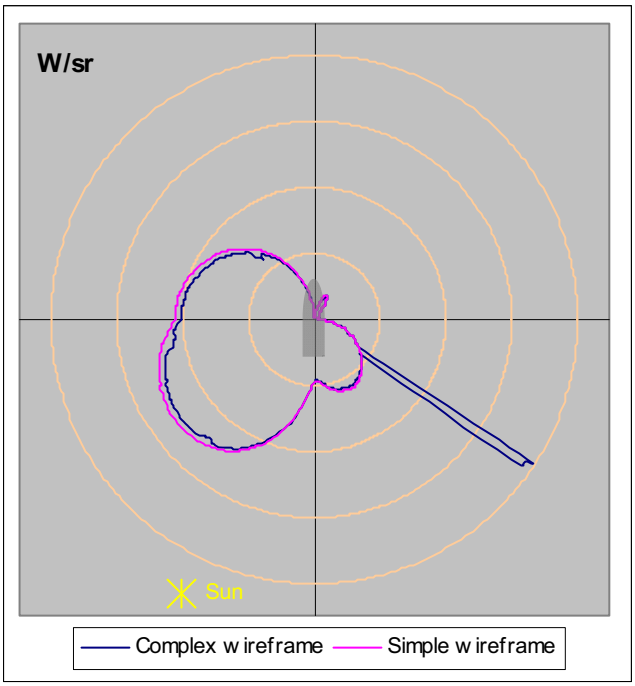

(a) Visible band

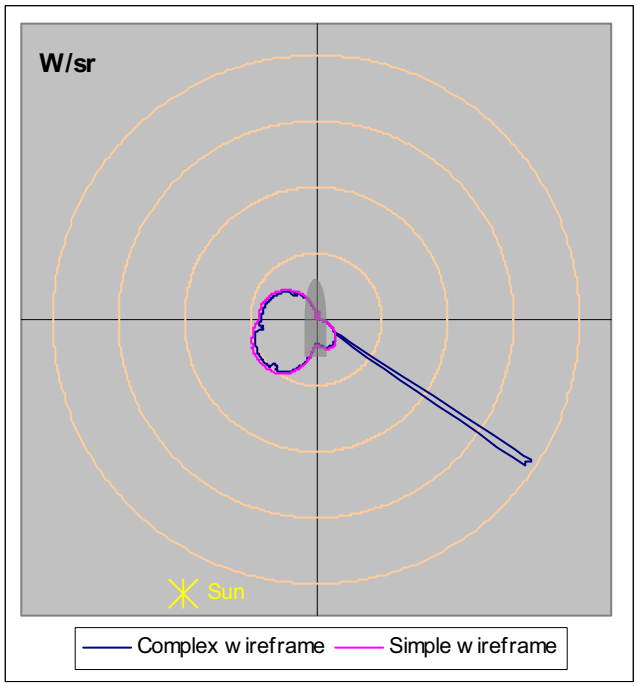

(b) Near-visible IR band

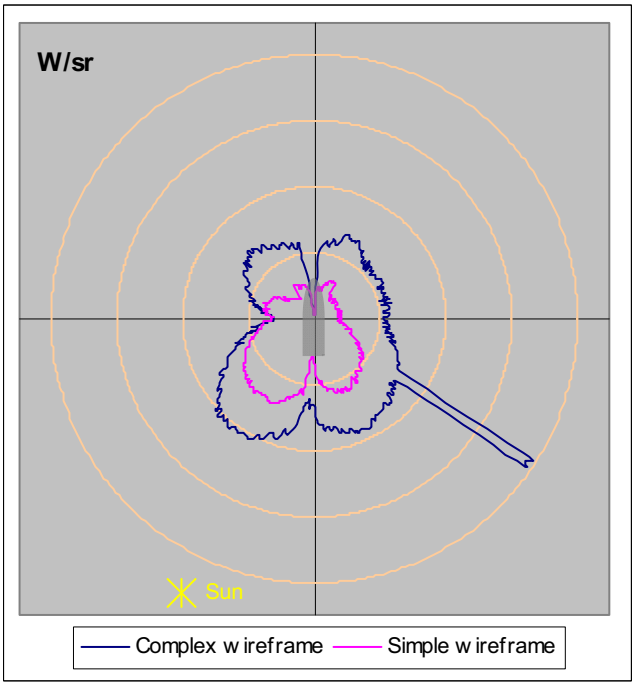

(c) Mid-wave IR band

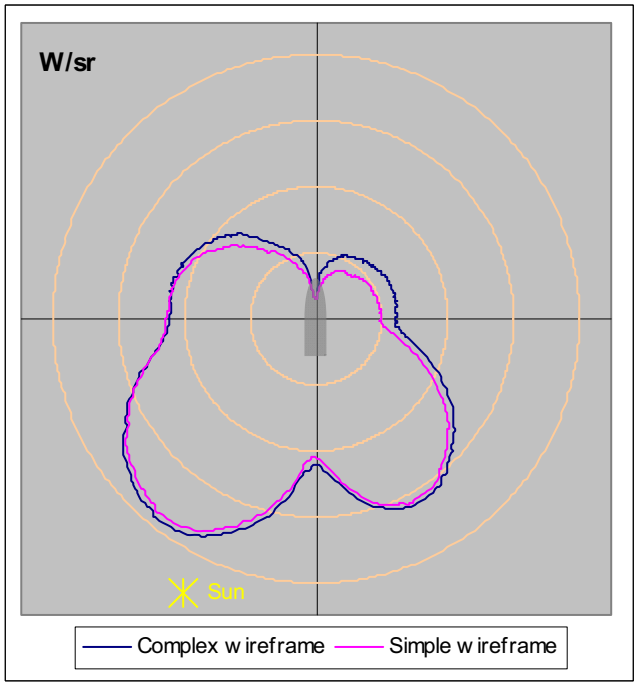

(d) Long-wave IR band

Figure D2 Background 1, 10 km viewing distance

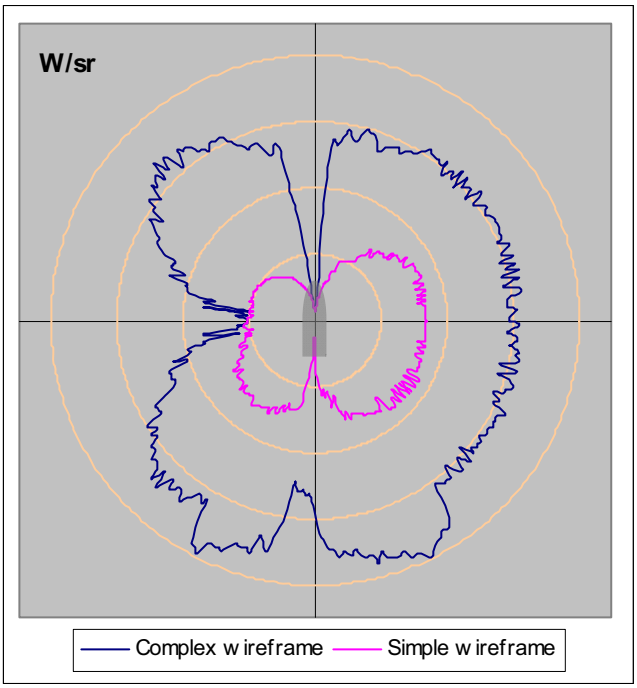

(a) Mid-wave IR band

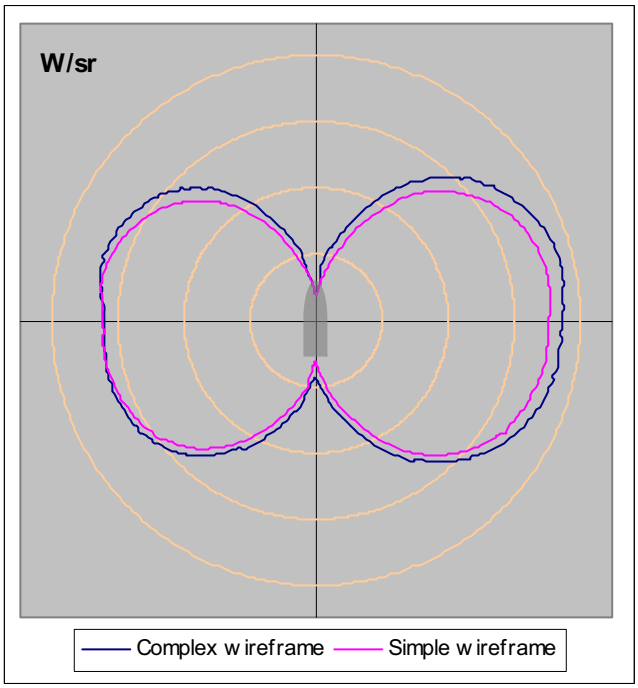

(b) Long-wave IR band

Figure D3 Background 2, 2 km viewing distance

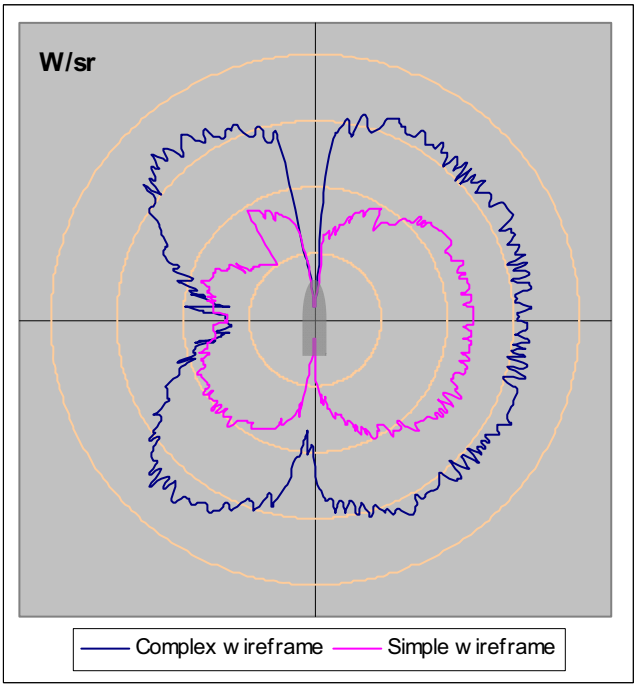

(a) Mid-wave IR band

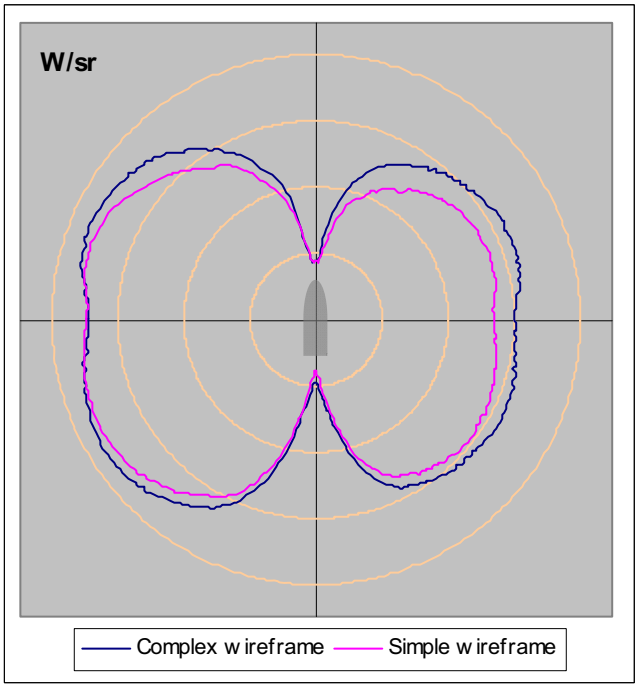

(b) Long-wave IR band

Figure D4 Background 2, 10 km viewing distance

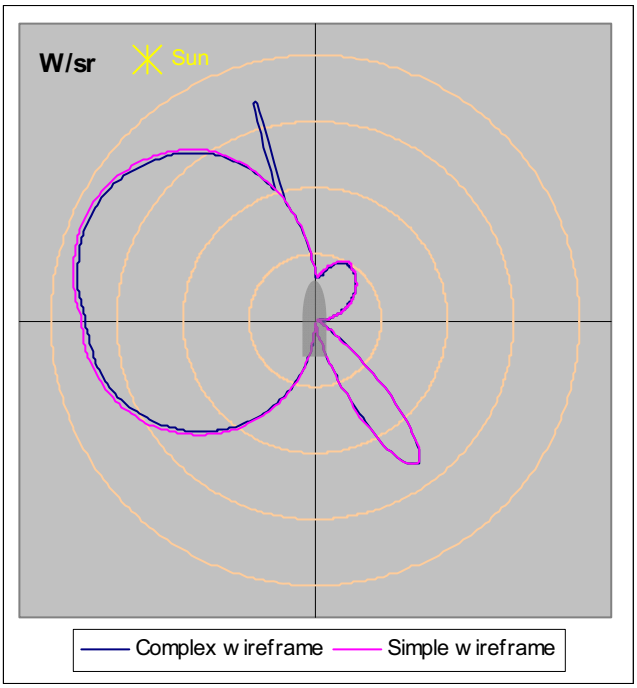

(a) Visible band

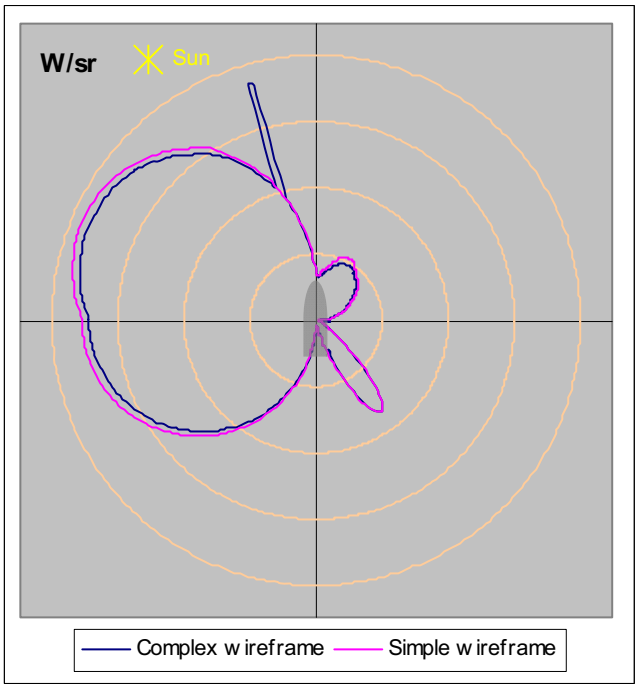

(b) Near-visible IR band

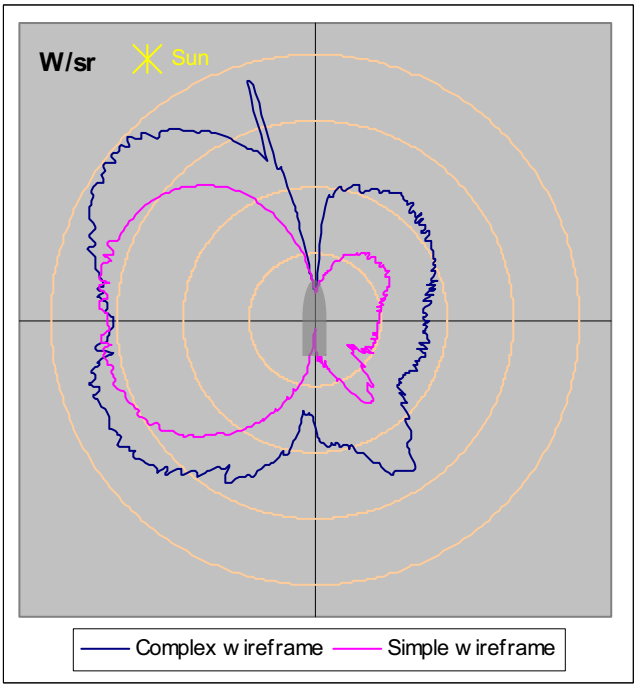

(c) Mid-wave IR band

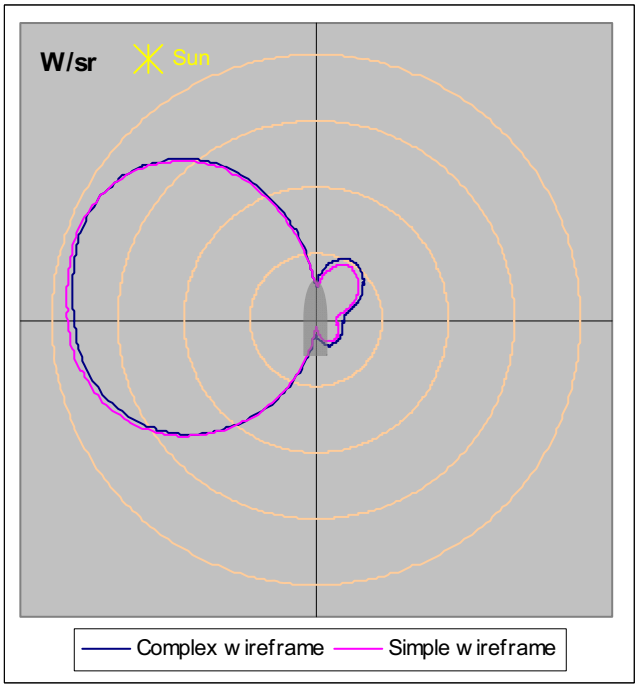

(d) Long-wave IR band

Figure D5 Background 3, 2 km viewing distance

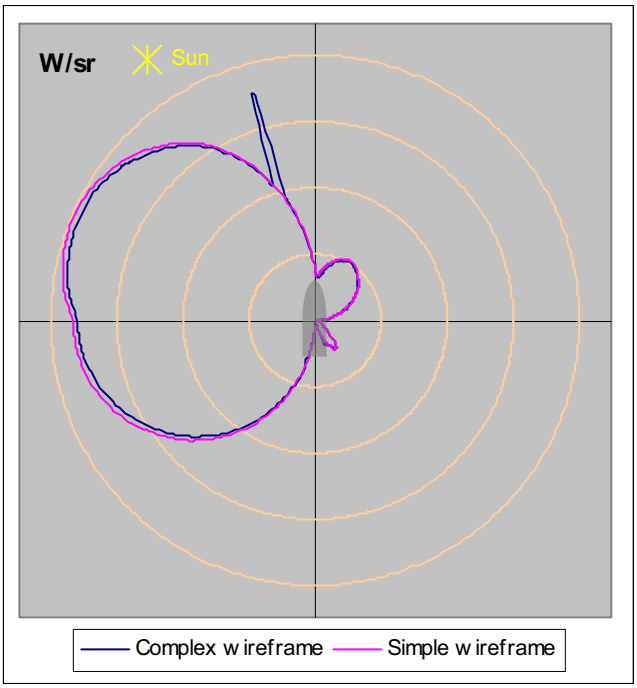

(a) Visible band

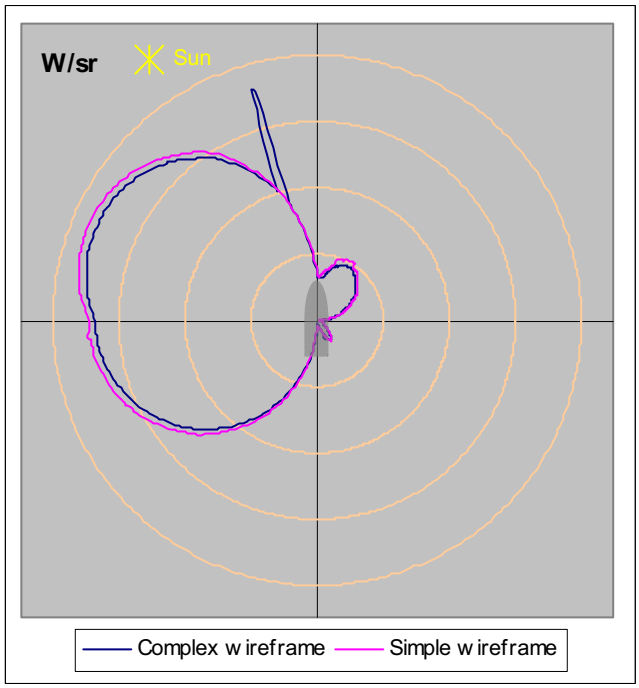

(b) Near-visible IR band

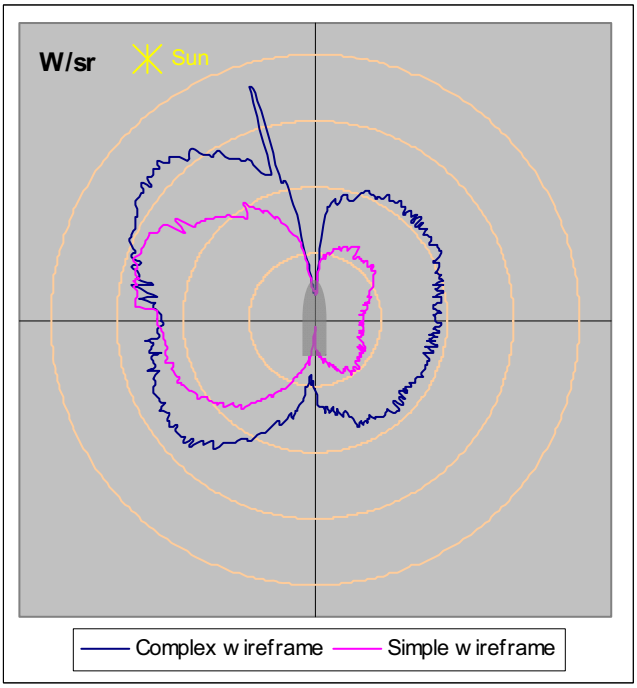

(c) Mid-wave IR band

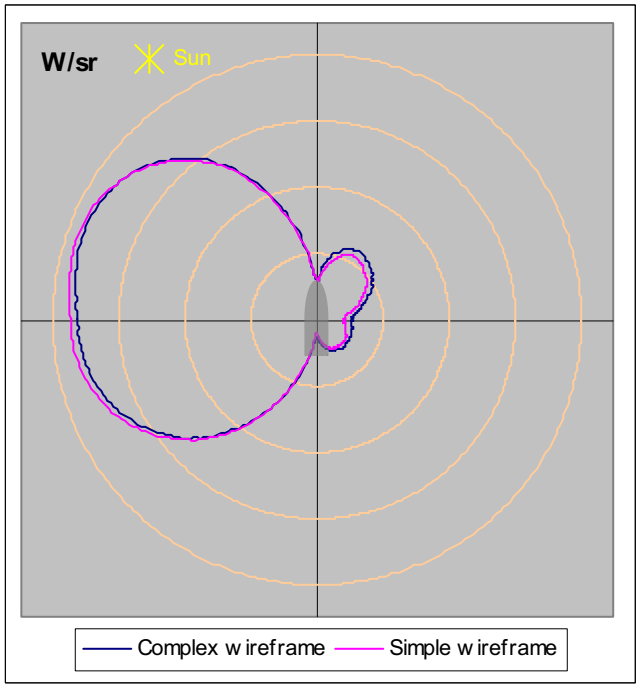

(d) Long-wave IR band

Figure D6 Background 3, 10 km viewing distance

D.2. Contrast signature plots for the two models, both with user-defined thermal boundary conditions but no exhaust plume

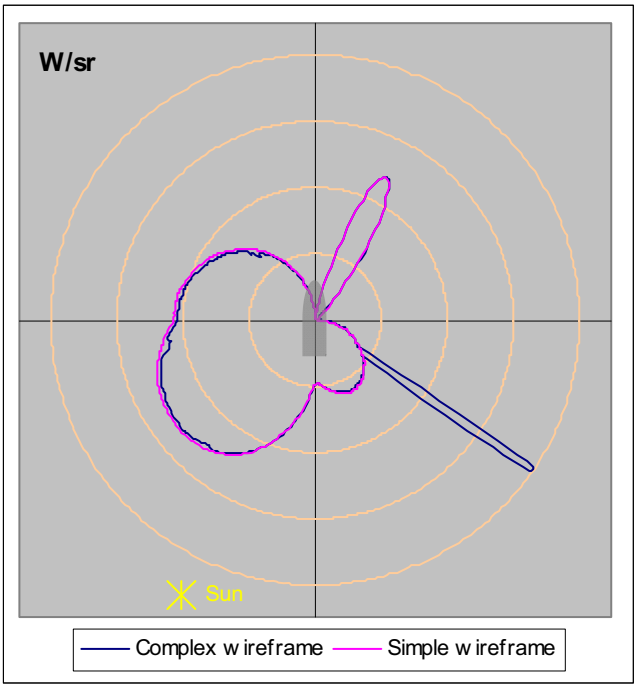

(a) Visible band

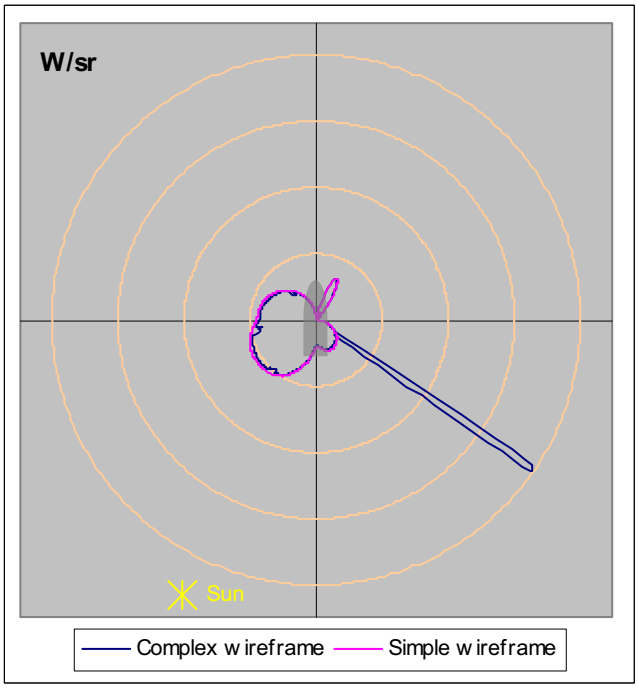

(b) Near-visible IR band

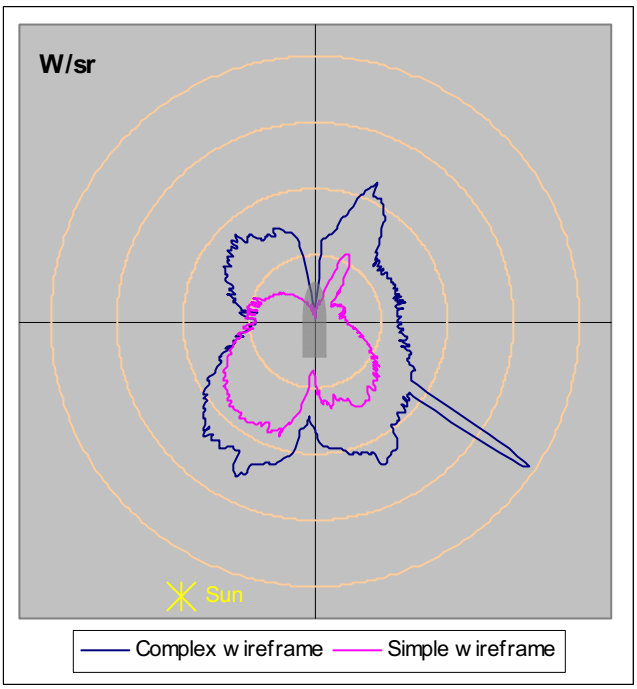

(c) Mid-wave IR band

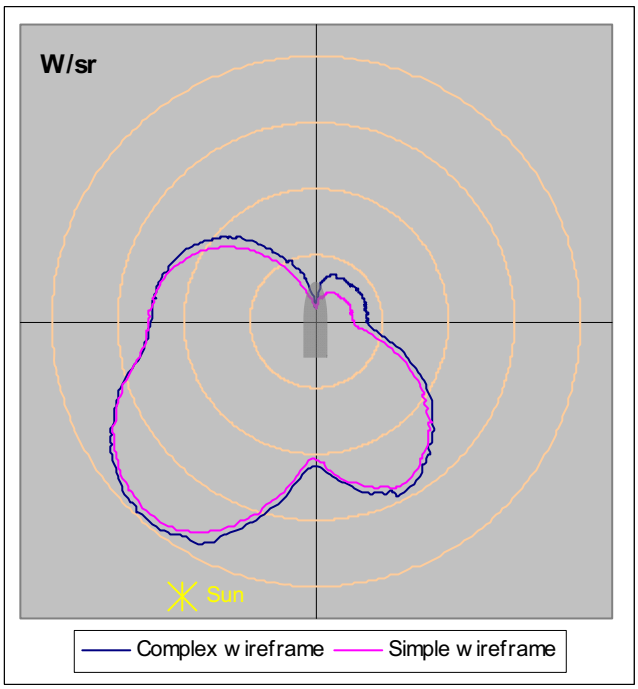

(d) Long-wave IR band

Figure D7 Background 1, 2 km viewing distance

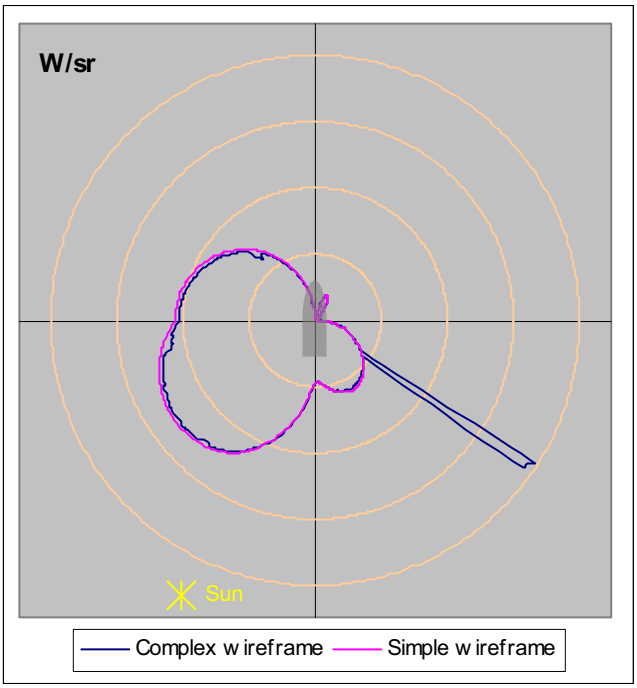

(a) Visible band

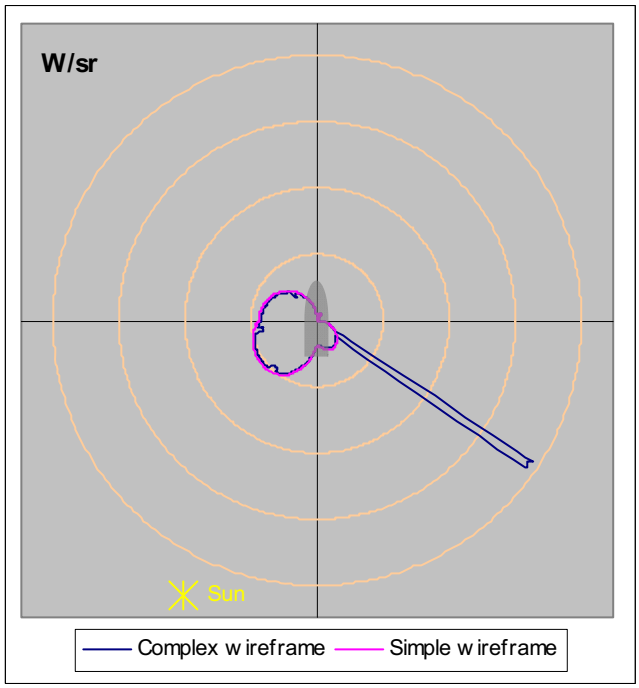

(b) Near-visible IR band

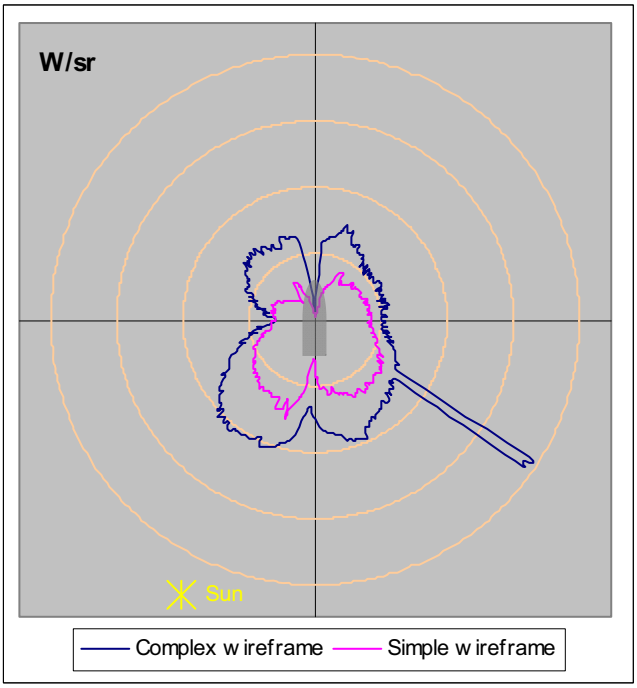

(c) Mid-wave IR band

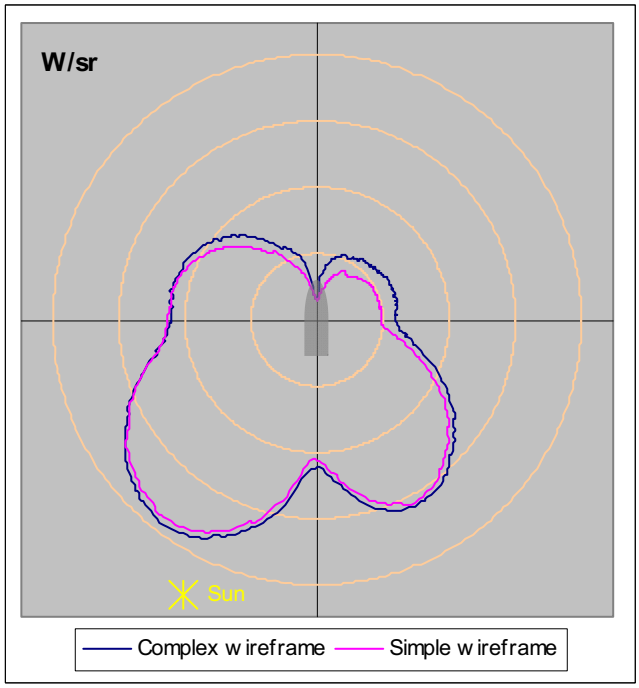

(d) Long-wave IR band

Figure D8 Background 1, 10 km viewing distance

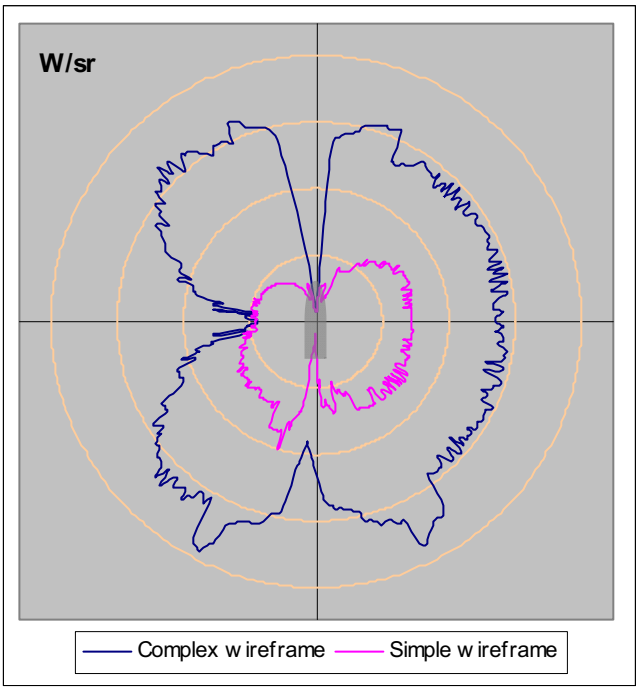

(a) Mid-wave IR band

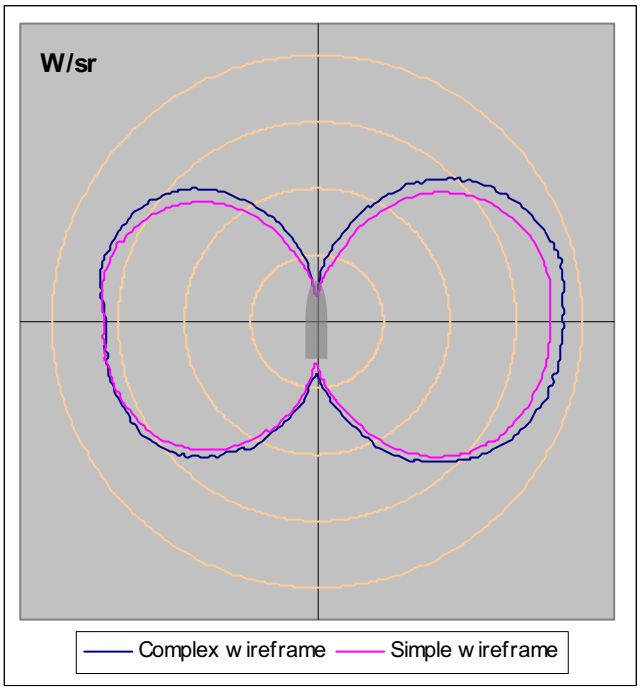

(b) Long-wave IR band

Figure D9 Background 2, 2 km viewing distance

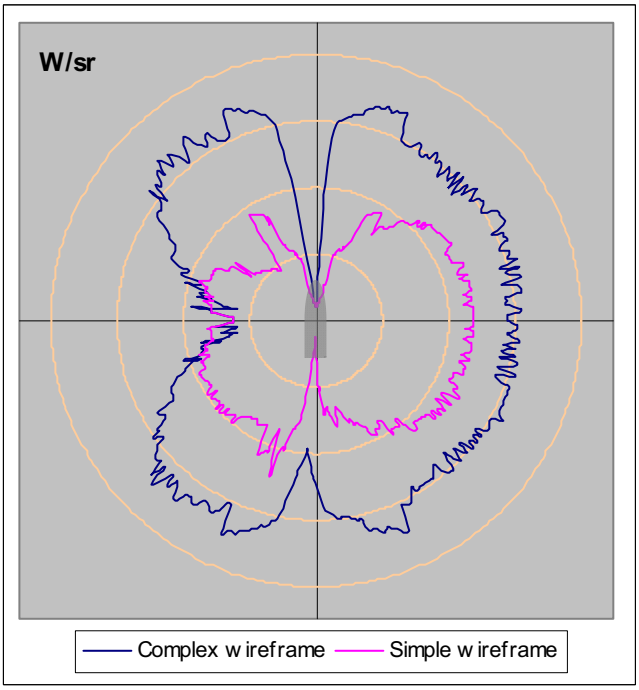

(a) Mid-wave IR band

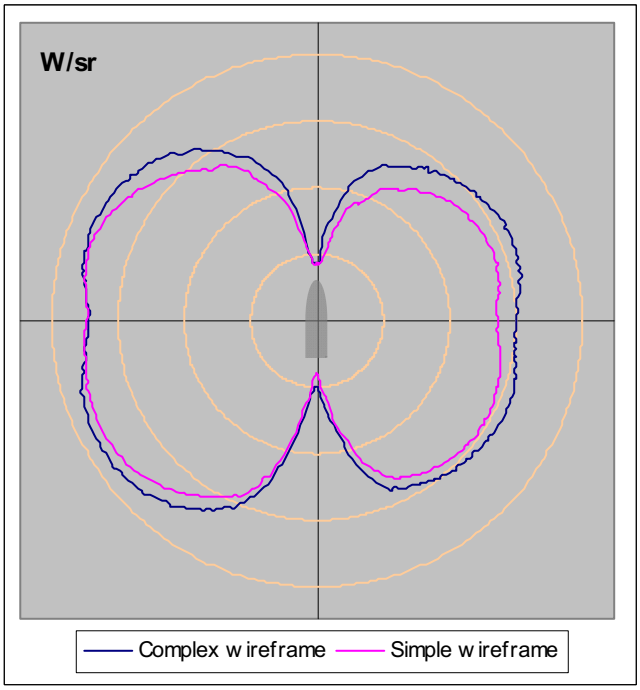

(b) Long-wave IR band

Figure D10 Background 2, 10 km viewing distance

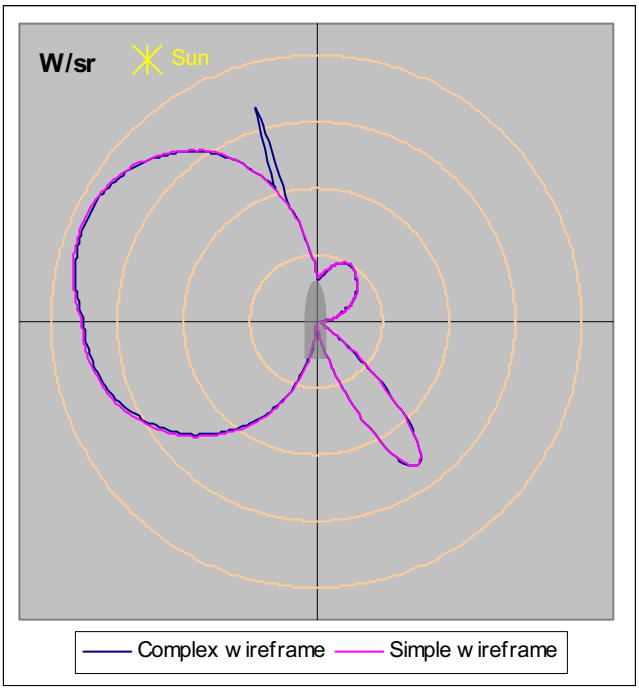

(a) Visible band

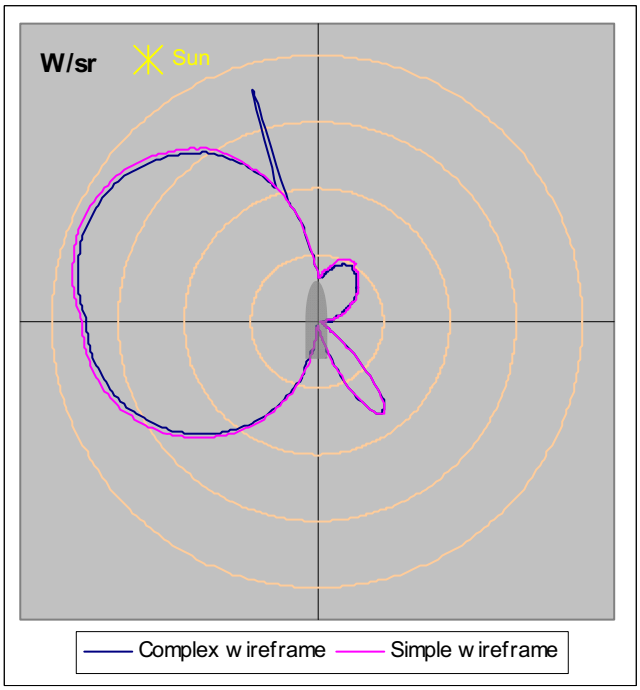

(b) Near-visible IR band

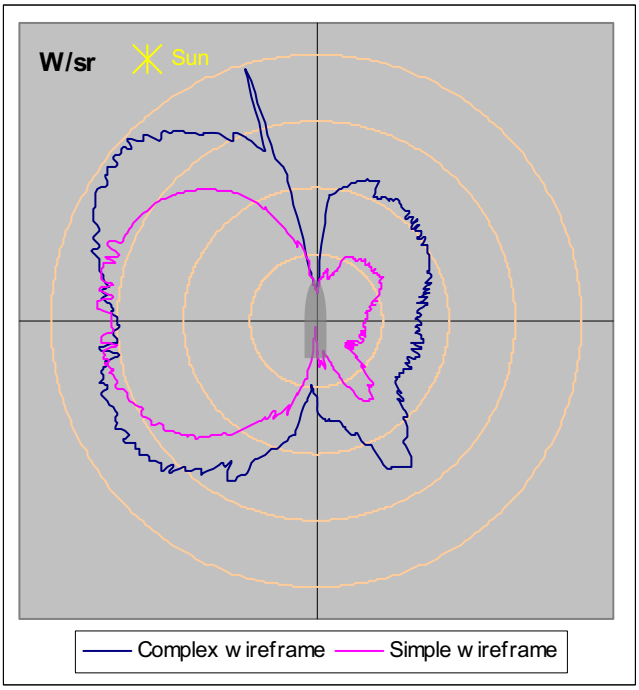

(c) Mid-wave IR band

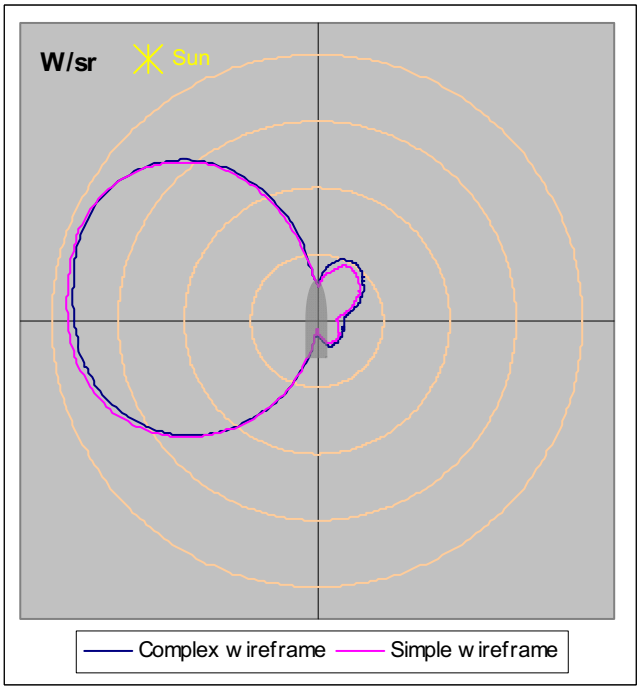

(d) Long-wave IR band

Figure D11 Background 3, 2 km viewing distance

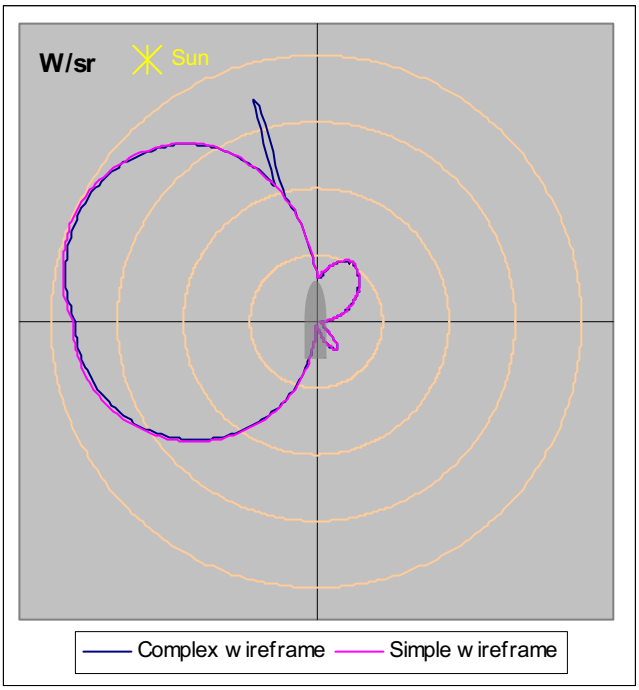

(a) Visible band

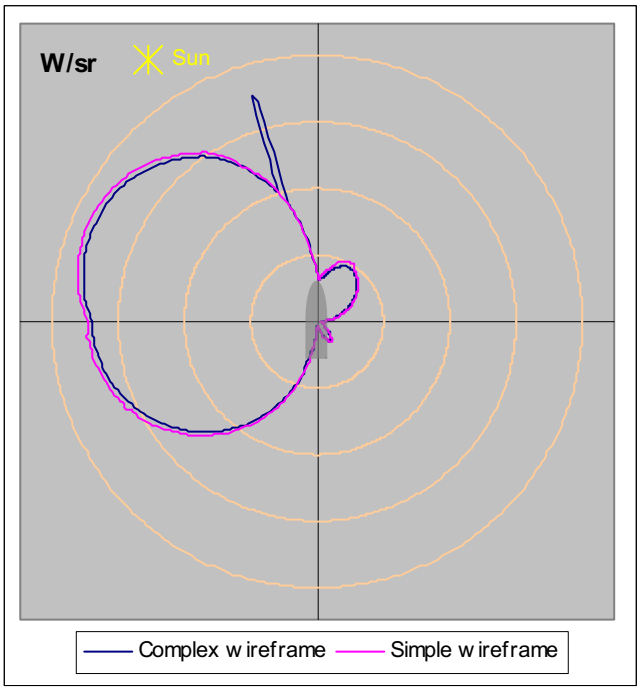

(b) Near-visible IR band

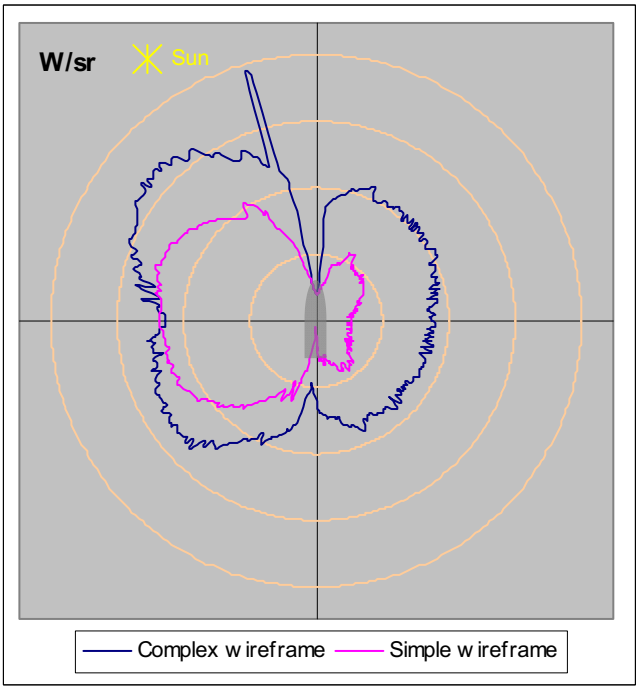

(c) Mid-wave IR band

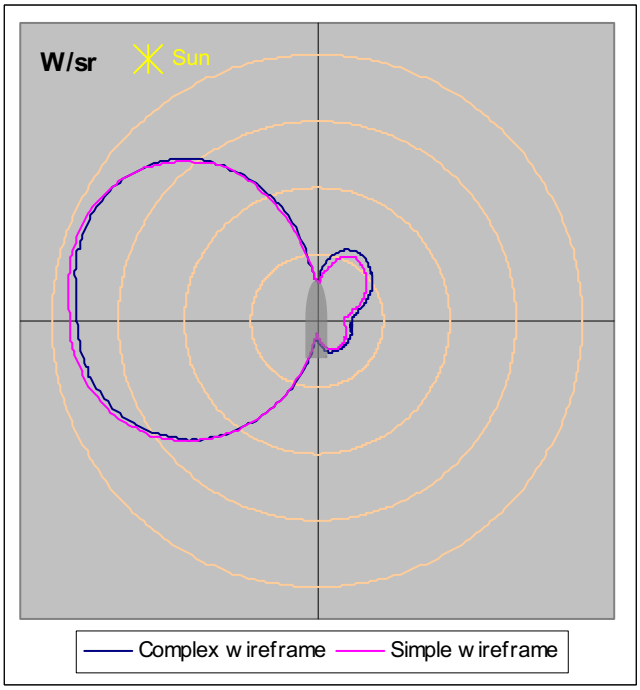

(d) Long-wave IR band

Figure D12 Background 3, 10 km viewing distance

D.3. Contrast signature plots for the two models, both with no user-defined thermal boundary conditions or exhaust plume

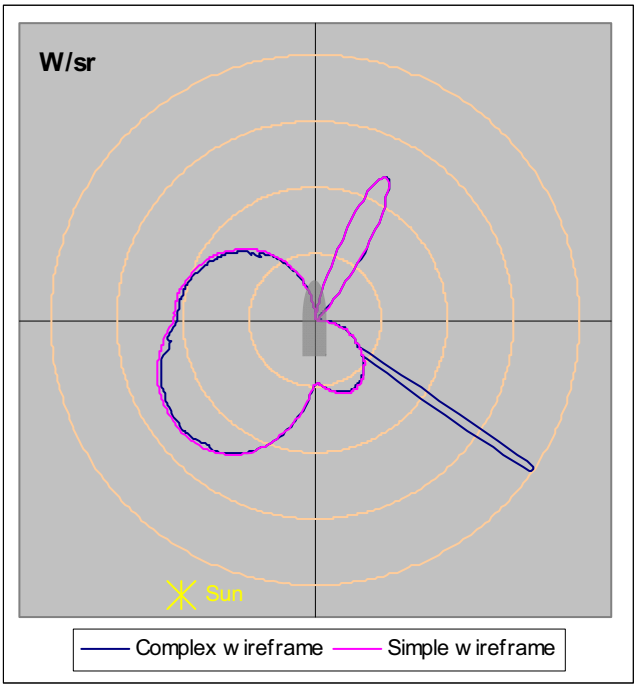

(a) Visible band

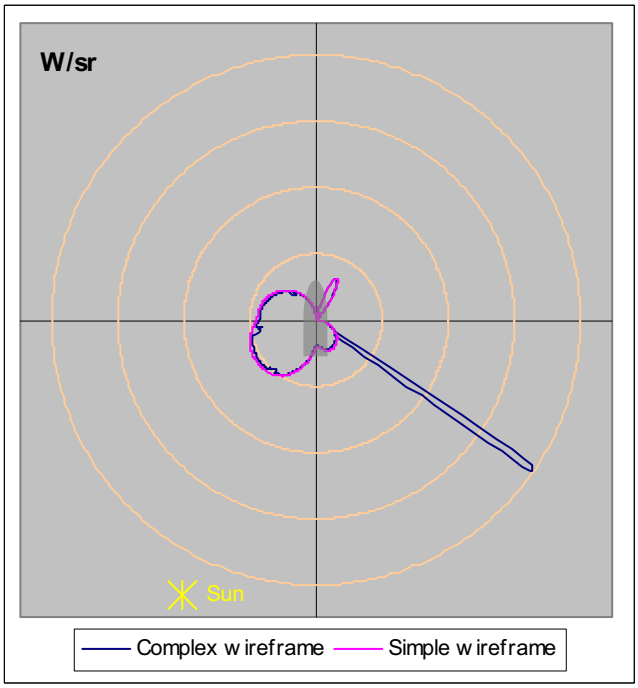

(b) Near-visible IR band

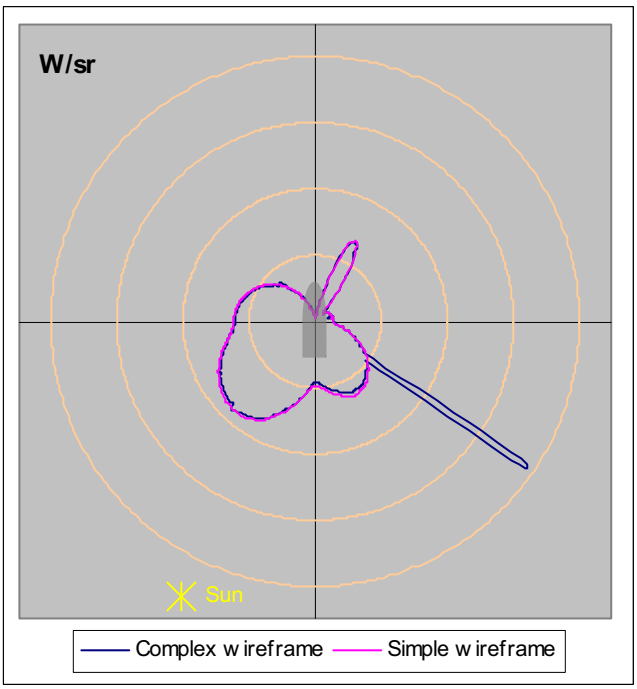

(c) Mid-wave IR band

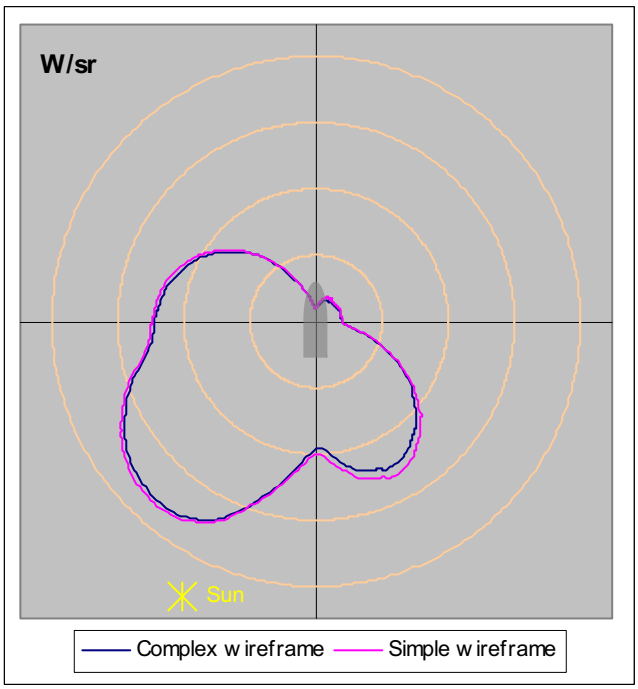

(d) Long-wave IR band

Figure D13 Background 1, 2 km viewing distance

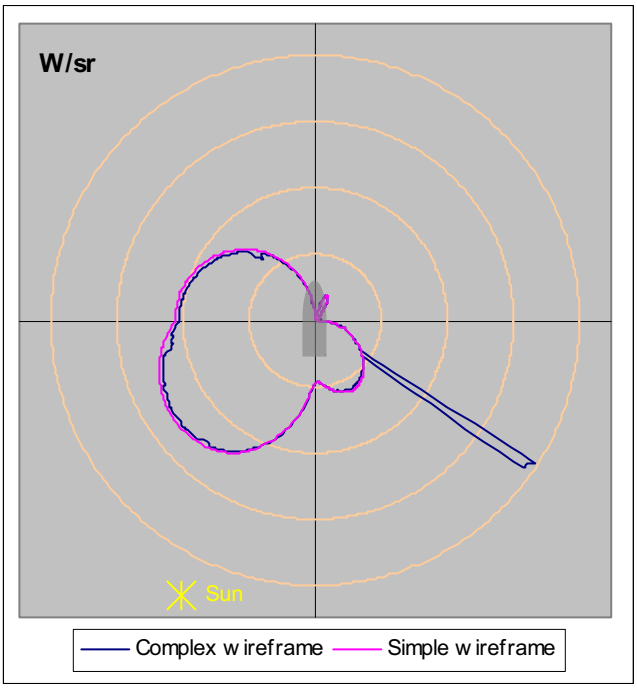

(a) Visible band

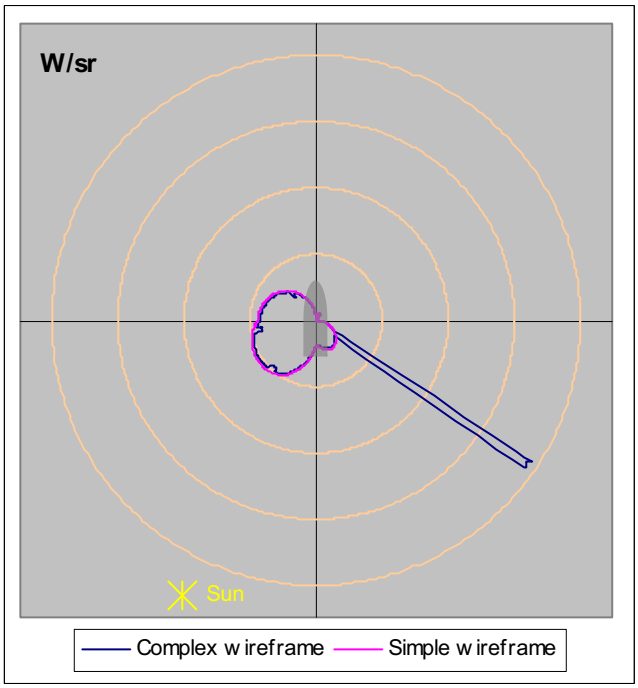

(b) Near-visible IR band

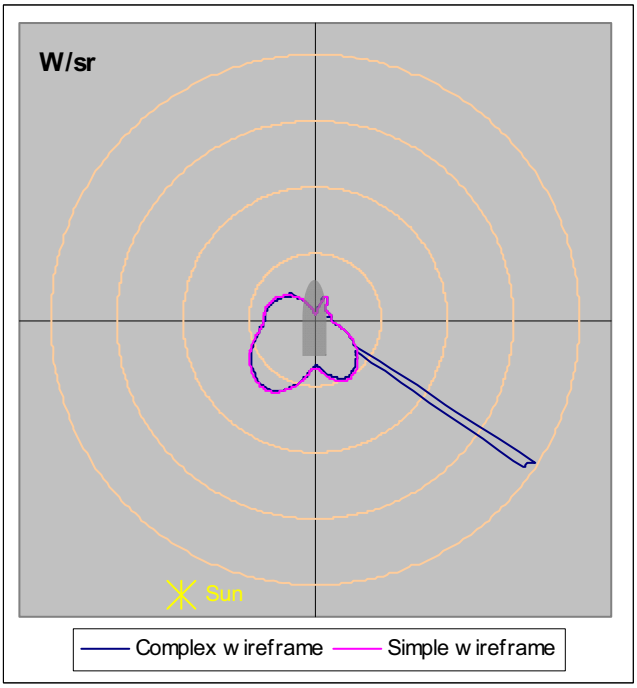

(c) Mid-wave IR band

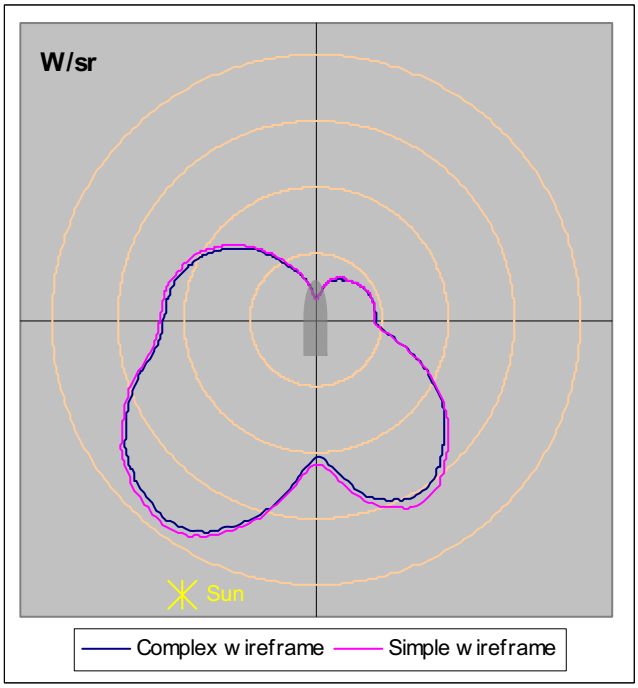

(d) Long-wave IR band

Figure D14 Background 1, 10 km viewing distance

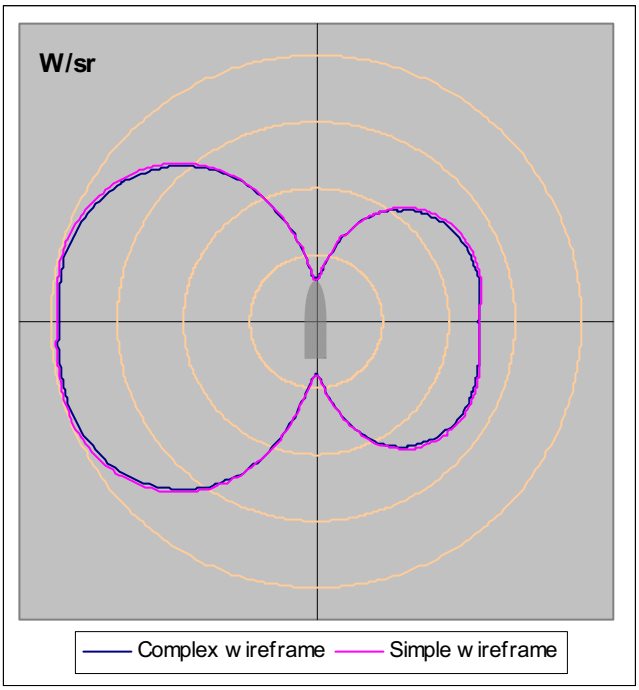

(a) Mid-wave IR band

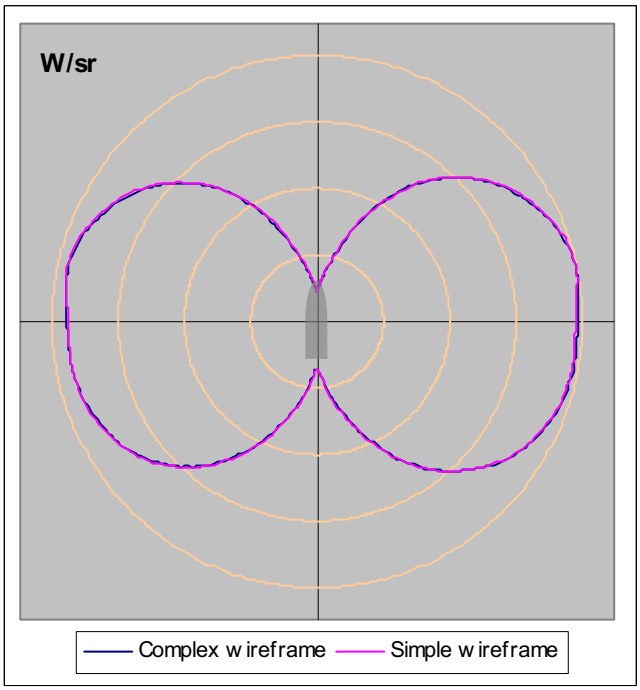

(b) Long-wave IR band

Figure D15 Background 2, 2 km viewing distance

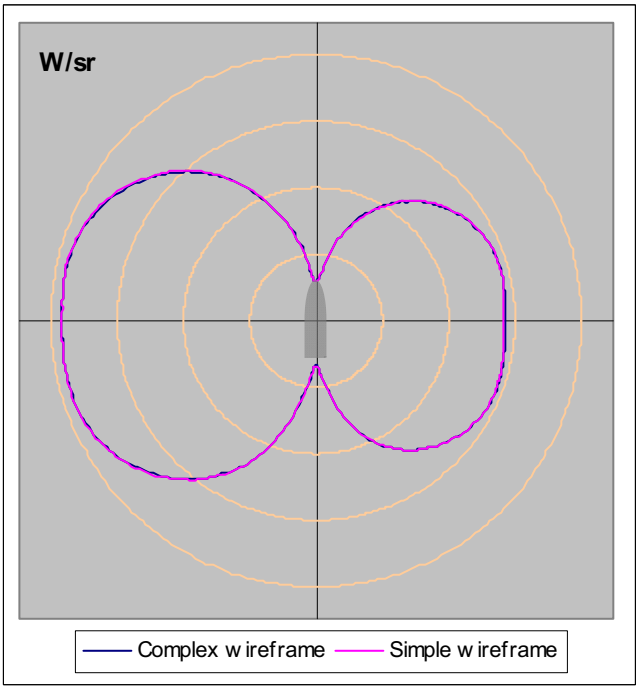

(a) Mid-wave IR band

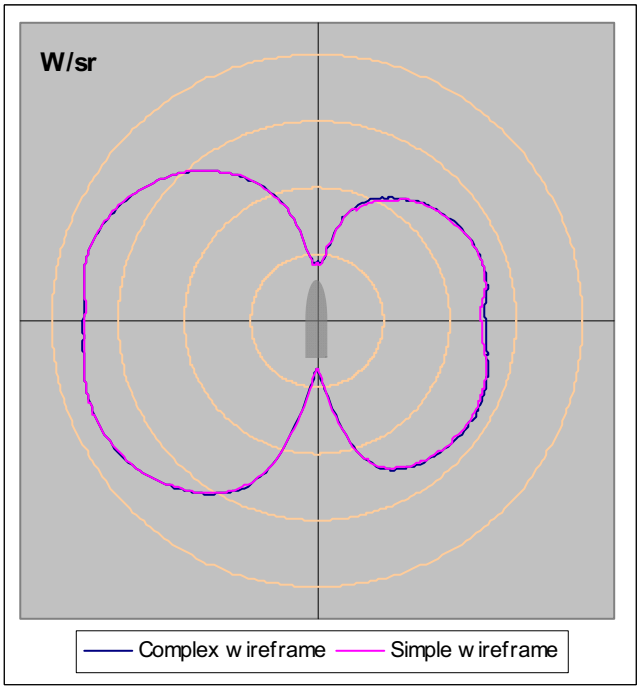

(b) Long-wave IR band

Figure D16 Background 2, 10 km viewing distance

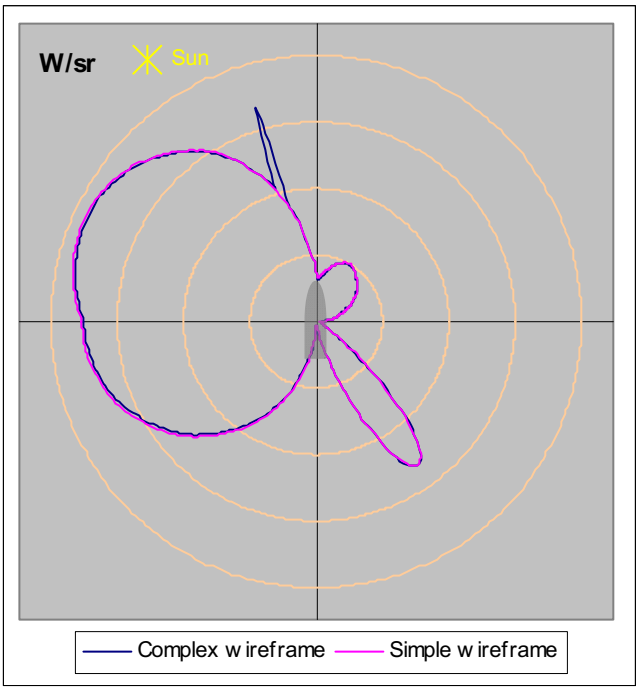

(a) Visible band

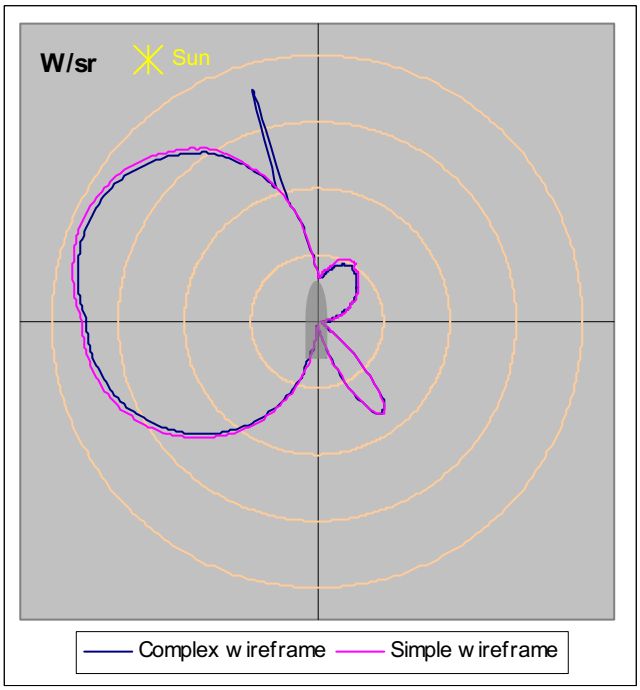

(b) Near-visible IR band

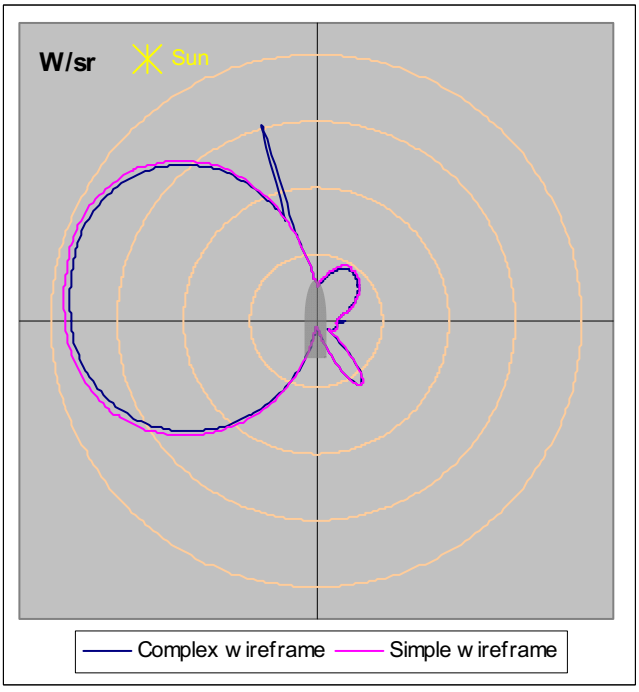

(c) Mid-wave IR band

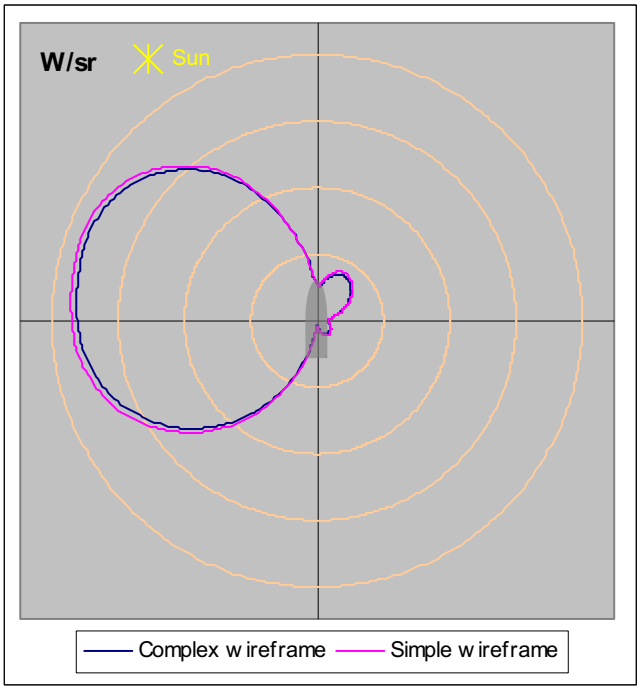

(d) Long-wave IR band

Figure D17 Background 3, 2 km viewing distance

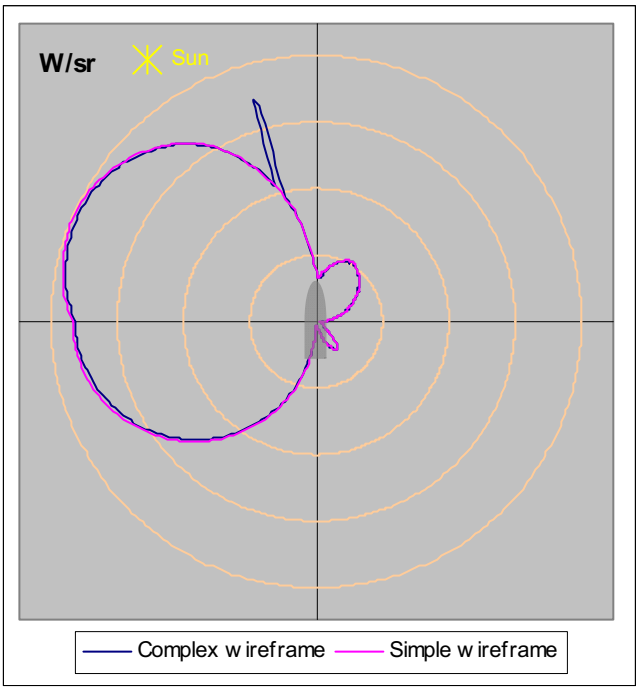

(a) Visible band

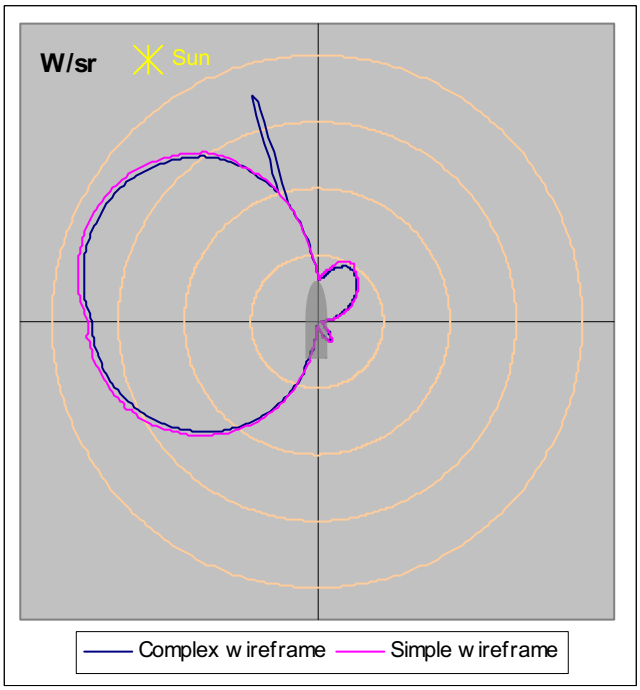

(b) Near-visible IR band

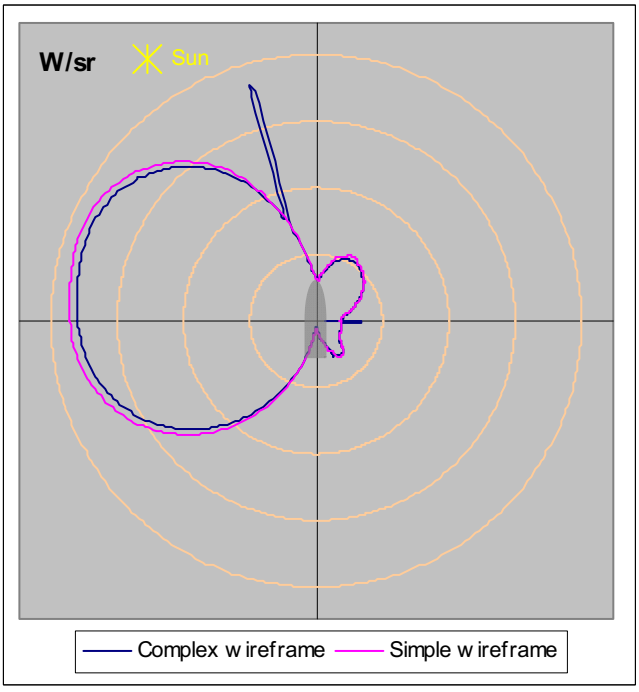

(c) Mid-wave IR band

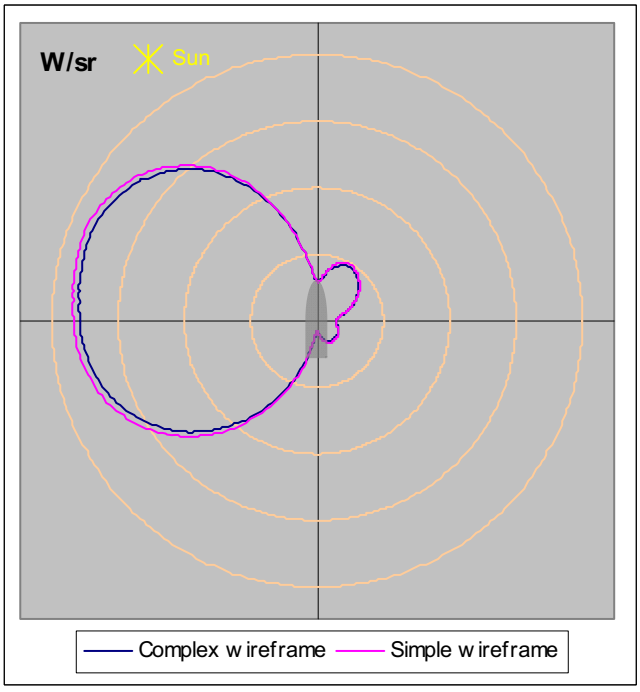

(d) Long-wave IR band

Figure D18 Background 3, 10 km viewing distance

DEFENCE SCIENCE AND TECHNOLOGY ORGANISATION
DOCUMENT CONTROL DATA

1. PRIVACY MARKING/CAVEAT (OF DOCUMENT)

2. TITLE

The Effects of Selected Modelling Parameters on the Computed Optical Frequency Signatures of Naval Platforms

3. SECURITY CLASSIFICATION (FOR UNCLASSIFIED REPORTS THAT ARE LIMITED RELEASE USE (L) NEXT TO DOCUMENT CLASSIFICATION)

Document	(U)
Title	(U)
Abstract	(U)

4. AUTHOR(S)

Susan Smith

5. CORPORATE AUTHOR

DSTO Defence Science and Technology Organisation
506 Lorimer St
Fishermans Bend Victoria 3207 Australia

6a. DSTO NUMBER	6b. AR NUMBER	6c. TYPE OF REPORT	7. DOCUMENT DATE
DSTO-TR-2277	AR-014-501	Technical Report	April 2009

8. FILE NUMBER	9. TASK NUMBER	10. TASK SPONSOR	11. NO. OF PAGES	12. NO. OF REFERENCES
2008/1012214	NAV 07/070	CCSG	86	13

13. URL on the World Wide Web

http://www.dsto.defence.gov.au/corporate/reports/DSTO-TR-2277.pdf

14. RELEASE AUTHORITY

Chief, Maritime Platforms Division

15. SECONDARY RELEASE STATEMENT OF THIS DOCUMENT

Approved for public release

OVERSEAS ENQUIRIES OUTSIDE STATED LIMITATIONS SHOULD BE REFERRED THROUGH DOCUMENT EXCHANGE, PO BOX 1500, EDINBURGH, SA 5111

16. DELIBERATE ANNOUNCEMENT

No Limitations

17. CITATION IN OTHER DOCUMENTS Yes

18. DSTO RESEARCH LIBRARY THESAURUS http://web-vic.dsto.defence.gov.au/workareas/library/resources/dsto_thesaurus.shtml

Platforms, naval ships, signatures, computer systems

19. ABSTRACT

An investigation has been carried out into the effects of wireframe detail and model sub-processing on the predicted optical frequency (OF) signature of a platform. This report describes the results of that investigation. Overall it is concluded that to be able to compare the computed OF signatures of different platforms with validity, the models of the platforms have to incorporate the same level of wireframe detail, especially in internally-heated regions such as their stacks. They also have to be processed using subdivisions of very similar size, based on the same method of facet subdivision.